# INVESTIGATING THE FRACTURE BEHAVIOUR OF X70M LINEPIPE STEEL GIRTH WELDMENTS VIA SINGLE EDGE NOTCHED TENSION AND BEND TESTS

A THESIS SUBMITTED TO
THE GRADUATE SCHOOL OF NATURAL AND APPLIED SCIENCES
OF
MIDDLE EAST TECHNICAL UNIVERSITY

BY

UYGAR TOSUN

IN PARTIAL FULFILLMENT OF THE REQUIREMENTS
FOR
THE DEGREE OF MASTER OF SCIENCE
IN
METALLURGICAL AND MATERIALS ENGINEERING

JULY 2018

Approval of the thesis:

**INVESTIGATING THE FRACTURE BEHAVIOUR OF X70M LINEPIPE STEEL GIRTH WELDMENTS VIA SINGLE EDGE NOTCHED TENSION AND BEND TESTS**

submitted by **UYGAR TOSUN** in partial fulfillment of the requirements for the degree of **Master of Science in Metallurgical and Materials Engineering Department, Middle East Technical University** by,

Prof. Dr. Halil Kalıpçılar
Dean, Graduate School of **Natural and Applied Sciences** _____

Prof. Dr. C. Hakan Gür
Head of Department, **Metallurgical and Materials Eng.** _____

Prof. Dr. C. Hakan Gür
Supervisor, **Metallurgical and Materials Eng. Dept., METU** _____

Dr. Süha Tirkeş
Co-Supervisor, **Weld. Tech. and NDT Res./App. C., METU** _____

**Examining Committee Members:**

Prof. Dr. Rıza Gürbüz
Metallurgical and Materials Eng. Dept., METU _____

Prof. Dr. C. Hakan Gür
Metallurgical and Materials Eng. Dept., METU _____

Prof. Dr. Cevdet Kaynak
Metallurgical and Materials Eng. Dept., METU _____

Prof. Dr. A. Tamer Özdemir
Metallurgical and Materials Eng. Dept., Gazi University _____

Assist. Prof. Dr. Mert Efe
Metallurgical and Materials Eng. Dept., METU _____

Date: 05.07.2018

**I hereby declare that all information in this document has been obtained and presented in accordance with academic rules and ethical conduct. I also declare that, as required by these rules and conduct, I have fully cited and referenced all material and results that are not original to this work.**

Name, Last name: UYGAR TOSUN

Signature :

## ABSTRACT

### INVESTIGATING THE FRACTURE BEHAVIOUR OF X70M LINEPIPE STEEL GIRTH WELDMENTS VIA SINGLE EDGE NOTCHED TENSION AND BEND TESTS

Tosun, Uygar
M.Sc., Department of Metallurgical and Materials Engineering
Supervisor: Prof. Dr. C. Hakan Gür
Co-Supervisor: Dr. Süha Tirkeş

July 2018, 86 pages

Increasing competition in the global market motivates the producers to invest in novel and cost-effective manufacturing technologies in pipeline construction. Gas metal arc welding multi-pass process has been proven for as-rolled low-alloy steels. Engineering of welding is a special concern in terms of fracture mechanics because the joint yields a fusion line between chemically and physically dissimilar structures. Engineering Critical Assessments (ECA) suggest more realistic scenarios for material's elastic-plastic behaviors at proximity of the discontinuities compared to conventional good workmanship criterion, and thus lower the repair rates dramatically by allowing more generous discontinuity dimensions. In this study, fracture toughness parameters and properties affecting the fracture behavior of as-welded API 5L X70M steels were investigated. After validating the integrity of girth welds with conventional non-destructive and destructive tests, Single Edge Notched Tension (SENT) and Single Edge Notched Bend (SENB) tests were performed to obtain single critical values and tear resistance curves. The fracture surfaces were examined. Then, the effects of crack tip constraint and plastic deformation were investigated. The results show that, the SENT specimens demonstrate better resistance to both located crack and propagation of tearing compared to SENB specimens due to lower crack tip constraint.

Keywords: High strength low alloy steel, fracture toughness, structural integrity, elastic-plastic fracture mechanics, line pipe

# ÖZ

## X70M BORU HATTI ÇELİĞİ ÇEVRESEL KAYNAKLARININ KIRILMA DAVRANIŞININ TEK KENARI ÇENTİKLİ ÇEKME VE EĞME TESTLERİ İLE İNCELENMESİ

Tosun, Uygar
Yüksek Lisans., Metalurji ve Malzeme Mühendisliği Bölümü
Tez Yöneticisi: Prof. Dr. C. Hakan Gür
Ortak Tez Yöneticisi: Dr. Süha Tirkeş

Temmuz 2018, 86 sayfa

Küresel pazardaki artan rekabet boru hattı inşasında özgün ve uygun maliyetli üretim teknolojileri yatırımlarına motivasyon sağlamaktadır. Çok pasolu gaz metal ark kaynağı düşük alaşımlı ve paslanmaz çeliklerde rüştünü ispatlamıştır. Kaynağın mühendisliği kırılma tokluğu bağlamında özel bir öneme sahiptir çünkü birleşme bölgesinde birbirinden kimyasal ve fiziksel olarak farklı iki yapının kesişim hattı bulunmaktadır. Mühendislik Kritik Değerlendirmesi (MKD) malzemenin hatalı bölgedeki elastik-plastik davranışı için geleneksel iyi işçilik kriterlerine göre daha gerçekçi bir alternatif sunar, bu sebeple daha büyük hata boyutlarına izin vererek tamir oranlarını önemli ölçüde azaltır. Bu çalışmada, kaynaklı X70M çeliğinin kırılma tokluğu parametreleri ve kırılma davranışını etkileyen özellikler incelenmiştir. Çevresel kaynağın bütünlüğü geleneksel tahribatsız ve tahribatlı testlerle doğrulandıktan sonra, tekil kritik değerleri ve kırılma dayanım eğrilerini elde etmek için, Tek Kenarı Çentikli Çekme (TKÇÇ) ve Tek Kenarı Çentikli Eğme (TKÇE) testleri yapıldı. Kırılma yüzeyleri incelendi ve çatlak ucu kısıtlaması ve plastik deformasyon incelendi. Sonuçlarda, TKÇÇ numunelerinin, daha düşük çatlak ucu kısıtlaması sebebiyle, TKÇE numunelerine göre hem üzerlerinde bulunan bir çatlağa hem de yırtılmaya daha iyi direnç gösterdiği belirlenmiştir.

Anahtar Kelimeler: Yüksek dayançlı düşük alaşımlı çelik, kırılma tokluğu, yapısal bütünlük, elastic-plastik kırılma mekaniği, boru hattı

**To Ever-Advancing Civilization…**

## ACKNOWLEDGMENTS

I sincerely thank my supervisor Prof. Dr. C. Hakan Gür and co supervisor Dr. Süha Tirkeş for their guidance, advice, criticism, encouragements and insight throughout the research.

I sincerely appreciate Dr. Koray Yurtışık for his motivation, guidance and support.

I deeply appreciate Dr. Göksu Gürer, M. Tolga Ertürk, Baran Tunç, Mehmet Çağırıcı and Burcu Anık whose help and advices were invaluable.

Orhan Aydın, Arif Atalay Özdemir, Cemal Yanardağ, Yücel Ateş, Kubilay Savcı Yeşildemir and Mevlüt Bağcı were very supportive and altruistic during fabrication and testing processes.

Hasan Özgür Taşcı was very helpful and generous in sharing his welding engineer knowledge comes directly from field experience. I sincerely appreciate fruitful discussions we had.

I want to extend my deep appreciation to my family; my mother and father Tahire and Daver Tosun and my wife Pınar Tosun for their infinite support, their faith in me, to all my friends and to whomever eased the load on me walking this path.

This work is financially supported by METU Welding Tech. and Non-destructive Testing Research/Application Center R&D Division.

## TABLE OF CONTENTS

## LIST OF TABLES

## LIST OF FIGURES

## LIST OF ABBREVIATIONS

| | |
|---|---|
| AE | Arc energy |
| ao | Initial crack length |
| ASTM | American Society of Testing and Materials |
| AUT | Automated ultrasonic testing |
| BS | British Standards Institution |
| CGHAZ | Coarse-grain heat affected zone |
| COD | Crack opening displacement |
| CTOD | Crack tip opening displacement |
| DBTT | Ductile to brittle transition temperature |
| DNV | Det Norske Veritas |
| ECA | Engineering critical assessment |
| EGF | European Group of Fracture |
| EPFM | Elastic-plastic fracture mechanics |
| FCAW | Flux cored arc welding |
| FEA | Finite element analysis |
| FFS | Fitness-for-service |
| FGHAZ | Fine-grain heat affected zone |
| FL | Fusion line |
| GMAW | Gas metal arc welding |
| GTAW | Gas tungsten arc welding |
| HAZ | Heat affected zone |
| ICHAZ | Inter-critical heat affected zone |
| IRCGHAZ | Inter-critically reheated coarse-grain |
| IRFGHAZ | Inter-critically reheated fine-grain |
| K | Stress intensity factor |
| LBZ | Local brittle zone |
| LEFM | Linear-elastic fracture mechanics |

| | |
|---|---|
| LSAW | Longitudinal sub-merged arc welding |
| MCAW | Metal cored arc welding |
| MT | Magnetic particle testing |
| NDT | Non-destructive testing |
| RT | Radiographic testing |
| SCCGHAZ | Sub-critically reheated coarse-grain |
| SCHAZ | Sub-critical heat affected zone |
| SCRCGHAZ | Super-critically reheated coarse-grain heat affected zone |
| SCRFGHAZ | Super-critically reheated fine-grain heat affected zone |
| SEM | Scanning electron microscope |
| SENB | Singe edge notched bending |
| SENT | Single edge notched tension |
| SMAW | Shielded metal arc welding |
| SZW | Stretch zone width |
| TANAP | Trans-Anatolian Natural Gas Pipeline |
| VT | Visual inspection |
| WM | Weld metal |
| $\Delta a$ | Tearing length |

# CHAPTER 1

# INTRODUCTION

## 1.1 Motivation

Fracture is a damage mechanism in materials that should be taken under consideration in engineering practices, such as design and maintenance programs. Describing the initiation and propagation mechanisms of cracking are still of great interest in the field of fracture mechanics where deterministic approaches should be supported by empirical works due to the complexity and versatility of material behavior.

As industrial infrastructures, pipelines consist enclosing and supporting assemblies where ductile materials are used under severe physical stress and environmental conditions that degrade and age the materials. Understanding the material's elastic-plastic behavior at the proximity of material discontinuities becomes tricky especially when material nonhomogeneities, such as welding joints, present.

Engineering of welding is a special concern in terms of fracture mechanics because the joint yields a fusion line between chemically and physically dissimilar structures. Mismatch in the mechanical properties between the fusion zone and the parent metal is inevitable and in fact intentionally optimized to the benefit of the fusion zone. This engineering optimization is technically called strength over-matching. Despite the over-matching is an engineering criterion, degree of it is important since as its degree gets higher, then general fracture toughness properties of the joint are affected in negative ways.

Nonetheless, the heat introduced to the materials during welding operations alters their microstructures significantly. Concerning deformations due to expansion and

contraction of the metal, this heat not only cause thermal processes but also complex mechanical processes through the joints. These thermomechanical processes yield quite nonhomogenous and anisotropic material structure especially through the fusion line and proximity of it. Therefore, anisotropic hardening during crack extension and propagation becomes and important issue.

The motivation behind this thesis work, and some other previous and in-progress works, is the Trans Anatolian Natural Gas Pipeline (TANAP) Project, which is about to be commissioned for delivery of natural gas from Shah Deniz-2 in Azerbaijan to Turkey and Europe. TANAP is globally one of the biggest pipeline projects where 1850 km of line was constructed under one management agent. Welding Technology and Non-destructive Testing Research / Application Center in Middle East Technical University and Ion Industrial Metallurgy have played an important role in mechanical and microstructural characterization and validation of pre-construction and construction weldments.

Another motivation of this study is the recent developments in test and evaluation methods of elastic-plastic fracture mechanics which are employed for assessments to evaluate allowable flaw sizes. New standards are emerging and the existing standards are dramatically revamped. All recent studies have proposed new approaches or developed methods. Results of this thesis work are expected to lay the groundwork for contributing international endeavor to evaluate the fracture behavior of line pipes more realistically and precisely.

## 1.2 Scope

Rules and requirements of API Standard 1104 [1], Welding of Pipelines and Related Facilities, were followed during the project TANAP. The purpose of API 1104 is to specify methods for the production of reliable weldments employing validated welding procedures. The standard provides two alternative criteria for dimensions of the discontinuities that are formed inevitably during welding operations. The standard conventionally introduces acceptance conditions that are based on empirical criteria

for workmanship and place primary importance on imperfection length. Such conventional criteria have provided and a satisfactory record of reliability in pipeline service for many years. 21st edition (2013) of the standard additionally provides an alternative method that is based on fracture mechanics analyses and fitness-for-service (FFS) criteria for the evaluation of both discontinuity height and length. However, using FFS requires tests to determine fracture toughness parameters or sometimes generate fracture resistance curves in addition to conventional mechanical tests, as well as stress analyses and inspection using state-of-art techniques. Performing analyses based on the principles of FFS is commonly termed Engineering Critical Assessment (ECA). ECA presents more realistic scenarios for material's elastic-plastic behaviors at proximity of the discontinuities. Therefore, ECA provides, generally, more generous allowable discontinuity dimensions. There are other standards and codes available for several industrial infrastructures, in which the discontinuity evaluation methodologies are based on ECA, like DNVGL-ST-F101 [2] for off-shore pipelines or RCC-M [3], R5 for high-temperature damage and R6 for fracture avoidance assessment procedures for nuclear power plants.

Tests for fracture toughness determination and resistance curve generation have been conducted on more than 500 SENB and SENT specimens, as well as tensile, bending, hardness and Charpy impact toughness tests. Introducing the testing data to ECA, tolerable flaw sizes were determined to be larger than the ones from conventional workmanship criteria, quite low repair rates and consequently quite high production rates have been achieved. TEKFEN Construction Co., one of the contractors of the project, reached 140 joints (Ø 56'', WT 19.45 mm) per day, which corresponds to highest number of joints commissioned in a working day during a pipeline construction in the world.

This thesis work has mainly concentrated on the variation in fracture toughness and resistance parameters of a specific material, which was a thermomechanically processed high strength low alloy line pipe steel grade X70M [4], with respect to the initial crack length and the loading condition. Testing of single edge notched specimens with different initial crack lengths and under bending/tensile loading,

contribution of the initial crack length and the loading condition to the crack-tip plasticity, thus fracture resistance behavior of the material, were simulated practically. These empirical efforts have been supported by numerical analyses and also other researchers who published their works. During data analysis, the parameter called initiation fracture toughness has taken a special concern, which has several definitions that are suggested by ASTM, BS, DNV and European Group of Fracture (EGF). As the most realistic approach, this parameter was also estimated employing geometrical parameters of the stretch zone. Moreover, micro-damage mechanisms that took place during stable crack extension were examined using post-test metallography and fractography.

# CHAPTER 2

# THEORY

## 2.1 General

Theory chapter is comprised of five sections. Firstly, an introduction to pipeline construction is presented. Secondly, brief overview on girth welding of line pipes is given. Thirdly, weldability of high strength low alloy (HSLA) steels and weld related defects are described in detail. Then, Structural integrity of line pipe structure is discussed. Lastly, the main focus of the thesis, fracture mechanics is broadly described in light of both historical overview and recent studies which are shaping the line pipe construction standards.

## 2.2 Pipeline construction

Despite renewable sources are being increasingly used, oil and natural gas are still highly competitive energy sources. One of the biggest challenges of all energy resources are the transportation of the energy. Reserves of them usually are remotely located from the end-users. Thin wall pipelines made of micro alloyed and thermo-mechanically rolled HSLA steel plates offer an additional competitive advantages by reducing transmission costs.

Long distances and ever increasing demand compel investors of energy industries to undertake massive construction projects. Cost efficient line pipes are vitally important for those projects. HSLA steels are number one selection for those projects. High strength is needed to overcome loads caused by massive gas streams, environmental effects and stress concentrations caused by locating and jointing pipes. Various standards share many similar mechanical properties required for line pipe steels. Steel

grades of API 5L [4], EN 10025-4 [5] and DNVGL-OS-B101 [6] sharing similar mechanical properties is tabulated in Table 1. API 5L is widely used line pipe materials standard for production of steel pipes, mainly used in petroleum and natural gas transmission.

*Table 1. Steel grades of similar mechanical properties from different standards.*

| **Yield Strength (MPa)** | **Temperature to show ductile behavior** | **API 5L** | **EN 10025** | **DNVGL-OS-B101** |
|---|---|---|---|---|
| **≥450** | 0°C | X65 PSL 2 | S450 J0 | VL AO460 |
| **≥275** | -20°C | X46 PSL 2 | S275 M | VL B27S |

High strength could be resulted with a decrease in toughness which can damage the structural integrity by increasing the risk of crack propagation [7, 8]. The high strength has to be achieved without decreasing the ductility properties of the line pipe [9]. TMCP assures such properties by micro-alloying and decreasing the grain size [10]. The grain refining effect is shown in Figure 1.

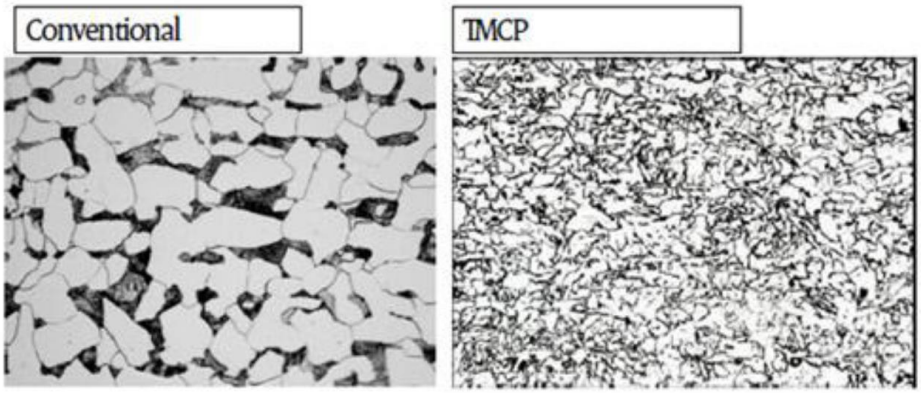


*Figure 1. The grain refining effect of TMCP [11]*

Pipeline construction projects typically are broken into manageable lengths called spreads because of the massive scale of those projects. Projects utilize highly trained, specialized and qualified crews comprise of technicians, engineers and managers. Crews have different responsibilities vary from coordinating the transportation of

specific pipes to related sections to coating jointed pipes to protect from environmental effects such as corrosion.

After the project is planned the first step is the pre-construction survey. Detailed environmental surveys are conducted to determine the most suitable construction techniques. Secondly, Clearing and grade easement is carried out to clear and grade along the pipeline route. Temporary erosion control measures are installed prior to any earth-moving activities. Removed soil is stored at the edge of the opened path for later reinstatement. Thirdly, pipeline trench excavation is completed with trenching machines by the crew. Then, pipes are laid end to end for stringing and bending process. Some pipes are cold bended with specialized equipment. After the stringing and bending are complete, aligned pipe sections are welded above ground in a protective tent usually by an automatic or mechanized welding machine as shown in Figure 2.

*Figure 2. Automatic GMAW on 56" line pipe steel [12]*

All the weldments are subject to X-ray and/or ultrasound testing and some coupons are cut for destructive testing to ensure they meet natural and international standards.

Weld joints are covered with a protective coating to prevent corrosion and protect against impacts that can occur when lowering in. Approximately one kilometer of line pipe is lowered into the trenches with the help of side boom tractors as shown in Figure 3. A tie-in welding is carried out to joint two lowered-in pipe strings together. Then fine soil is placed around the pipe in the trench to act as padding. After padding the original topsoil is backfilled. Water is pumped to a higher pressure than the operating gas pressure to further verify integrity of the pipeline by hydrostatic testing. The path of the pipeline is restored to its original state as much as possible. Safety measures like marker posts are used to warn of the location of the buried pipeline.

Aforementioned constructed phases are subjected to strict supervision with audits from third parties and internal quality assurance units. All inspections are carried out in accordance with the technical specifications of the project. Projects have unique technical manuals based on the requirement and location of the projects. Commonly technical specifications widely follow API 1104 standard [1].

*Figure 3. Pipe lowering process applied by side boom tractors [12]*

American Petroleum Institute has issued codes for welding and testing of pipelines in API 1104 [1]. The standard comprehend guidelines for various weld methods such as shielded metal arc welding, submerged arc welding, gas tungsten arc welding, gas metal arc welding, flux-cored arc welding, plasma arc welding, oxyacetylene welding used in not only pipelines but also in the compression and pumping facilities. It designates acceptance criteria for weld and related tests. Acceptance standards are given based on both empirical criteria for workmanship and engineering critical assessment criteria determined by fracture mechanics analysis.

One of the biggest challenges for pipeline construction is off-shore construction. Vast distances under seas or lakes have to be passed in the quest of transmitting the gas to end-users. There are three methods used for off-shore construction which are J-laying, S-laying and reeling [13]. Basic schematics of those methods are presented in Figure 4.

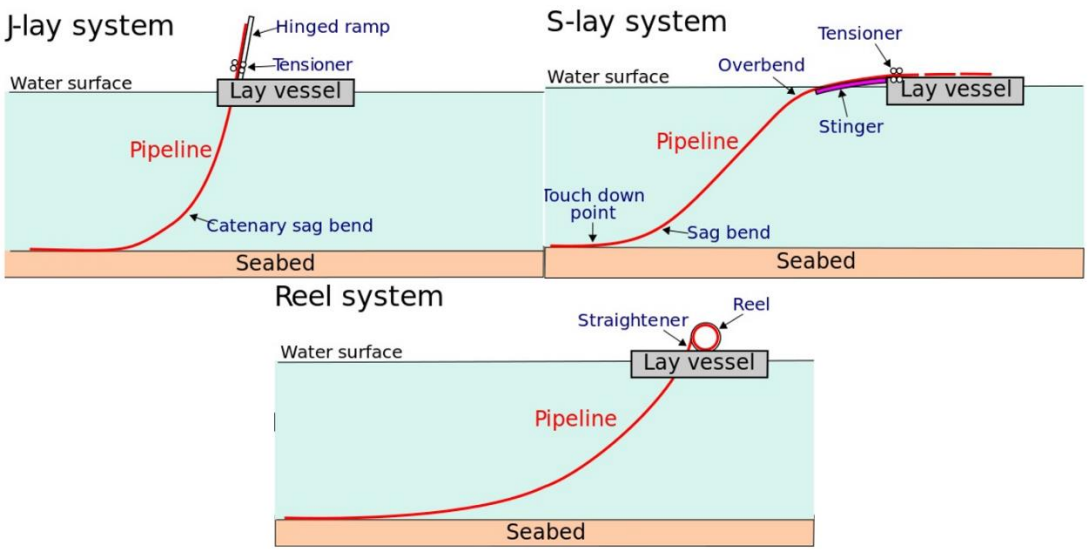


*Figure 4. Basic schematics of off-shore pipeline construction methods*

Compared to the onshore construction, independently from the chosen method off-shore constructing is quite troublesome because of occurrence of high loads and nominal plastic strains during the laying process. Norwegian standard of DNVGL-ST-F101 for off-shore constructing is followed worldwide [2]. Det Norske Veritas

provides guidance and requirements to concept development, design, construction operation and abandonment of submarine pipeline systems. The effects of off-shore constructing to the structural integrity is further investigated in section 2.5.

### 2.2.1 Parent Metal

As one of the highest demanded steels for main line pipes, API 5L X70M PS2 has increasingly produced since its invention in 1974 [14]. Even though new and higher strength HSLA's are available it is highly used in recent massive projects such as Trans Anatolian Pipeline Project (TANAP) because of its cost-benefit ratio compared to other steels.

5L is the coding of API for line pipes suitable for oil and gas transsmission. X followed by two or three integer represents the minimum yield strength of the material in ksi. PSL 2 stands for the mandatory mininmum and maximum values for notch toughness and carbon equivalent properties while PS1 defines only the minimum values of yield and tensile strength.

Mechanical properties of X70M makes it a viable option for both offshore and onshore construction. The line pipe steel has 485 to 635 MPa yield strength and 570 to 760 MPa tensile strength with a minimum elongation of 17% [4]. The chemical composition and carbon equivalent limits are tabulated in Table 2 [4]. Fraction of micro alloying elements may vary as long as the steel meets with the mechanical requirements. Regardless of their fraction, those elements increase the strength of the steel drastically. Thermo-mechanically controled process (TMCP) and alloying element combinitons are resulted with bainitic or acicular ferrite, granular bainitic ferrite, polygonal ferrite and quasi-poligonal ferrite or massive ferrite microstructures [15, 16].

*Table 2 Chemical composition constraints of API 5L X70M grade line pipe steels [4]*

| | Mass Fraction (% maximum) | | | | | | | Carbon Equivalent (% maximum) | |
|---|---|---|---|---|---|---|---|---|---|
| | **C** | **Si** | **Mn** | **P** | **S** | **V+Nb+Ti** | **Other*** | **$CE_{IIW}$** | **$CE_{Pcm}$** |
| X70M | 0.12 | 0.45 | 1.70 | 0.025 | 0.015 | 0.15 | | 0.43 | 0.25 |

* Cu, Ni, Cr and Mo ≤ 0.50%; B ≤ 0.001 %

2.3 Girth welding of line pipes

Arc welding is a fusion process for joining metals. Applying high amount of heat in a relatively small region between two parts melting and causing a joining. This high energy needed to melt metal is produced by an electrical arc in arc welding. A schematization of arc welding is presented in Figure 5. Arc is created across the gap between the electrode and the work piece producing a molten metal pool. This pool is vulnerable to oxides and nitrides caused by the contact with air that damage the strength and toughness of the weld joint. Thus, a protective shielding is created by gas or electrode coating that protects the pool.

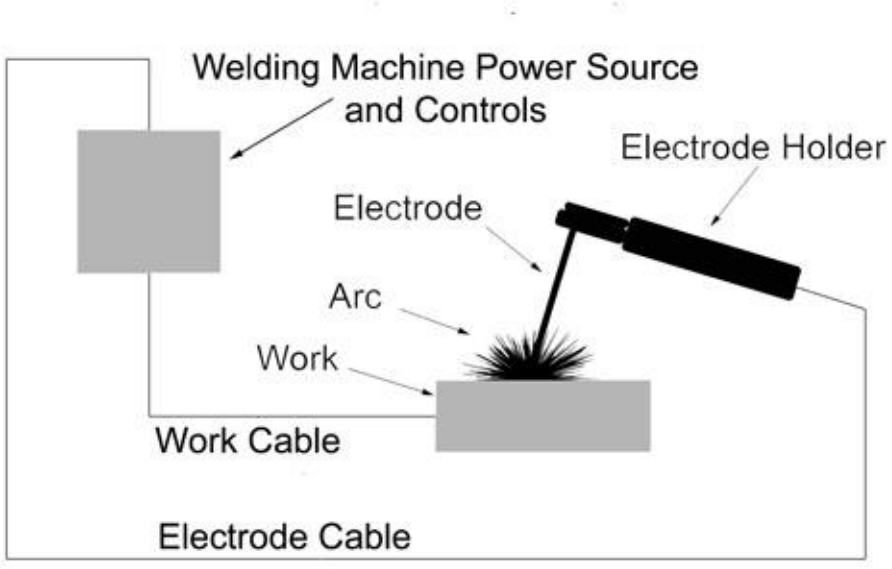


*Figure 5. Schematic view of arc welding*

Girth welding is performed by arc welding techniques. Mainline pipes are jointed automatically with GMAW and semi-automatic gas-shielded FCAW and MCAW methods or manual GTAW and SMAW methods are used for tie-ins.

GMAW is an arc welding process that uses the heat of an electric arc established between a consumable metal electrode and the part to be welded. The electrode is a bare metal wire fed by a mechanism across the arc and into the molten weld pool. The schematic view of the weld method is presented in Figure 6. GMAW is a versatile method when the electrode is flux cored it is called FCAW and if it is metal cored it is called MCAW.

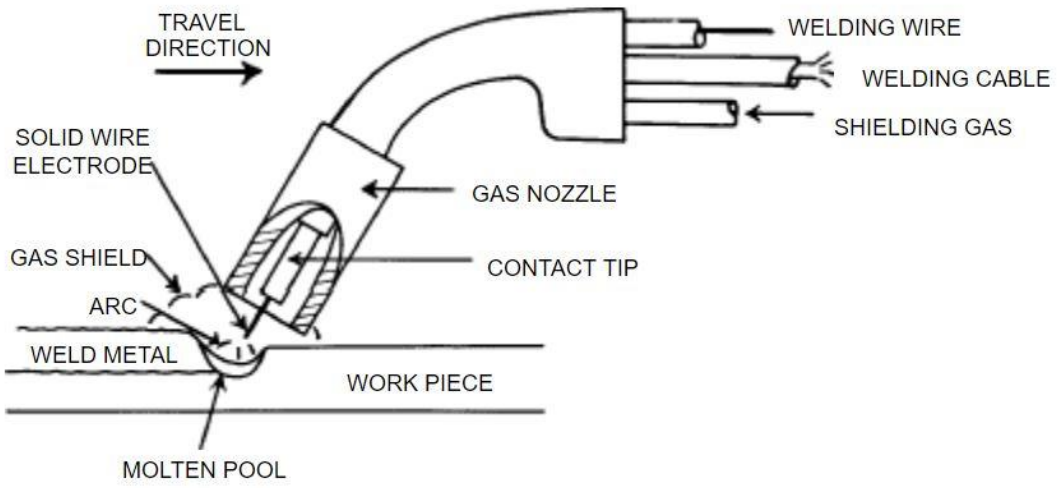


*Figure 6. Schematic view of the GMAW process*

GTAW is a manual welding process. The arc is established between work piece and non-consumable tungsten electrode. An inert gas is released by the nozzle of the torch to protect the weld metal. Use of filler metal is optional. If it is added it melts between the electrode and work piece. GTAW requires highest skill from a welder and it is the most time consuming weld application. Therefore, it is usually used only for root passes and sometimes second pass which is called hot pass. The schematic view of the weld method is presented in Figure 7.

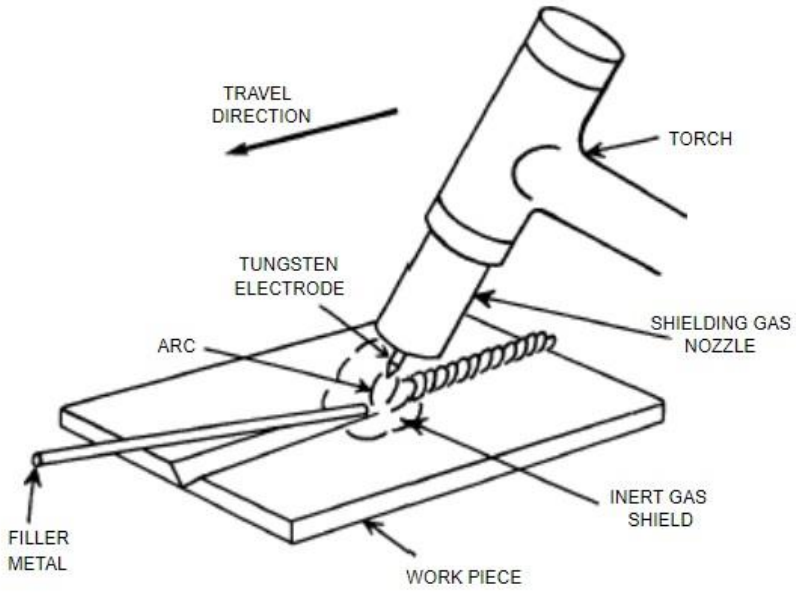


*Figure 7. Schematic view of the GTAW process*

SMAW is a manual metal arc welding widely used for various arc welding processes because of its compact and adaptable design. Welding is performed with the heat of an electric arc that is maintained between the end of a coated metal electrode and the work piece. The coat protects the molten metal from air and increases its properties by alloying it. During solidification slag forms on the molten metal. Slag is removed before starting the next pass. The schematic view of the weld method is presented in Figure 8.

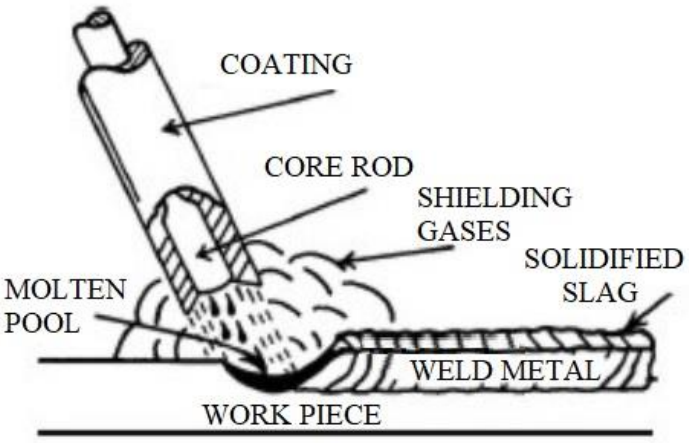


*Figure 8. Schematic view of the SMAW process*

There are many weld parameters such as weld metal type, shielding gas type, welding speed, etc. One of the most important parameters regardless of the chosen method is heat input. Heat input is the energy supplied to the work piece in the welding process. HI is calculated from equation 1.

$$HI = \eta \times AE \quad (1)$$

η is the arc heat transfer efficiency coefficient (or thermal efficiency) and values of η are tabulated with respect weld methods in Table 3. AE is the Arc Energy and calculated from the equation 2.

$$AE = \frac{60VI}{1000v} \quad (2)$$

where V is the voltage used, in volts, I is the current used, in amperes and v is the travel speed of the welding torch, in mm per minute.

*Table 3. Heat transfer efficiency coefficient if different weld processes*

| **Process** | **Efficiency factor (η)** |
|---|---|
| Submerged arc welding (SAW) | 1.0 |
| Shielded metal arc welding (SMAW) | 0.8 |
| Flux cored arc welding (FCAW) | 0.8 |
| Gas Metal Arc Welding (GMAW) | 0.8 |
| Gas tungsten arc welding (GTAW) | 0.6 |
| Plasma arc welding | 0.6 |

## 2.4 Weldability of HSLA steels

Constructing a homogeneous pipeline by joining steels with any of the weld methods described in section 2.3 is an impossible task. Welding processes may introduce discontinuities to the material. Aside from weld related discontinuities the original

mechanical and microstructural properties are suffer a change. HSLA steels are subjected to complex thermal process cycles during the rolling and production [17]. That makes the welding even more challenging since the high heat input resulting in a growth on grain size. All welding processes result in a heat-affected zone (HAZ). HAZ is a band like region along with the fusion line between weld metal and parent metal. Macro examination of a cross weld section is presented in Figure 9. HAZ does not melt during the welding but undergoes microstructural changes.

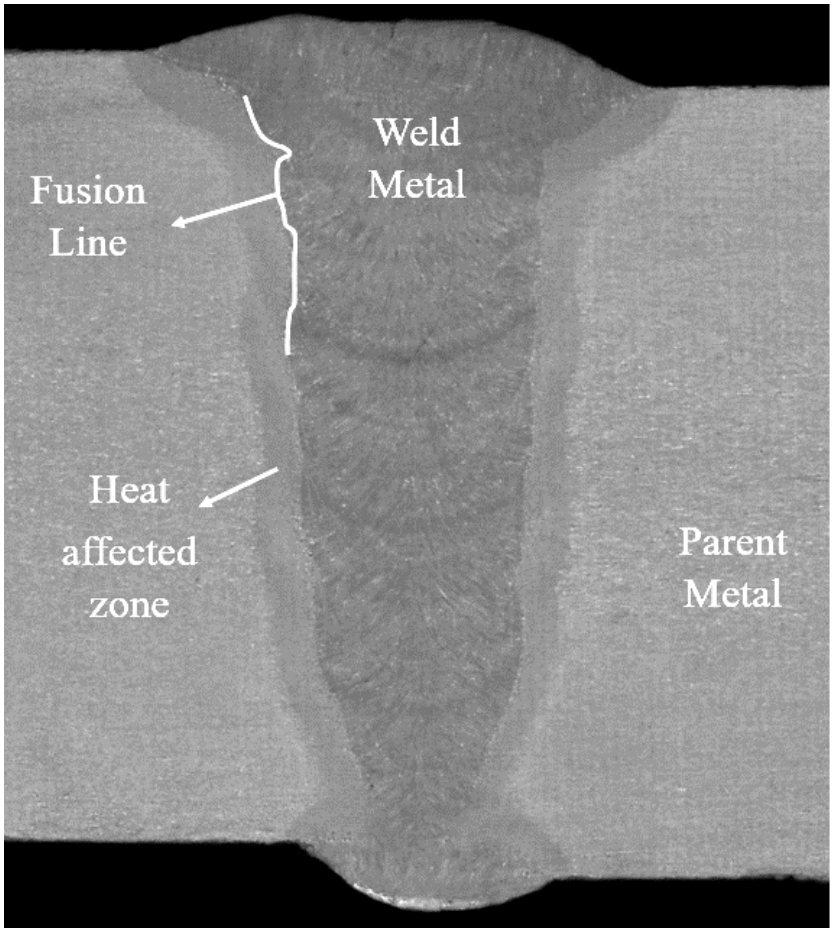


*Figure 9. Macro section of a weldment.*

The properties of HAZ play a significant role in deciding the performance of welding joint [18]. Welding process is usually followed by strength mismatches between weld metal, HAZ and parent metal.

The number of the passes needed to complete the joining of plates depends on the weld method and material thickness. HSLA steels used as line pipes are joined with multiple passes because decreasing the number of passes also means increasing the heat input. Higher heat inputs decrease weld pool viscosity and can cause weld metal dropping in welding position used in pipeline joining. The positions are defined with similar reasoning with a different designation in ISO 15614-1 [19], ASME SEC. IX [20] and AWS D1.1 [21]. 5G position according to ASME and AWS or PH according to ISO is used for pipeline welding which is shown in Figure 10 schematically.

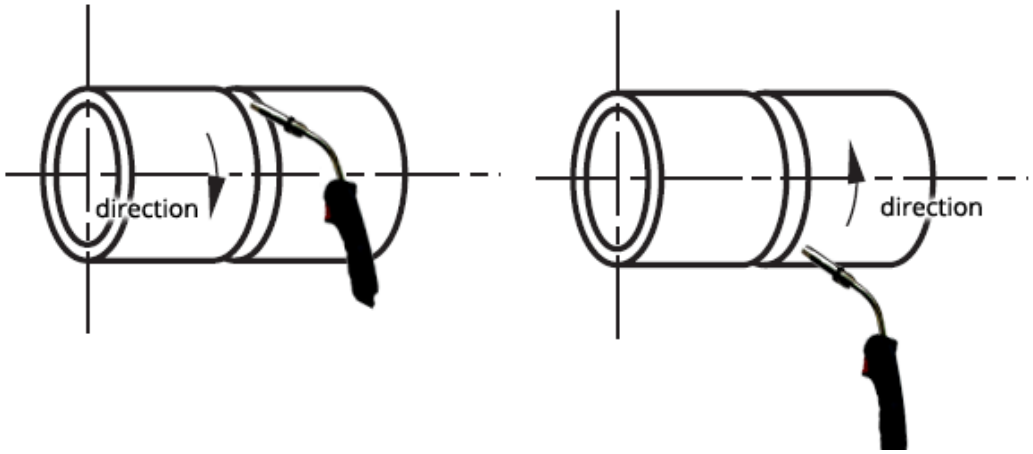


*Figure 10.. PH / 5G position with downhill and uphill direction.*

Even though it is actively used on line pipes, multi-pass welding has its own drawbacks. Severe effects of re-heated HAZ regions of first pass is reported by Celin et al. [22]. Sub-regions of HAZ are presented in Figure 11.

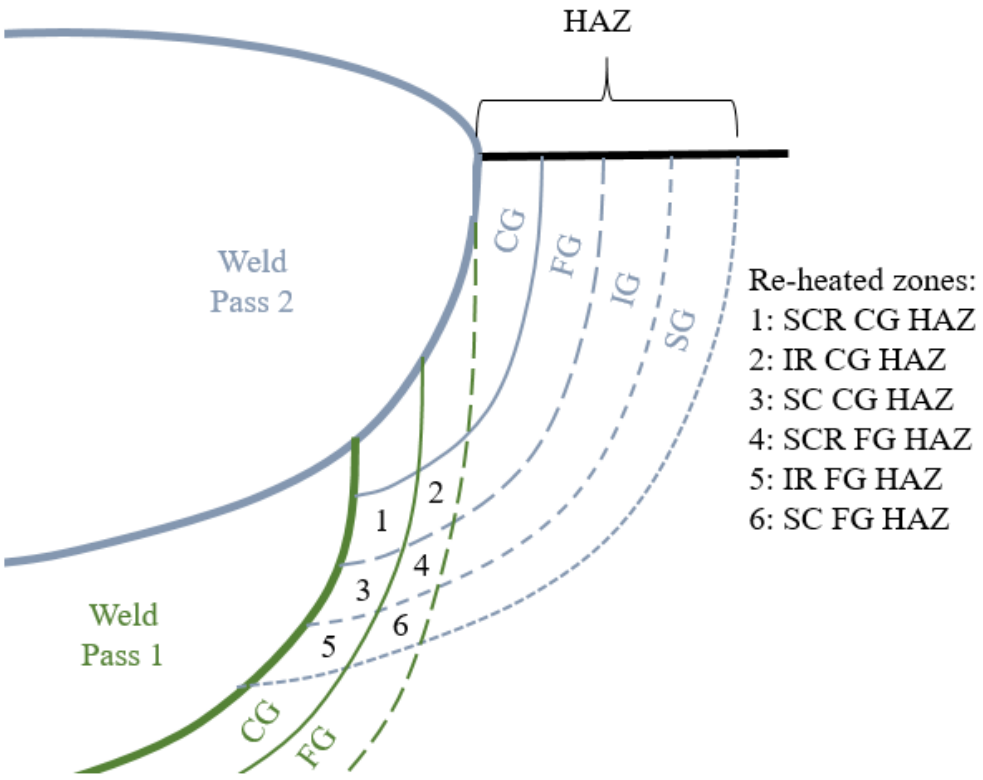


*Figure 11. Sub-regions of HAZ.*

The sub-regions are named by the relations with the phase-transition temperatures of the material ($A_{C1}$ and $A_{C3}$) $A_{C3}$ and 1300 °C.
CGHAZ occurs when the temperature of region reaches above 1300 °C,
FGHAZ occurs when the temperature of the region is between 1300 °C and $A_{C3}$,
ICHAZ occurs when the temperature of the region is between $A_{C3}$ and $A_{C1}$,
SCHAZ occurs when the temperature of the region is lower than $A_{C1}$.

A micro examination photo of transition from weld metal to parent metal is presented in Figure 12.

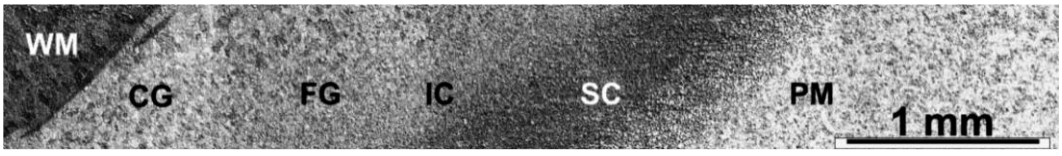


*Figure 12. Transition from weld metal to parent metal [22].*

Worst fracture resistance and highest DBTT is observed in CGHAZ of girth welds of HSLA steels [23]. Higher size of the HAZ region extends the negative mechanical effects [24]. The main reason of this metallurgical deterioration in the HAZ is the change of original microstructure mentioned in 2.2.1 to other ferritic and austenitic phases due to thermal cycles of welding. Local brittle zones (LBZs) in multi-pass welding occur in inter-critically reheated coarse grain heat affected zone (IRCGHAZ) as a result of this transformation [25].

Parameters such as thermal cycles, cooling rates, number of weld passes and heat inputs indirectly affect the size and distribution of LBZ [18]. However, low heat input brings weld related flaws like lack of fusion or incomplete penetration which are as dangerous to structural integrity as the microstructural adverse change in HAZ. Lack of fusion occurs when the weld filler metal fails to properly fuse with the base metal. Incomplete penetration is a condition when the weld metal does not properly penetrate the weld joint through weld direction. One of the most common imperfection is porosity which can be caused by insufficient inert gas shielding.

All those dangers are addressed by a good workmanship and right weld parameters. Both of those requires experience and strict supervision. As a result, a recipe for carrying out a particular weld occurs, which is called the welding procedure.

## 2.5 Structural integrity

Structures are expected to retain its strength, function and form under service conditions such as different stresses and corrosive environmental effects. Structural integrity is the ability of the structure to operate through a designated life span [26]. Effective inspection, analysis and risk management ensure engineered structures remain safe and productive. A structural integrity assessment is fundamental to provide limitations for design and prevent any kind of catastrophic failure.

In pipelines this assessment is called Engineering Critical Assessment (ECA) or in other words Fitness-For-Service (FFS) assessment. The welding processes are a rate

limiting step in pipeline construction [27]. Most welding fabrication codes are based on “good workmanship” criteria which is over conservative. Nevertheless, limitations of this criteria successfully specify maximum tolerable flaw sizes and minimum tolerable Charpy energy to sustain structural integrity.

“Good workmanship” criteria preserve its importance for manual welding operations where the quality threshold hast to be high since the skill of the welder is an important parameter. However, more than 80% of the girth welds are performed automatically or semi-automatically at the present time. Automatic applications enable weld parameters to remain in a very limited range which contributes to metallurgical and mechanical results to be consistent. As a result, ECA based on fracture mechanics principles to determine the defect tolerance for safety of the structure is emerged. ECA is a more realistic and mostly less conservative assessment since it is accurately measures material toughness with modern fracture mechanics parameters obtained from both computer aided finite element analysis and testing of specimens.

Modern standards such as BS 7910 present extensive evaluation methods for a standardized ECA and limit fracture toughness parameters [28]. A visual presentation of requirements for an ECA in accordance with BS 7910 is presented in Figure 13. Stresses acting on the region containing the flaw, size, orientation to the weld and position of the flaw and tensile and toughness properties of the related region is required to carry out an ECA.

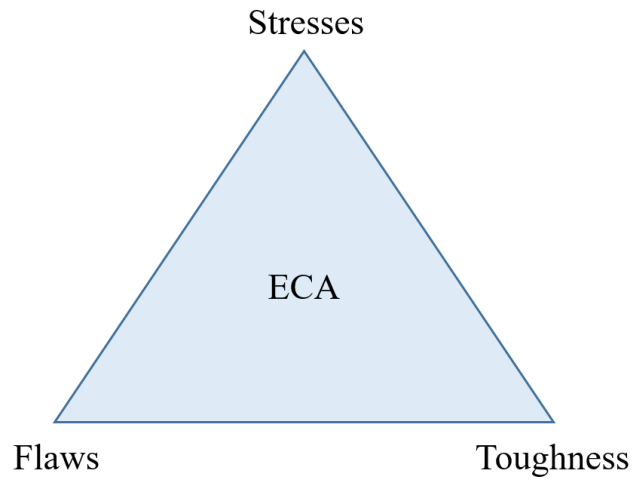


*Figure 13. Parameters required for an ECA*

One of the most vital models that structural integrity assessment built around is weak link model. This model is an assumption that inhomogeneous components contain randomly distributed small regions of low toughness [29]. Once a crack front close enough to nearest weak, stress concentration shifts into the weak link guiding crack front to the link. Crack propagates rapidly and the component "fails" because of a chain reaction connecting weak links. Weak link is referred to as LBZ in weldments. IRCGHAZ region neighboring the fusion line is a potential host for LBZ with lower toughness [30]. Consequently, a fracture toughness analysis targeting that specific region is required.

## 2.6 Fracture mechanics

Fracture toughness is the resistance of material under stress to crack extension [31]. Measurement of fracture toughness by standardized parameters plays an imperative role in engineering applications of fracture mechanics to structural integrity assessment. Stress intensity factor (K) is the first parameter widely accepted and it defines the stress intensity of elastic crack-tip fronts in Linear Elastic Fracture Mechanics (LEFM) where a linear crack growth without any plastic resistance is expected [32]. LEFM is inadequate in realistic assessments of linepipe steels where a higher resistance to fracture is obtained by the plastic region occurs on crack tip. Crack

Tip Opening Displacement (CTOD) is an Elastic-Plastic Fracture Mechanics (EPFM) parameter proposed in 1963 to serve as an engineering parameter [33]. CTOD occurrence after a force applied to a specimen with crack is shown in Figure 14. The J-integral is introduced in 1968 and widely accepted as a measure of the crack driving force and measures the energy release associated with crack growth or tearing [34]. CTOD is commonly used in United Kingdom since it is developed in there, on the other hand, J was originally developed in the United States of America and more common to use in there [27].

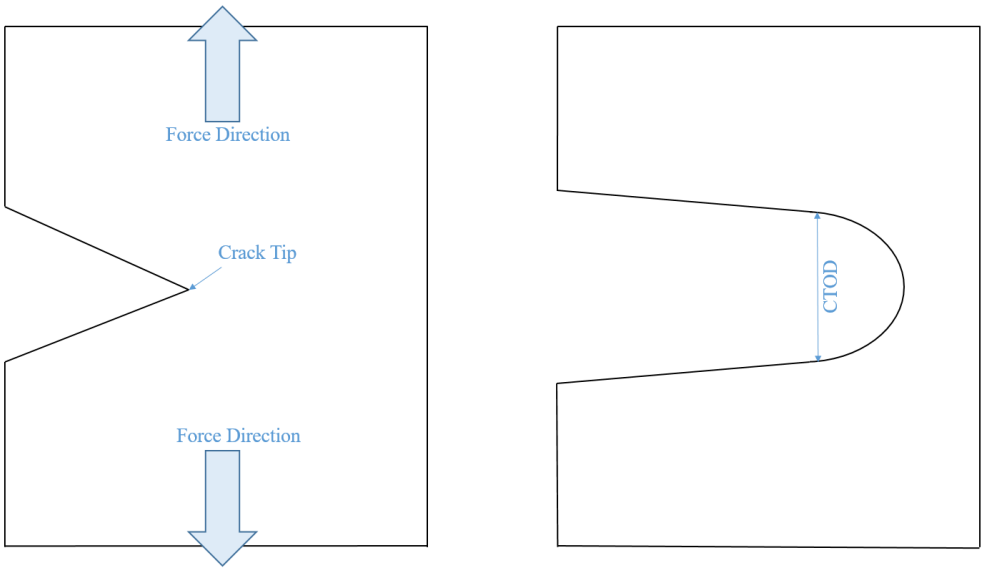


*Figure 14. CTOD occurance after a force applied to specimen with a crack*

Standards such as ASTM E1820 [35], ISO 12135 [36], DNVGL-RP-F108 [37] and BS 8571 [38] offer specimen preparation guidance, testing procedures, validity evaluations, calculations for fracture toughness parameters and conversion formulas between the parameters. Testing procedures has an extended range of variety from different loading types to different conditioning methods which grants different assessments to be carried out. This diversity is further discussed in experimental chapter.

# CHAPTER 3

# EXPERIMENTAL

## 3.1 Methodology

This chapter begins with the introduction to the properties of parent and filler metals with respect to international standards. Next, the welding procedures used to achieve seamless joining is presented. It is followed by the integrity confirmation and characterization which contains inspection and testing methods to qualify the structure by examining most vulnerable section with both destructive and non-destructive tests. Then, post-test metallography and fractography is addressed to scrutinize the validity of crucial fracture toughness testing. The last section describes R curve generation to further examine the main focus of the thesis.

Experimental investigations on different material zones are tabulated with respect to reference standards in Table 4.

## 3.2 Parent and filler metals

24.01 mm thick API X70 grade line pipe steel was the parent metal. The parent metal was a pipe with 48” outside diameter and delivered in the as-welded condition. Pipe 1 steel number was 15418169, and pipe number was BAO051011. Pipe 2 steel number was 15418186, and pipe number was BAO051018. Both steels were manufactured by Baowu Steel Group, China which is one of the biggest steel producers in the world in terms of production rates.

*Table 4. Experimental investigations on different material zones with respect to reference standards.*

| | Specimen Designation | Standards | PM | HAZ | WM |
|---|---|---|---|---|---|
| Elemental constituents | SP | ASTM E 415 | | | |
| Integrity Confirmation | MT | ISO 17638 & ISO 23279 | | | |
| | RT | ASTM E1742, ASTM E2007 & ASME BPV Code | | | |
| | XL | ISO 17639 | | | |
| | XN | ISO 5173 | | | |
| | A (CWT) | API 1104 | | | |
| Microstructural constituents | OM | ASTM E112 | | | |
| | SEM | | | | |
| Hardness (Vickers) | M3 (HV10) | ISO 6507 | | | |
| | M3 (HV0.5) | ASTM E 384 | | | |
| Strength and Ductility | AA, AB | ISO 6892-1 | | | |
| Fracture Toughness | N | ASTM E23 | | | |
| | PC (CTOD) | ISO 12135 & ISO 15653 | | | |
| | PJ (J-R curve) | ISO 12135 & DNVGL-RP-F108 | | | |

The parent metal was confirmed to be API 5L Grade X70M PSL2 grade by the qualification report BGSAR1512230000400 of the supplier. The chemical composition of both steel numbers are presented in Table 5. The metals were joined by Longitudinally Submerged Arc Welding (LSAW) method. Macro section of the weld intersection is presented in Figure 15.

*Table 5. The chemical compositions of steels as presented in the qualification report.*

| Steel No | Weight fraction (%) | | | | | | | | | | |
|---|---|---|---|---|---|---|---|---|---|---|---|
| | C | Mn | Si | Ni | Cr | Ti | Mo | V | P | Cu | S |
| 15418169 | 0.05 | 1.76 | 0.24 | 0.19 | 0.24 | 0.015 | 0.14 | <0.01 | 0.007 | 0.01 | 0.002 |
| 15418186 | 0.05 | 1.75 | 0.25 | 0.20 | 0.24 | 0.015 | 0.14 | <0.01 | 0.006 | 0.01 | <0.001 |

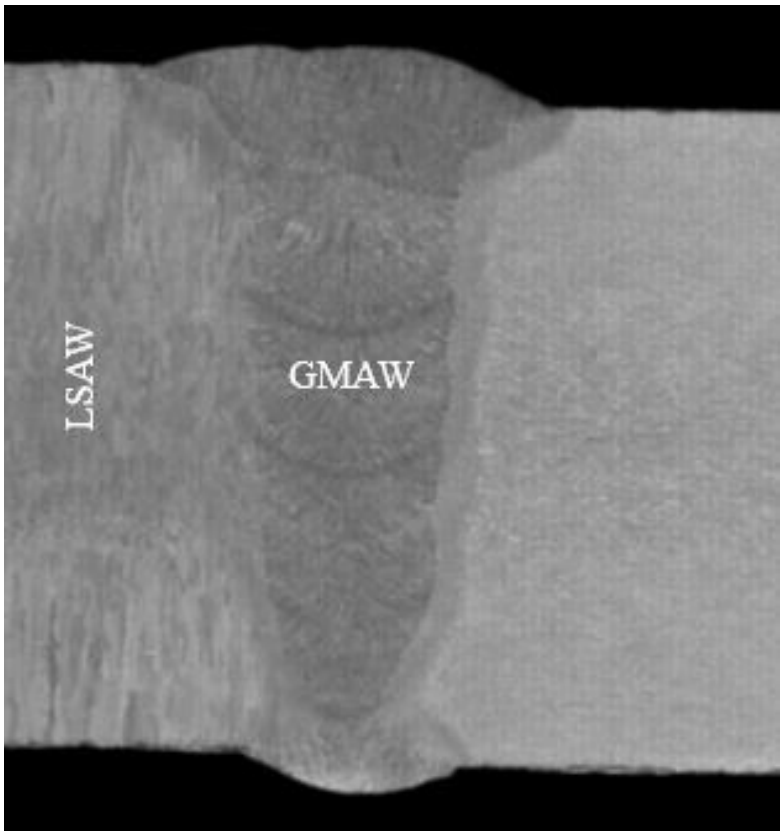


*Figure 15. Macro section of weld intersection.*

The pipe was sectioned, and characterized by employing optical emission spectral analyses for elemental constituents and carrying out tensile test for mechanical properties. The parent metal found to be consistent with the material certificate as per EN 10204 type 3.1 and API 5L [4].

Filler metal was SFA 5.18 ER70S-6 with 0.9 mm diameter for the root pass and supplied by Lincoln Electric Co. which is a multinational manufacturer of welding products and its heat number was 101901. SFA 5.28 ER80S-Ni1 with 1 mm diameter was used for all other passes from hot to cap and supplied by Voest Alpine Bohler

which is also a global manufacturer of welding consumables and its heat number was 1293Z. Both filler metals were introduced during GMAW operations. The chemical compositions of the wires and the filler metal under M21 shielding gas combination (5% to 25% $CO_2$ and balance Argon) and mechanical properties of the as-welded filler metal are tabulated in Table 6 and Table 7, respectively as presented in their certificates.

*Table 6. The chemical compositions of the wire and as-welded filler metal with M21 shielding gas.*

| | | Weight fraction (%) | | | | | | | | | | |
|---|---|---|---|---|---|---|---|---|---|---|---|---|
| | | C | Mn | Si | Ni | Cr | Ti | Mo | V | P | Cu | S |
| Wire | ER70S-6 | 0.08 | 1.47 | 0.83 | 0.02 | 0.02 | <0.001 | <0.001 | <0.01 | 0.006 | 0.19 | 0.007 |
| | ER80S-Ni1 | 0.06 | 1.49 | 0.64 | 0.92 | 0.03 | 0.07 | <0.01 | 0.01 | 0.009 | 0.08 | 0.008 |
| As-welded filler metal | ER70S-6 | 0.09 | 1.26 | 0.77 | 0.01 | 0.02 | <0.001 | <0.001 | <0.01 | 0.006 | 0.19 | 0.007 |
| | ER80S-Ni1 | 0.07 | 1.29 | 0.58 | 0.88 | 0.02 | 0.04 | <0.01 | <0.01 | 0.008 | 0.08 | 0.008 |

*Table 7. Mechanical properties of as-welded filler metal with M21 gas combination.*

| | ER70S-6 | ER80S-Ni1 |
|---|---|---|
| $R_{p0.2}$ (MPa) | 590 | 576 |
| $R_m$ (MPa) | 670 | 644 |
| Elongation (%) | 24 | 25.5 |
| Charpy V notch (J) at RT | 170 | - |
| Charpy V notch (J) at -50 °C | 90 | - |
| Charpy V notch (J) at -20 °C | - | 173 |
| Charpy V notch (J) at -40 °C | - | 129 |

3.3 Welding parameters and integrity of the joint

The pipes were aligned and clamped with pneumatic internal line-up clamp "re-rounder type" by Internal Welding Machine. After clamping, the roots of bevels were joined automatically by Internal Welding Machine. Bevel design and pass sequence are presented in Figure 16. All other passes were completed by P-625 mechanized welding machine. Welding is completed in horizontal fixed position. Both welding machines used in jointing were CRC-Evans products.

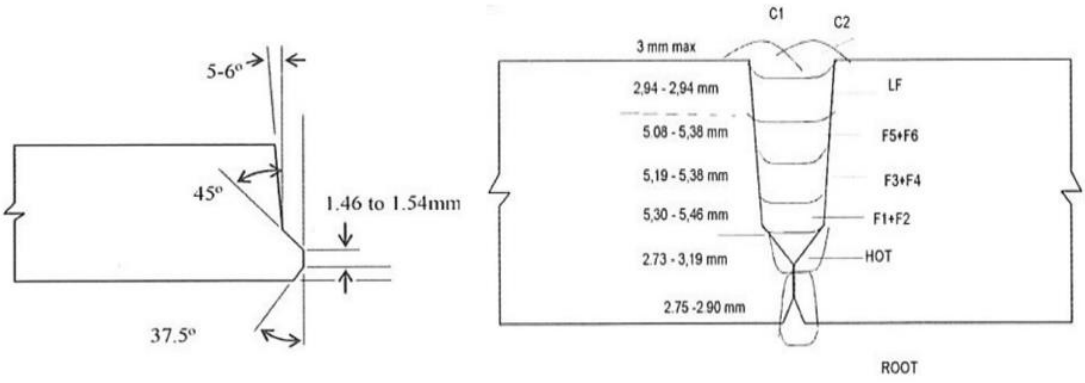


*Figure 16. Bevel design and pass sequence.*

Root welding was carried out by low voltage short circuiting GMAW [39] and from hot pass to cap passes high frequency pulsed GMAW was operated [40]. The shielding gases were applied during GMAW operations to protect the weld pool from atmospheric contamination. The shielding gas mixture was Argon-20% $CO_2$.

Heat input, voltage, amperage and torch travel speed with respect to the passes are tabulated in Table 8. Pre-heating was applied to control cooling rates since the heat input was relatively low due to small filler metal diameter. Pre-heat temperature obtained by induction coils was 152°C and interpass temperature was set to below 205°C. The temperatures measured at a distance ≥ 75 mm from the toe on both sides of bevel by digital contact thermometer.

*Table 8. Heat Input, voltage, amperage and torch travel speed per pass.*

| Passes | Root | Hot | F1-F6 | LF | C1-C2 |
|---|---|---|---|---|---|
| Welding Unit | IWM | P625 | | | |
| Heat Input (Kj/mm) | 0.34 | 0.35 | 0.59 | 0.67 | 0.46 |
| Voltage (Volts) | 19.2 | 24.7 | 22.9 | 23.2 | 23.5 |
| Amperage (ampers) | 183-236 | 259-305 | 163-244 | 146-244 | 119-147 |
| Travel Speed (mm/min) | 691-716 | 1137-1222 | 401-511 | 366-488 | 353-488 |

Test and validation methods of API 1104 were utilized for integrity assessments and procedure qualifications of the weldments since it is an on-shore mainline joining procedure. Before sectioning for specimen extraction the integrity of the joint is validated by VT, MT, RT and AUT. A representative radiographic image of the coupon is presented in Figure 17.

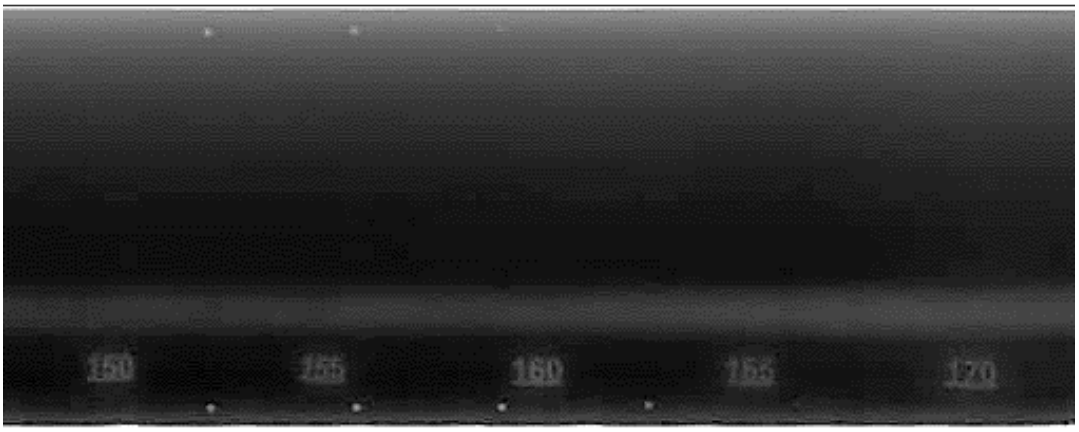


*Figure 17. Radiogrpahic image of the coupon.*

The number of test specimens dictated by the related section of the standards are given in Table 9. Welded joint is divided to 8 arcs and specimens are sectioned from those arcs. Cut plan of the arcs and specimen designation with respect to position is presented in Figure 18. The location and quantity of the specimens and the dimensional tolerances were taken from the related reference section of API 1104. The specimens were extracted from different positions to represent the whole circumference since welding parameters vary with respect to the position as explained in section 2.4.

Different heat inputs in different welding directions might influence the mechanical properties of welded joint in some positions.

*Table 9. Number of specimens tested according to API 1104*

| Testing Method | # of Specimens | Related Section in API 1104 |
|---|---|---|
| Cross-weld Tensile Test | 4 | 5.6.2 |
| Bend Test | 8 | 5.6.5 |
| Macro-section Examination | 3 | 10.3.7.2 |
| Hardness Test | 3 | 10.3.7.3 |

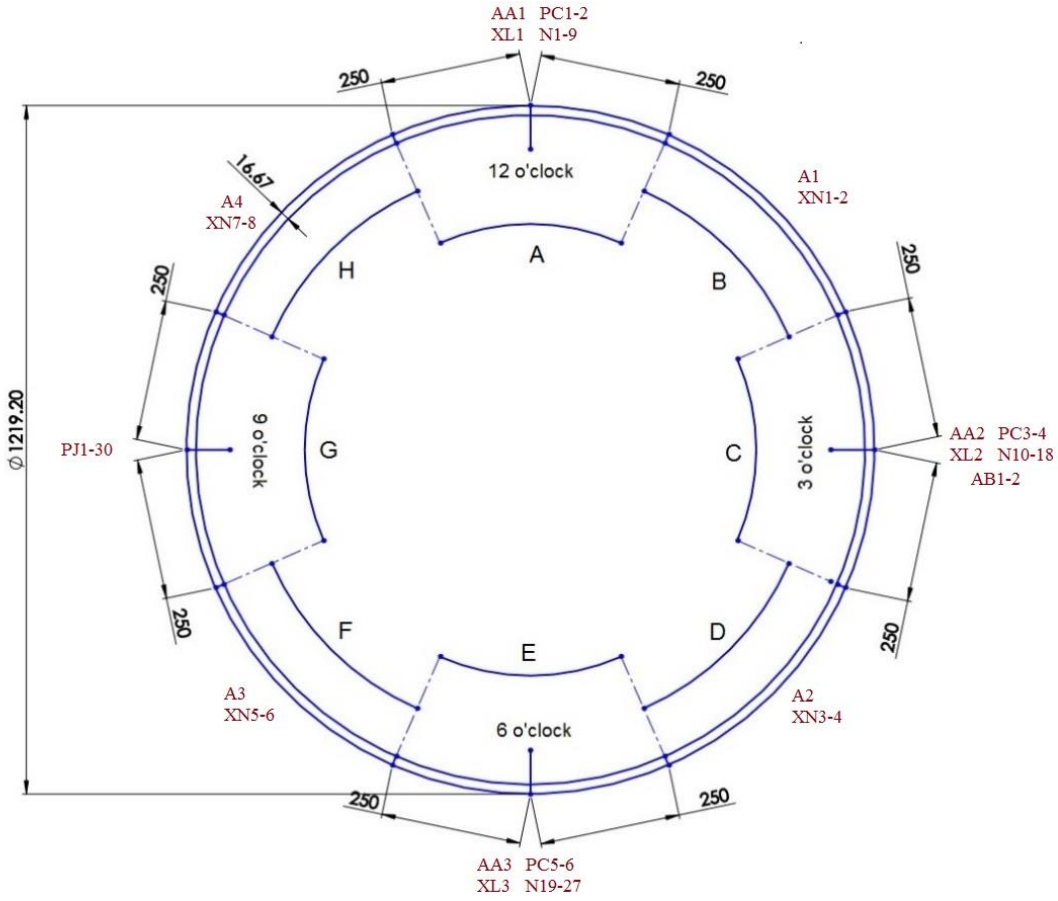


*Figure 18. Pipe sectioning to 8 arcs and specimen designation with respect to the position.*

Cross weld tensile testing was conducted to determine weld related imperfections that can cause the fracture and overmatch between weld metal and base metal. Test

specimens were of rectangular cross section with reduced width at the mid-length as shown in Figure 19. The specimens were extracted from Arc B, D, F and H and prepared in accordance with the requirements of API 1104 [1]. The weld reinforcement was removed. Ultimate tensile stress was determined and fracture location as recorded.

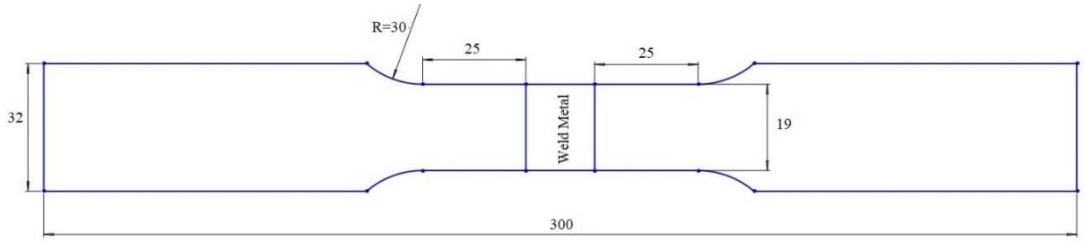


*Figure 19. Top view of transverse (cross weld) tensile test specimen.*

Bend tests were carried out to ensure the soundness of the joints in accordance with ISO 5173 [41] as its referenced in API 1104 [1]. Side bend specimens were 300 mm long and 13 mm in width. The long edges were rounded and sides were smooth and parallel. The cap and root bead reinforcements were removed. Diameter of the plunger and span length were 90 mm and 120 mm, respectively. Specimen and test setup dimensions are shown in Figure 20. The specimens were extracted from Arc B, D, F and H.

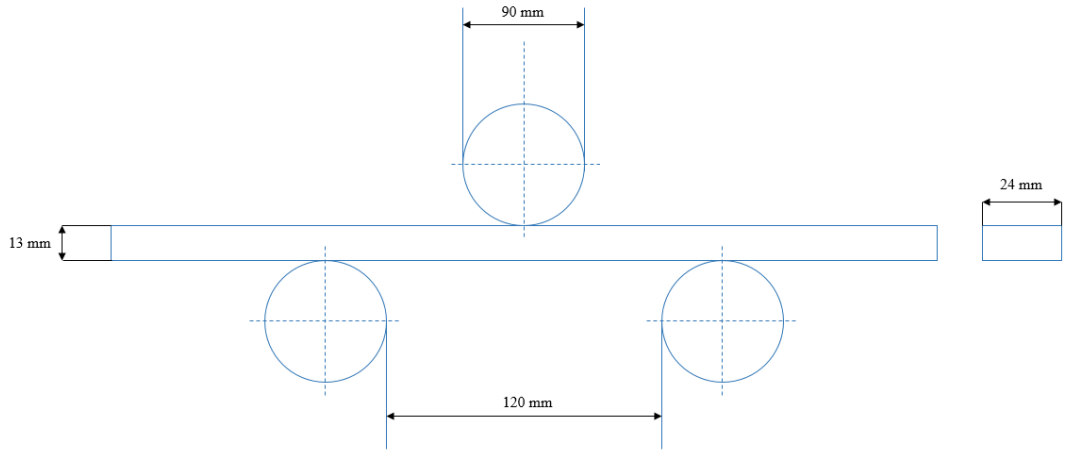


*Figure 20. Bend specimen and test setup.*

Weld transverse macro examination specimens were sectioned properly from Arc A, C and E for visual examination of the fusion zone and base metal. The weld transverse macro-section specimens were 15 mm-thick. The specimens were saw cut and machined down to the specified thickness. One face of each specimen was ground and polished to at least 600 grit finish, and then, etched with Nital (10% nitric acid + ethyl alcohol) per ISO/TR 16060 to reveal weld macro structure [42].

All three cross sectional macro examination specimens were subjected to HV10 hardness test in accordance with ISO 6507 [43]. Location of Vickers hardness indentations were shown in Figure 21. 10 kg-force is applied for 10 seconds per indentations.

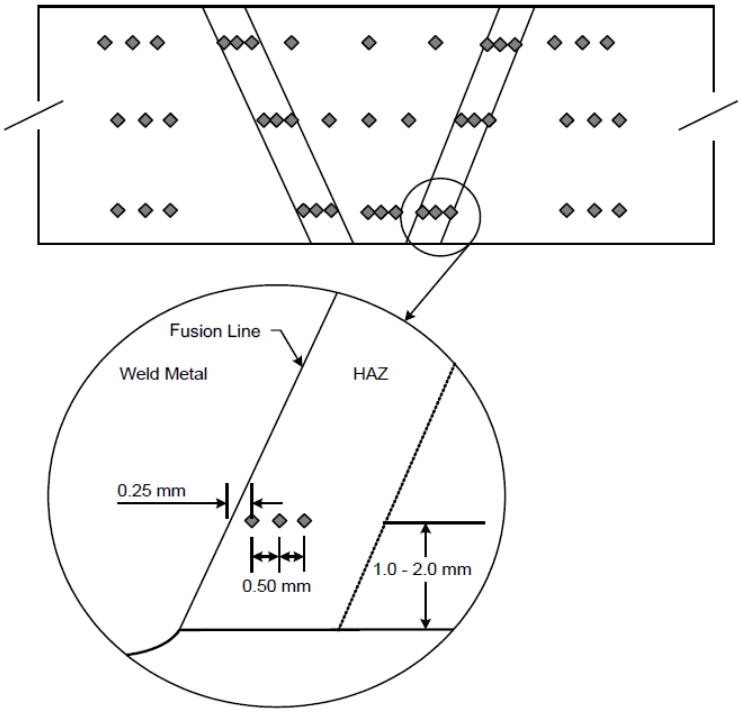


*Figure 21. Locations of Vickers hardness indentations.*

## 3.4 Mechanical characterization

Integrity confirmation was followed by the tests tabulated in Table 10 in accordance with Annex A of API 1104 [1]. Annex A presents alternative acceptance criteria that

employs fracture toughness mechanics and ECA to determine the minimum tolerable flaws less conservative than workmanship criteria. ECA and workmanship was previously explained in section 2.5.

*Table 10. Number of specimens tested according to Annex A of API 1104.*

| **Testing Method** | **# of Specimens** | **Related Section in API 1104** |
|---|---|---|
| Charpy Impact Test (-10 °C) | 27 | A.3.4.2 |
| Fracture Toughness Test (-10 °C) | 6 | A.3.4.3 |
| All Weld Tensile Test | 4 | A.3.4.3 (prerequisite of fracture toughness test) |
| Base Metal Tensile Test | 2 | A.3.4.3 (prerequisite of fracture toughness test) |

Tensile strength and ductility parameters were determined by all-weld tensile test at room temperature (23°C ± 5°C). The testing procedure and specimen geometry conforms to ISO 6892-1 [44]. The test specimens were of circumferential cross section with reduced width at the mid-length and were extracted from Arc A, C and E. Base metal tensile specimens were also prepared with same dimensions and orientation from neighboring regions of specimen AA2 and named AB1 and AB2. A basic drawing of the specimen is given in Figure 22. Diameter of reduced section (d) was 6 mm and gauge distance ($L_o$) was calculated from the following equation:

$$L_o = 5.65\ (\frac{\pi d^2}{4})^{1/2} \quad (3)$$

Maximum crosshead test speed was calculated from the maximum strain rate ($\dot{e}_{L_c}$) given by standard as 0,00025 $s^{-1}$ multiplyed by the paralel length. The specimens were tested with a speed of 0.6 mm/min up to yield point, and then, with a speed of 5 mm/min.

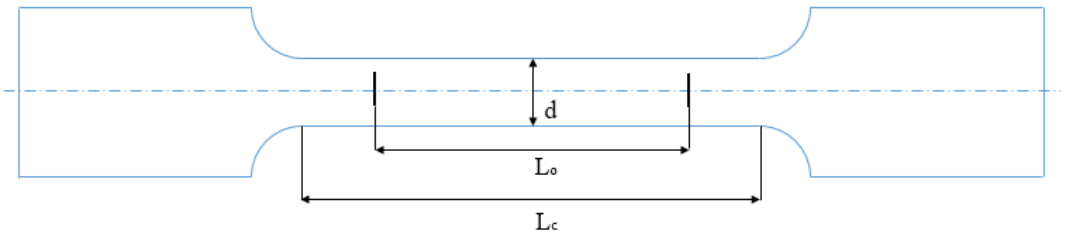


*Figure 22. Dimensions of tensile specimens.*

Yield strength was determined in terms of $R_{t0.5}$ and $R_{p0.2}$ was schematically shown in Figure 23. Young's modulus (E) was calculated from the slope of the elastic region. Ultimate tensile strength was determined from the following equation:

$$R_m = \frac{4F_{max}}{\pi d^2} \quad (4)$$

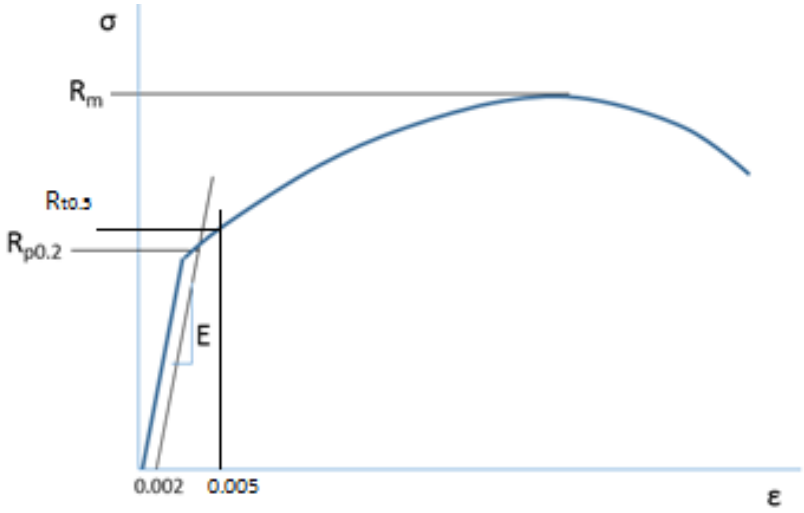


*Figure 23. Representative engineering stress vs engineering strain curve and strength parameters.*

All toughness tests were carried out at -10°C which is the minimum temperature expected in pipeline through service span since ductility is a feature that might dramatically change with temperature.

3 sets of Charpy impact toughness specimens were prepared from each arcs of A C and E. All sets are containing 3 identically notched specimens. Notch locations were:

- weld centerline (WCL),
- fusion line (FL) which is 50% weld metal and 50% HAZ,
- FL+1 mm as shown in Figure 24.

The whole notch is on HAZ in FL+1 specimens therefore, the results obtained from those specimens represent the toughness of HAZ. Specimen dimensions were 10x10x55 $mm^3$. The tests were conducted at the design temperature, i.e., -10°C.

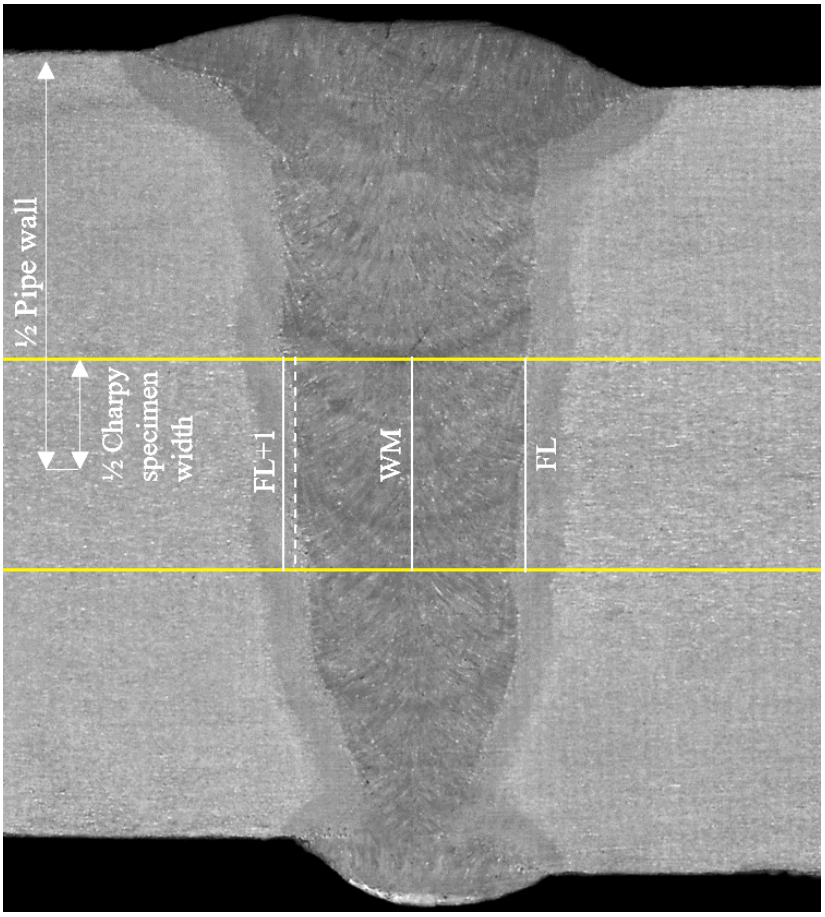


*Figure 24. Charpy specimen and V-notch location.*

Aside from conventional impact toughness, resilience to fracture was measured with elastoplastic fracture toughness parameter, CTOD, in accordance with ISO 15653 [45]. Single Edge Notched Bend (SENB) specimens were extracted from Arc A, C and E and prepared with NP orientation presented in Figure 25. Single value parameters were

calculated from two sets of specimens. Specimen notch locations were WM and FL. Specimens were tested at -10°C.

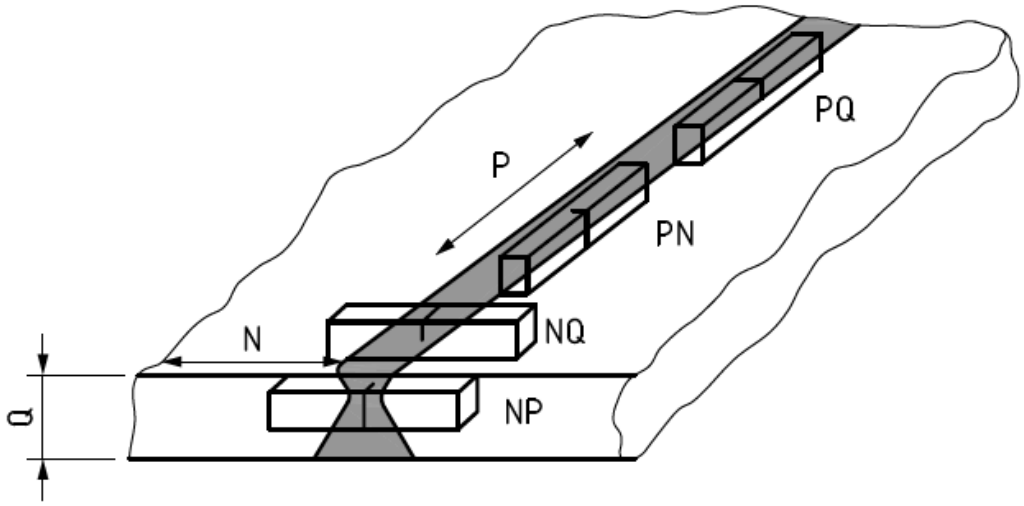


*Figure 25. Crack plane orientation code for fracture toughness specimens.*

Thickness of the specimen, B=22 mm was determined by the pipe thickness less the minimum amount of milling and grinding necessary to produce a specimen with the rectangular cross section and surface finish from a curved pipe segment. Width of the specimen (W) was chosen 2B and Bx2B cross sectional specimens were prepared. After specimens were machined down to rectangular cross section, notches were opened with electrical discharge machining (EDM). The geometry of the notch with internal knife edges is presented in Figure 26. Local compression is applied to reduce residual stress to obtain sufficiently straight fatigue pre-crack shapes. A 1.5 mm pre-crack was created at the tip of the notch by dynamical loading. Bending test was carried out with a speed of 0.7 mm/min crosshead displacement rate and the load is applied from a span length (S) of 4W. Tests were terminated when the load was passed its highest peak and load versus crack opening displacement (COD) graph was acquired. COD measurements were done by a COD gauge placed on top of the notch opening. Additional both SENB and single edge notched tension (SENT) fracture toughness specimens were prepared and tested for J R-curve generation which is explained in detail in section 3.6.

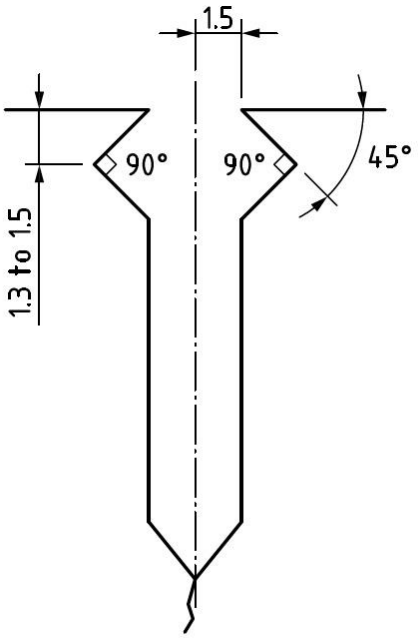


*Figure 26. Notch geometry with the integral knife edges.*

## 3.5 Metallography and fractography

Macro hardness tests were carried out to satisfy the API 1104 criteria while the purpose of micro hardness test was to distinguish LBZs. Opposite side of the macro specimen from arc C is further polished to 1200 grit finish and again etched with 10% Nital according to ASTM E 384. HV0.5 indentations were inserted with 0.4 millimeter interspacing from weld center line to BM in every 2 millimeters through thickness. The macro specimen subjected to micro hardness testing is presented in Figure 27. Micro hardness test with 0.25 mm interspacing were carried out to examine strain hardening caused by the plasticity of the specimen after fracture toughness tests. A representative image used to measure the HV0.5 values is presented in Figure 28. The minimum distance between the center point of individual indentations were higher than 3 times the mean diagonal to prevent the influence of deformation caused by an indentation. 0.5 kg-force is applied for 10 seconds per micro indentations.

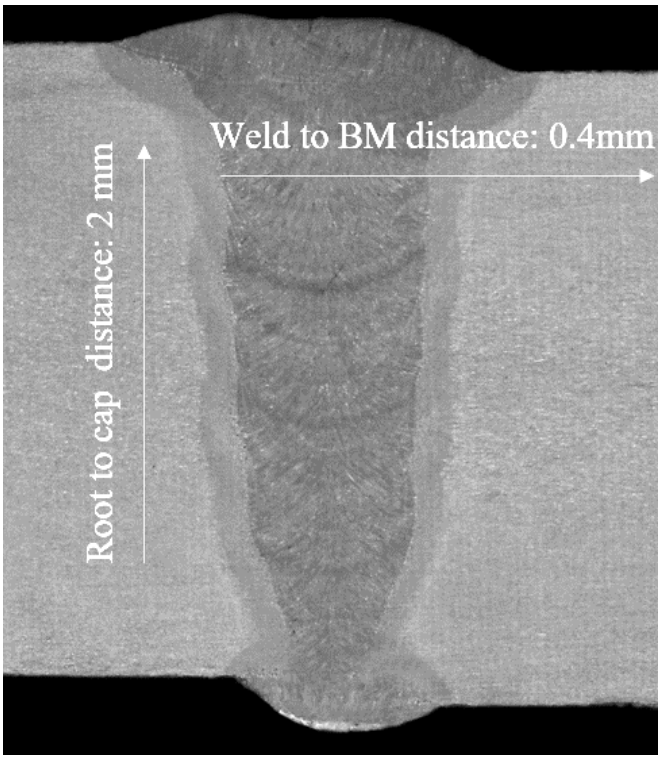


*Figure 27. Interspacing distance of micro hardness intendations.*

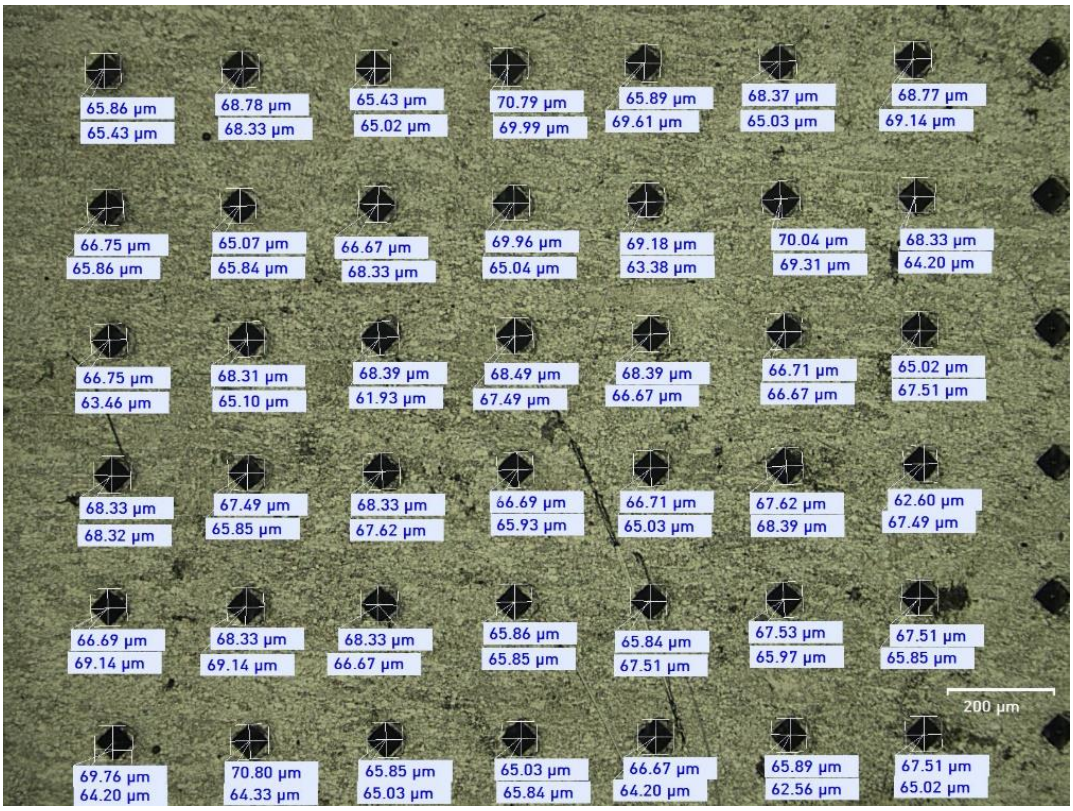


*Figure 28. A representative image of HV0.5 indentations with 0.25 mm interspacing.*

The specimens were sectioned after experiments at temperatures below the DBTT of the parent metal by applying liquid nitrogen. Fracture surfaces of the specimens were documented by digital photography. Initial crack length, $a_0$, and stable crack extension, $\Delta a$, was measured on the photographs by the nine-point average method and calculated and validated according to ISO 12135 [36]. An illustration of fracture surface is given in Figure 29.

The nine-point average method is presented in the equation:

$$a = \frac{1}{8}\left[\left(\frac{a_1+a_9}{2}\right) + \sum_{j=2}^{j=8} a_j\right] \qquad \text{X3}$$

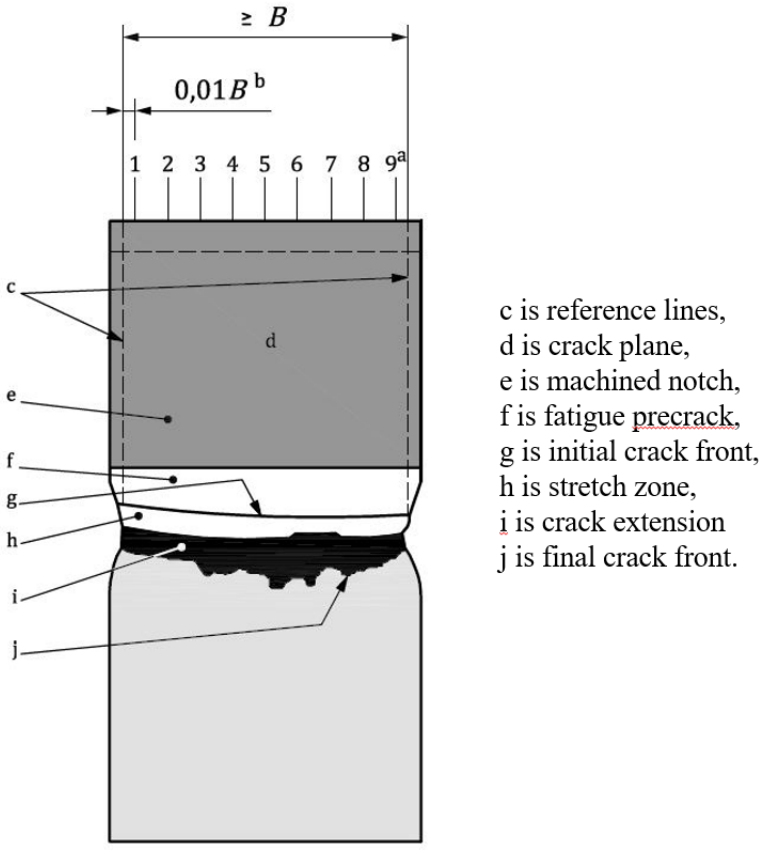


*Figure 29. Illustration of fracture surface [36].*

Fracture toughness specimens notched from FL were subjected to post-test metallography in order to control wheather the crack tip has been successfully located

in the target microstructure. Fracture surfaces of both SENB and SENT specimens were examined under SEM for microstructural examination and stretch zone measurement.

### 3.6 Analyses of testing data

Fracture toughnesses of the FL and WM were defined as single parameter by CTOD testing. Those critical values are sufficient when assessing the fracture resistance to a located flaw. Stable tearing assessment, on the other hand, requires to evaluate the change of fracture toughness associated with tearing. Such assessments have to be applied when high total nominal longitudinal strain ($\varepsilon_{l.nom}$) is expected due to off-shore installation or seismic fault zones. Resistance curve is required when $\varepsilon_{l.nom}$ is higher than 0.5 according to DNVGL-RP-F108 [37].

The welded joint subjected to testing is designed as on shore, seismic zone procedure. Consequently, it is necessary to generate information about both critical toughness values of flaw and fracture resistance curves. Even though, one curve was sufficient for tearing assessment, two curves were generated per SENB and SENT specimen sets, separately. SENT specimens were prepared and tested in accordance with DNVGL-RP-F108 [37] and SENB were prepared and tested in accordance with ISO 15653 [45]. All specimens were NQ oriented (see Figure 25), extracted from arc G, shared the same cross-section of 20x20 $mm^2$ and pre-cracked as described in section 3.4. Specimen numbers and notch locations are tabulated with respect to specimen type in Table 11. Minimum number of test specimens to generate J vs tearing length ($\Delta a$) curve is 6 where $\Delta a$ equals to initial crack length ($a_o$) subtracted from final crack length ($a_f$) and measured from fracture surfaces as described in section 3.5. Mean curve generation is required for SENB specimens and lower bound curve generation is required for SENT specimens. A representation of two curves generated from the same data points is shown in Figure 30. Thus, 2 additional SENT specimens were prepared since DNVGL-RP-F108 allows the lowest test result to be ignored before defining R-curve.

*Table 11. Fracture toughness specimen numbers and notch locations for curve generation.*

| Notch Location (see Figure 24) | Orientation (see Figure 25) | # of SENB specimens | # of SENT specimens |
|---|---|---|---|
| WM | NQ | 6 | 8 |
| FL | NQ | 6 | 9 |

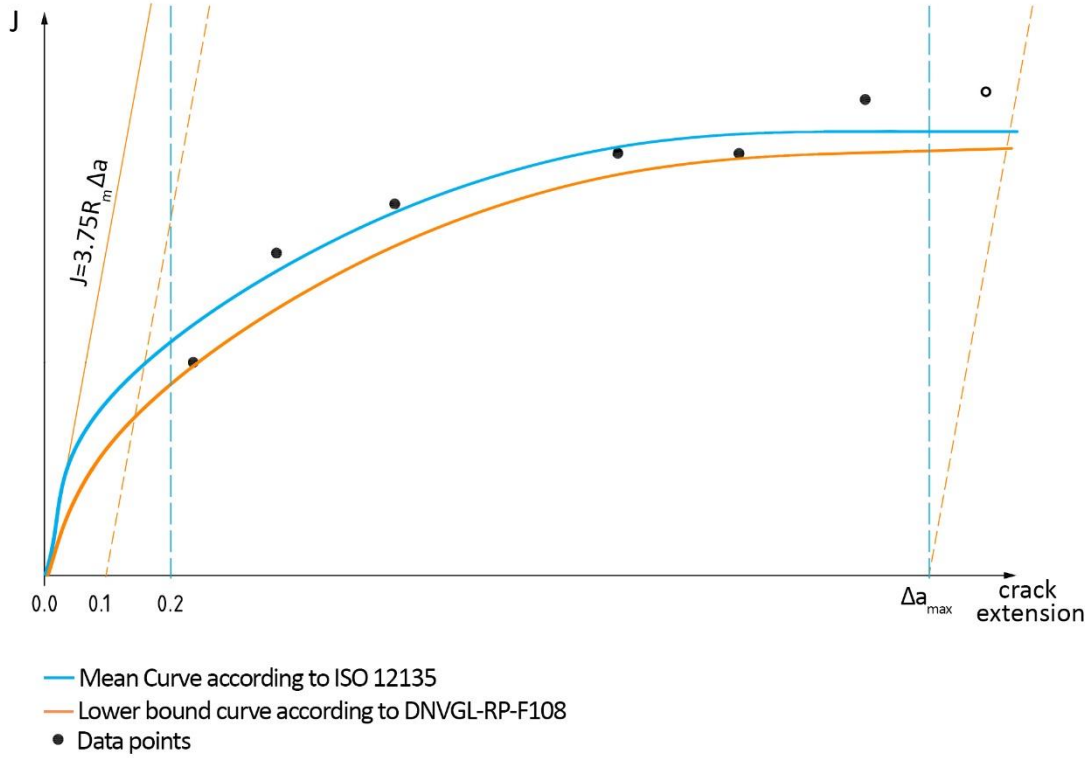


*Figure 30. Two resistance curves generated from the same data points.*

The loads applied to the specimens with respect to the specimen type is presented in Figure 31. All specimens in a set were loaded differently to acquire different data points for the curve between tearing lengths between 0.1 for SENB specimens and 0.2 for SENT specimens to $\Delta a_{max}$. $\Delta a_{max}$ is 25% of W-$a_o$ for SENB specimens and 10% for SENT specimens where W- $a_o$ is the remaining initial ligament.

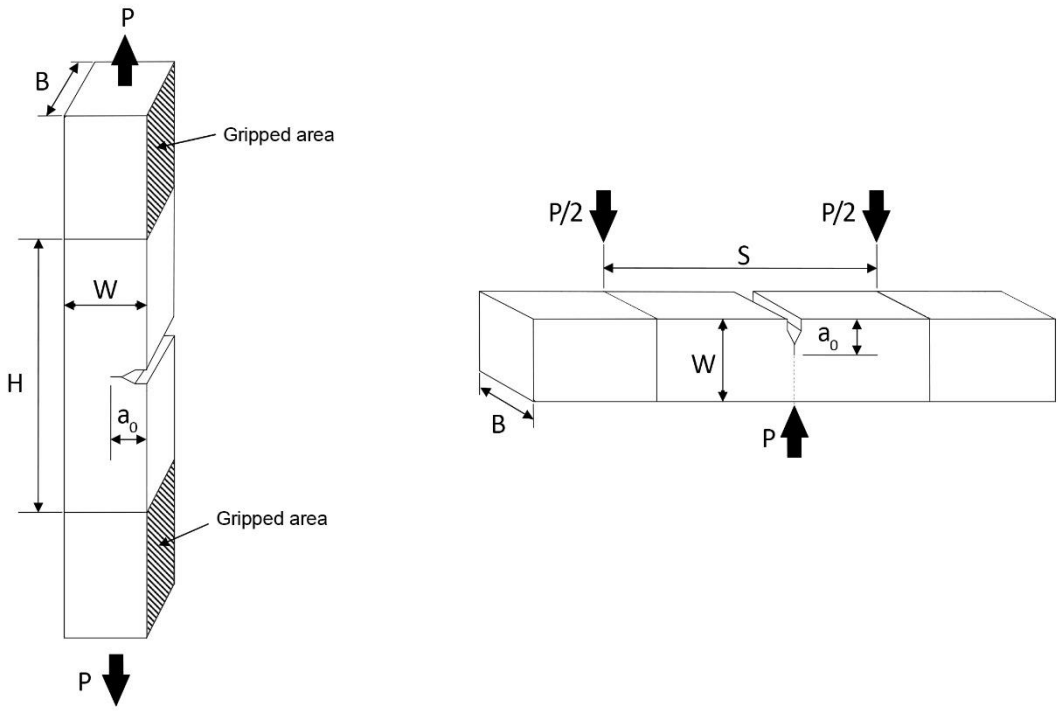


*Figure 31. The loads applied to the SENB and SENT specimens.*

J values of the SENB specimens were calculated according to following equations:

$$J = J_{Elastic} + J_{Plastic} \cdot C_{cor} \tag{5}$$

$$J = \frac{K^2}{E'} + \frac{1.9U_p}{B(W-a_0)} \cdot \left[1 - \frac{\Delta a}{2(W-a_0)}\right] \tag{6}$$

where,

$$K = \left[\frac{FS}{BW^{1.5}} G\left(\frac{a_0}{W}\right)\right] \tag{7}$$

$$G\left(\frac{a_0}{W}\right) = \frac{3\left(\frac{a_0}{W}\right)^{0.5}\left[1.99 - \frac{a_0}{W}\left(1-\frac{a_0}{W}\right)\left(2.15 - \frac{3.93a_0}{W} + \frac{2.7a_0^2}{W^2}\right)\right]}{2\left(1+\frac{2a_0}{W}\right)\left(1-\frac{a_0}{W}\right)^{1.5}} \tag{8}$$

$$E' = \frac{E}{(1-\upsilon^2)} \tag{9}$$

Above equations are derived from the equations in ISO 12135 [36]. $U_p$ is the plastic component of the area under the plot of force (F) versus specimen load-point displacement (q) at the load-line as presented in Figure 32.

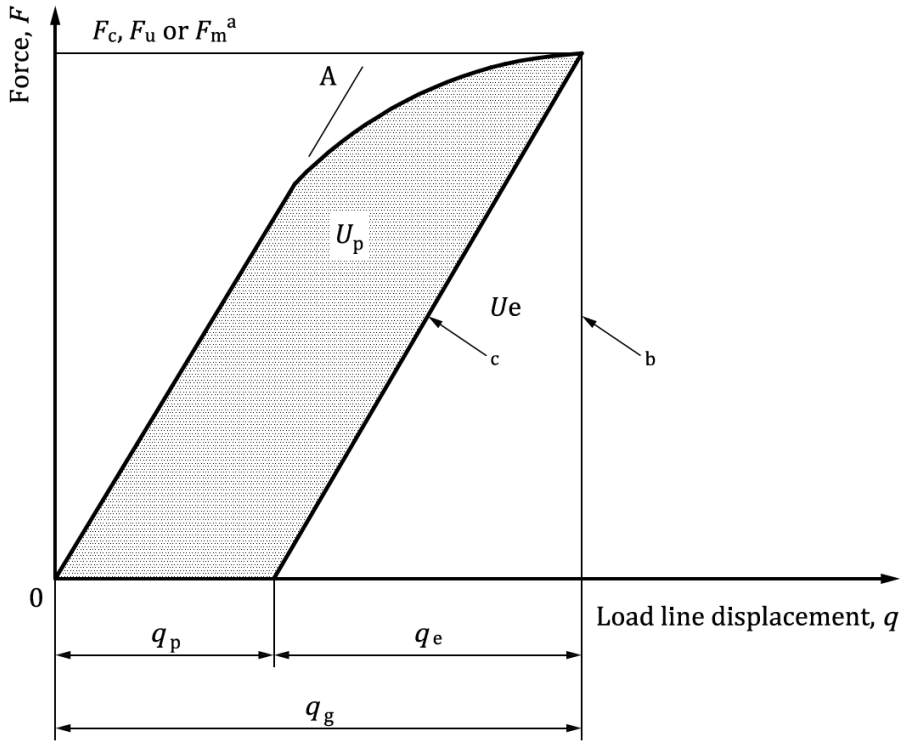


*Figure 32. Definition of Up [36].*

J values of the SENT specimens were calculated according to following equations which are derived from BS 8571 [38]:

$$J = J_{Elastic} + J_{Plastic} \cong J_{Elastic} + J_{Plastic} \cdot C_{cor} \quad (10)$$

$$J = \frac{K^2}{E'} + \frac{\eta_P U_p}{B(W-a_0)} \quad (11)$$

where $U_p$ is the area under the plot of F versus crack opening displacement (COD) instead of q shown in Figure 32.

$$K = \frac{F}{BW}\sqrt{\pi a_0}(f_1 - 6\xi_3 f_2) \quad (12)$$

$f_1$, $\xi_3$, and $f_2$ are defined as follows:

$$\xi_3 = \frac{\xi_1}{\xi_2 + 12\frac{H}{W}} \quad (13)$$

$$\xi_1 = 12\pi\left(\frac{a_0}{W}\right)^2 \sum_{i=0}^{8} q_i\left(-\frac{a_0}{W}\right)^i - U_+\left(\frac{a_0}{W} - 0.6\right)\left[19.95 - \frac{3.99(3a_0/W-1)}{(1-a_0/W)^2}\right] \quad (14)$$

$$\xi_2 = 72\pi(\frac{a_0}{W})^2 \sum_{i=0}^{8} r_i(-\frac{a_0}{W})^i - U_+\left(\frac{a_0}{W} - 0.6\right)[99.38 - \frac{15.9}{(1-a_0/W)^2}] \quad (15)$$

$$f_1 = U_-\left(0.6 - \frac{a_0}{W}\right)\sum_{i=0}^{4} n_i(-\frac{a_0}{W})^i - U_+\left(\frac{a_0}{W} - 0.6\right)\frac{(1+3a_0/W)}{3.545(a_0/W)^{1/2}(1-a_0/W)^{3/2}} \quad (16)$$

$$f_2 = U_-\left(0.6 - \frac{a_0}{W}\right)\sum_{i=0}^{4} m_i(-\frac{a_0}{W})^i - U_+\left(\frac{a_0}{W} - 0.6\right)\frac{0.375}{(a_0/W)^{1/2}(1-a_0/W)^{3/2}} \quad (17)$$

where $U_+$ and $U_-$ are Heaviside functions defined as follows:

$U_+(x) = 0$ for $x \leq 0$

$U_+(x) = 1$ for $x > 0$

$U_-(x) = 0$ for $x < 0$

$U_-(x) = 1$ for $x \geq 0$

$q_i$, $r_i$, $m_i$ and $n_i$ are constants given in Table 12.

*Table 12. The constants used in the J calculations.*

| $i$ | $n_i$ | $m_i$ | $q_i$ | $r_i$ |
|---|---|---|---|---|
| 0 | 1.120 | 1.122 | 0.629 | 0.629 |
| 1 | 0.231 | 1.400 | 0.609 | 1.047 |
| 2 | 10.550 | 7.330 | 5.093 | 4.602 |
| 3 | 21.720 | 13.080 | 11.097 | 9.975 |
| 4 | 30.390 | 14.000 | 26.757 | 20.295 |
| 5 | - | - | 48.997 | 32.993 |
| 6 | - | - | 81.820 | 47.041 |
| 7 | - | - | 77.953 | 40.693 |
| 8 | - | - | 42.456 | 19.600 |

$$\eta_P = 0.858\left[\left(196.719e^{-\left(\frac{B}{W}\right)} - 64.642\right)\left(\frac{a_0}{W}\right)^5 + \left(-493.511e^{-\left(\frac{B}{W}\right)} + 138.837\right)\left(\frac{a_0}{W}\right)^4 + \left(463.503e^{-\left(\frac{B}{W}\right)} - 106.207\right)\left(\frac{a_0}{W}\right)^3 + \left(-201.862e^{-\left(\frac{B}{W}\right)} + 34.532\right)\left(\frac{a_0}{W}\right)^2 + \left(39.413e^{-\left(\frac{B}{W}\right)} - 4.525\right)\left(\frac{a_0}{W}\right)^1 + \left(-2.064e^{-\left(\frac{B}{W}\right)} + 1.039\right)\right] \quad (18)$$

# CHAPTER 4

# RESULTS

## 4.1 Welding procedure qualification

No major indication was observed on non-destructive testing which means that the joint is flawless or flaws are below NDT range. The coupon is adequate for destructive tests in either case. No significant discontinuity was recorded from bending and cross weld tensile tests. Cross weld tensile specimens were fractured from base metal with a tensile strength higher than the minimum base metal requirement as presented in Table 13. This result is a conceivable outcome of overmatching between weld metal and base metal which is further examined in section 4.3.

*Table 13. Cross weld tensile test results*

| Specimen Code | A1 | A2 | A3 | A4 |
|---|---|---|---|---|
| Specimen Location | Arc B | Arc D | Arc F | Arc H |
| Tensile Strength (MPa) | 675 | 675 | 680 | 671 |
| Location of fracture | Base Metal | | | |

Macro examination specimens XL1, XL2 and XL3 were subjected to hardness test and designated M31, M32 and M33, respectively. XL2 with the rows of Vickers indentations are presented in Figure 33 and HV10 hardness test results are presented in Table 14. Macro hardness surveys yielded maximum hardness 265 HV10 on the specimen XL3 from Arc E where minimum heat input, maximum cooling rate and consequently higher brittle phase fraction are expected due to over-head welding direction. Highest HV10 result suggests brittle phases are in acceptable fractions. Which means, welding power parameters and pre-heat temperature were properly optimized along the circumference.

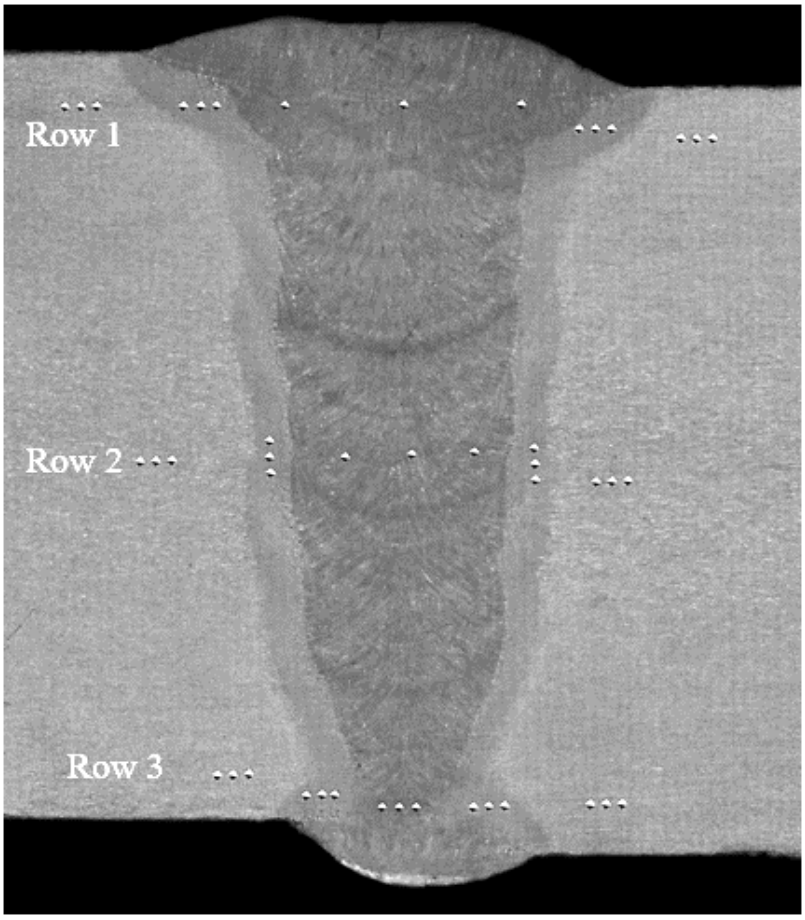


*Figure 33. HV10 indentations on XL2.*

*Table 14. Results of hardness measurements (HV10).*

| Test Code | Row | Base Metal | | | HAZ | | | Weld Metal | | | HAZ | | | Base Metal | | |
|---|---|---|---|---|---|---|---|---|---|---|---|---|---|---|---|---|
| | | 1 | 2 | 3 | 4 | 5 | 6 | 7 | 8 | 9 | 10 | 11 | 12 | 13 | 14 | 15 |
| M31 | 1 | 240 | 246 | 241 | 242 | 232 | 248 | 230 | 235 | 230 | 256 | 254 | 245 | 229 | 234 | 225 |
| | 2 | 212 | 213 | 217 | 213 | 231 | 231 | 217 | 236 | 232 | 240 | 224 | 219 | 219 | 212 | 213 |
| | 3 | 238 | 230 | 236 | 221 | 221 | 247 | 255 | 236 | 240 | 232 | 219 | 217 | 213 | 217 | 231 |
| M32 | 1 | 220 | 208 | 212 | 216 | 224 | 221 | 219 | 212 | 223 | 240 | 233 | 220 | 208 | 217 | 215 |
| | 2 | 218 | 205 | 208 | 209 | 219 | 224 | 223 | 221 | 219 | 213 | 200 | 212 | 198 | 201 | 202 |
| | 3 | 215 | 216 | 214 | 224 | 220 | 212 | 216 | 221 | 258 | 221 | 221 | 216 | 209 | 215 | 216 |
| M33 | 1 | 237 | 239 | 233 | 246 | 251 | 265 | 258 | 231 | 246 | 263 | 261 | 240 | 224 | 242 | 243 |
| | 2 | 208 | 213 | 213 | 216 | 220 | 222 | 250 | 240 | 249 | 249 | 228 | 224 | 219 | 218 | 216 |
| | 3 | 226 | 215 | 211 | 216 | 223 | 233 | 225 | 245 | 229 | 216 | 234 | 239 | 216 | 225 | 243 |

Elemental constituents of the weld metal and the base metal analyzed by optical emission spectrography is presented in Table 15. These results are matching with the requirement of the standard presented in Table 2 and compatible with the values obtained from qualification certificates presented Table 5 and Table 6. Weld metal results presented in this table was obtained from the middle of the weld metal where ER80S-Ni1 was used as filler.

*Table 15. Elemental constituents of WM and BM*

| | Weight fraction (%) | | | | | | | | | | |
|---|---|---|---|---|---|---|---|---|---|---|---|
| | C | Mn | Si | Ni | Cr | Ti | Mo | V | P | Cu | S |
| Base Metal | 0.041 | 1.76 | 0.23 | 0.22 | 0.22 | 0.019 | 0.134 | 0.004 | 0.014 | 0.027 | <0.001 |
| Weld Metal | 0.058 | 1.46 | 0.51 | 0.79 | 0.07 | 0.005 | 0.04 | 0.004 | 0.015 | 0.074 | <0.001 |

The girth welding procedure is also qualified per ECA in which high plastic strains are taken into consideration. Strength and ductility parameters, absorbed impact energies, fracture toughness parameters and resistance curves will be introduced in the following sections.

## 4.2 Microstructural features

Indentations of macro hardness are too large and the minimum interspacing required is too large to detect LBZs. HV 0.5 micro hardness scanning with higher resolution is employed to distinguish hardening spikes in IRCGHAZ which are clearly visible in Figure 34. HV 0.5 micro hardness measurements in the HAZ are presented in Table 16.

*Table 16. Results of the micro hardness measurements in the HAZ (HV0.5).*

| | | Specimen XL2 (HV0.5) HAZ FL to BM | | | | | | | |
|---|---|---|---|---|---|---|---|---|---|
| Rows from Cap to Root | 1 | 300 | 264 | 221 | 256 | 222 | 212 | 243 | 254 |
| | 2 | 342 | 311 | 286 | 260 | 286 | 290 | - | - |
| | 3 | 282 | 240 | 288 | 267 | 257 | - | - | - |
| | 4 | 224 | 214 | 207 | 197 | - | - | - | - |
| | 5 | 315 | 280 | 233 | 228 | - | - | - | - |
| | 6 | 220 | 252 | 236 | 215 | - | - | - | - |
| | 7 | 220 | 252 | 236 | 215 | - | - | - | - |
| | 8 | 341 | 291 | 257 | 255 | - | - | - | - |
| | 9 | 275 | 290 | 290 | - | - | - | - | - |
| | 10 | 237 | 197 | 230 | - | - | - | - | - |
| | 11 | 256 | 200 | 217 | 204 | - | - | - | - |
| | 12 | 251 | 223 | 274 | 225 | 250 | 214 | 241 | 248 |

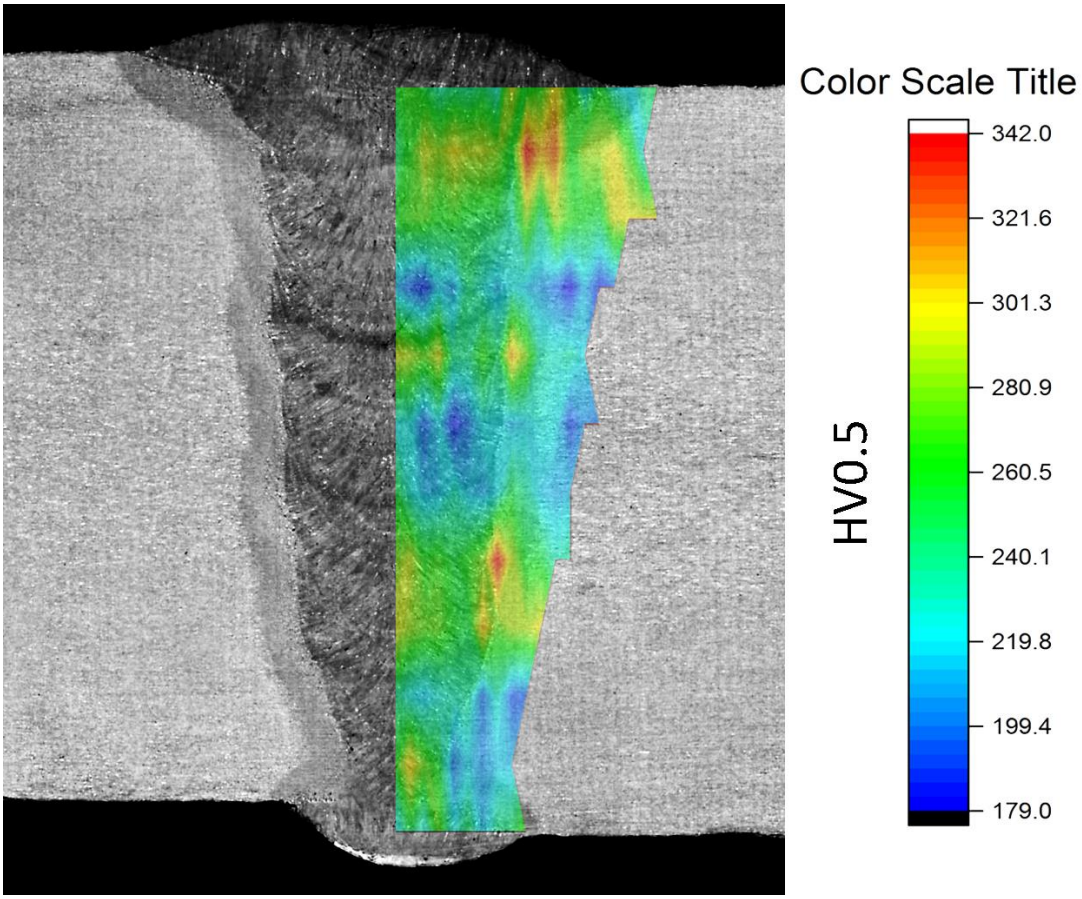


*Figure 34. Contour map of microhardness variation*

The proportion of LBZs and associated deterioration of mechanical properties increased with increased formation of martensitic-austenitic (MA) constituents in the CGHAZ as reported by Mohammadijoo et al [46]. MA constituents are randomly distributed alongside with the fusion line at grain boundaries and promotes crack initiation and propagation [47, 48]. This effect is further investigated in section 4.5. Coarsened grains that host MA islands at their boundaries from IRCGHAZ are visible in Figure 35.

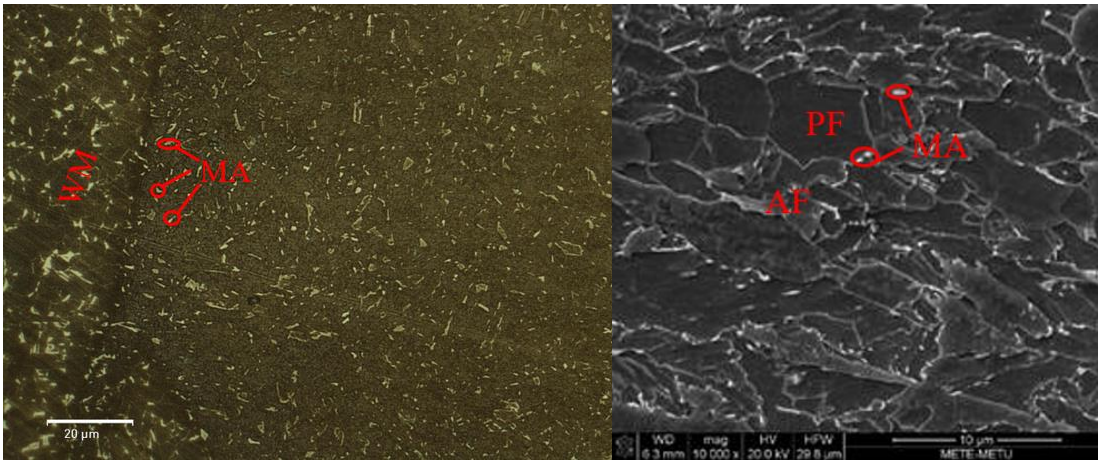


*Figure 35. OM and SEM micrographs of LaPera etched and %2 Nital etched IRCGHAZ.*

## 4.3 Strength and ductility parameters

All-weld tensile and base metal tensile test results are presented in Table 17. It is clearly visible that the requirement for the weld metal to have strength level equal to or higher than (overmatching) the base material is fulfilled in Figure 36. This is a prerequisite of both API 1104 and DNVGL-ST-F101 to minimize deformation in the area adjacent to any possible defects. However, more than 20% overmatch deteriorates toughness parameters such as J and CTOD [49].

*Table 17. All weld and base metal tensile test results*

| | Base Metal | | All-weld Metal | | | |
|---|---|---|---|---|---|---|
| Specimen Code | AB1 | AB2 | AA1 | AA2 | AA3 | AA4 |
| Specimen Location | Arc C | Arc C | Arc A | Arc C | Arc E | Arc G |
| Yield Strength $R_{t0.5}$ (MPa) | 620 | 615 | 681 | 685 | 715 | 708 |
| Tensile Strength $R_m$ (MPa) | 660 | 662 | 721 | 728 | 746 | 745 |
| Young's Modulus (GPa) | 206 | 200 | 203 | 210 | 206 | 206 |
| Elongation (%) | 20.3 | 22.1 | 22.0 | 21.9 | 19.5 | 22.2 |

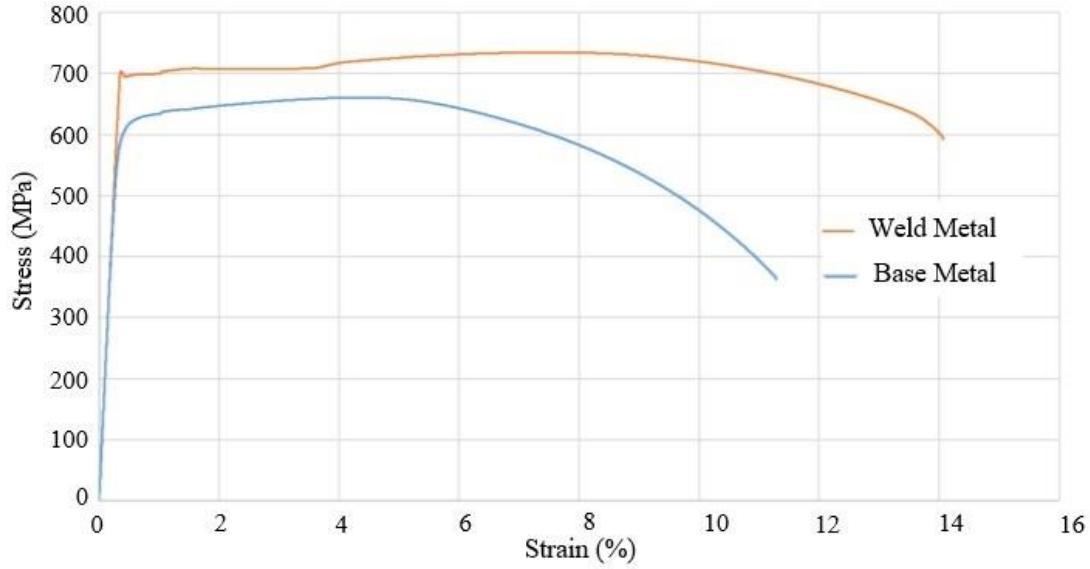


*Figure 36. Engineering stress- strain curves obtained by all weld metal and base metal tensile test*

Highest mismatch is 18.5% and it is between the yield strengths of AB1 and AA3. AA3 from Arc E shows the highest strength in all weld metal specimens as expected since Arc E is welded over-head direction with the lowest heat input. Low heat input result in high strength and hardness but low toughness which is presented in section 4.4.

## 4.4 Impact Toughness

Charpy V-Notch impact toughness results are presented in Table 18. Lower bound evaluation is the only applicable option for all toughness tests where the lowest single

value determines the toughness of set of specimens extracted and notched from the same location. All lower bound values from distinctive sets are underlined in this table. Specimens notched from fusion line have the highest standard deviation since most of the coarsened grains and LBZs that dramatically lower the toughness are randomly located in that region. High values of specimens notched from fusion line +1 mm certify that influence of deterioration caused by welding process is minimal.

Weld center notched specimens have the lowest absorbed energy as expected due to overmatch explained in section 4.3. The lowest impact toughness from weld notched specimens, 147 J is from Arc E (N19) followed by 158 Joules in Arc C (N11) and then 168 J from Arc E (N1) is matching with heat input alteration along the circumference. The lowest heat input resulted in the worst impact toughness and the highest heat input resulted in the best impact toughness.

*Table 18. Charpy V-Notch impact toughness test results at -10 °C.*

| | Location of the specimen | Location of the notch | Absorbed energy (J) |
|---|---|---|---|
| N1 | Arc A | Weld Center | 168 |
| N2 | Arc A | Weld Center | 183 |
| N3 | Arc A | Weld Center | 171 |
| N4 | Arc A | Fusion Line | >300 |
| N5 | Arc A | Fusion Line | 102 |
| N6 | Arc A | Fusion Line | 199 |
| N7 | Arc A | Fusion Line +1mm | >300 |
| N8 | Arc A | Fusion Line +1mm | >300 |
| N9 | Arc A | Fusion Line +1mm | >300 |
| N10 | Arc C | Weld Center | 161 |
| N11 | Arc C | Weld Center | 158 |
| N12 | Arc C | Weld Center | 162 |
| N13 | Arc C | Fusion Line | 180 |
| N14 | Arc C | Fusion Line | 161 |
| N15 | Arc C | Fusion Line | 171 |
| N16 | Arc C | Fusion Line +1mm | 292 |

*Table 18(Continued). Charpy V-Notch impact toughness test results at -10 °C.*

| | | | |
|---|---|---|---|
| N17 | Arc C | Fusion Line +1mm | 294 |
| N18 | Arc C | Fusion Line +1mm | >300 |
| N19 | Arc E | Weld Center | 147 |
| N20 | Arc E | Weld Center | 156 |
| N21 | Arc E | Weld Center | 175 |
| N22 | Arc E | Fusion Line | 205 |
| N23 | Arc E | Fusion Line | 200 |
| N24 | Arc E | Fusion Line | >300 |
| N25 | Arc E | Fusion Line +1mm | >300 |
| N26 | Arc E | Fusion Line +1mm | >300 |
| N27 | Arc E | Fusion Line +1mm | 298 |

4.5 Elastic-plastic fracture toughness parameters

Single CTOD parameters are presented in Table 19. The specimens notched from fusion line has better results compared to the specimens notched from weld metal as previously noted in section 2.4. When calculating the crack tip opening displacement or energy release of crack growth, single value parameters assume that the crack does not propagate even though crack tip widens. Therefore, J and CTOD single values neglect the crack propagation. Critical values of those single parameters are calculated from the highest load plateau since the crack propagation is neglected. Crack measurement from PC4 revealed almost 10 times higher Δa than PC1 but had better δ results since crack extension (Δa) is not used in single value calculations. Crack surfaces of PC1 and PC4 are presented in Figure 37.

*Table 19. Single CTOD (δ) values*

| | PC1 | PC2 | PC3 | PC4 | PC5 | PC6 |
|---|---|---|---|---|---|---|
| Location of Specimen | Arc A | Arc A | Arc C | Arc C | Arc E | Arc E |
| Notch Location | WM | FL | WM | FL | WM | FL |
| $a_0$ (mm) | 23.03 | 22.74 | 22.80 | 22.78 | 22.53 | 22.67 |
| Δa (mm) | 1.15 | 7.88 | 0.81 | 11.22 | 0.44 | 1.14 |
| δ (mm) | 0.423 | 0.681 | 0.454 | 0.659 | 0.436 | 1.171 |

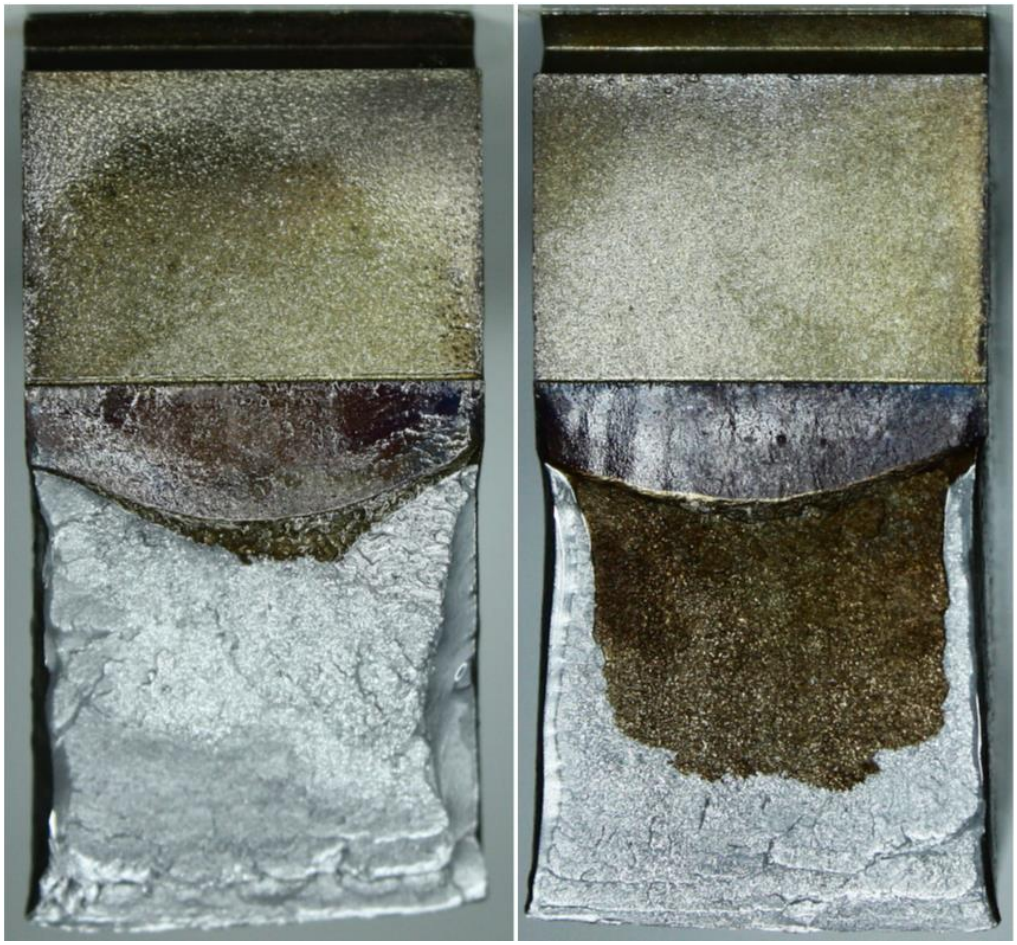

*Figure 37. Fracture surfaces of PC1 and PC4.*

Single value parameters characterize the resistance against the initiation of crack under static loads. However, the resistance curves characterize the resistance of the material against both initiation and propagation of the crack. Single value parameters are adequate for ordinary installation and work conditions. Crack propagation is inevitable and non-ignorable under conditions that involve high stress or high strain. Thus, more complex R-curve evaluation is required. J results of weld metal notched SENB specimens and R curve are presented in Table 20 and Figure 38, respectively.

*Table 20. J values of the weld metal notched SENB specimens*

| | PJ1 | PJ2 | PJ3 | PJ4 | PJ5 | PJ6 |
|---|---|---|---|---|---|---|
| $a_0$ (mm) | 10.75 | 10.70 | 10.80 | 11.03 | 11.16 | 10.64 |
| Δa (mm) | 0.27 | 0.43 | 0.81 | 1.15 | 2.06 | 2.31 |
| J (J/mm$^2$) | 0.291 | 0.445 | 0.569 | 0.654 | 0.836 | 0.917 |

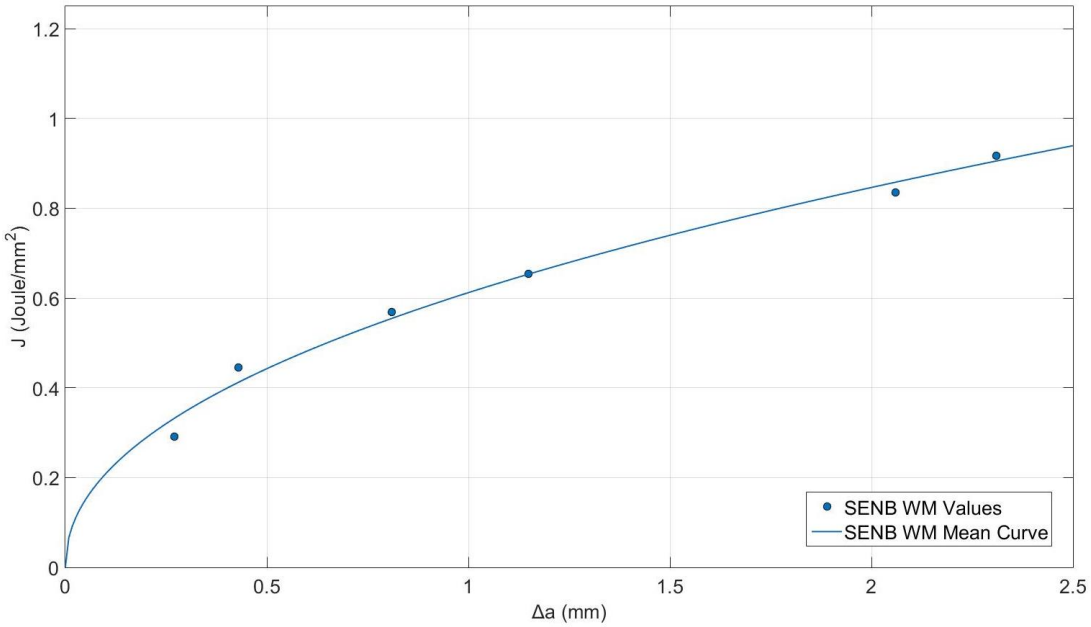


*Figure 38. J R-curve of the SENB weld metal notched specimens.*

J values of the fusion line notched SENB specimens and R curve are presented in Table 21 and Figure 39, respectively.

*Table 21. J values of the fusion line notched SENB specimens*

| | PJ7 | PJ8 | PJ9 | PJ10 | PJ11 | PJ12 |
|---|---|---|---|---|---|---|
| $a_0$ (mm) | 10.85 | 9.99 | 10.87 | 10.09 | 11.04 | 10.27 |
| Δa (mm) | 0.26 | 0.33 | 0.62 | 0.84 | 0.98 | 1.11 |
| J (J/mm$^2$) | 0.392 | 0.551 | 0.734 | 0.934 | 0.914 | 0.938 |

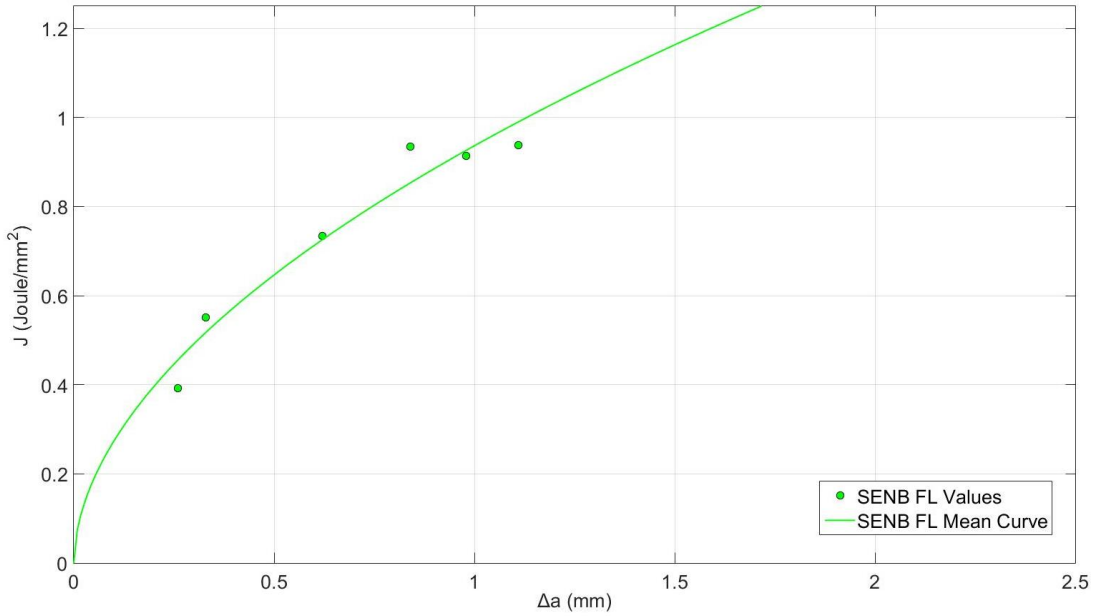


*Figure 39. J R-curve of the SENB fusion line notched specimens*

J values of the weld metal notched SENT specimens and R curve are given in Table 22 and Figure 40, respectively.

*Table 22. J values of the weld metal notched SENT specimens*

| | PJ13 | PJ14 | PJ15 | PJ16 | PJ17 | PJ19 | PJ20 | PJ21 |
|---|---|---|---|---|---|---|---|---|
| $a_0$ (mm) | 7.39 | 6.41 | 6.21 | 6.11 | 6.29 | 6.48 | 6.29 | 6.14 |
| Δa (mm) | 0.530 | 0.892 | 1.361 | 0.540 | 0.629 | 0.289 | 1.141 | 0.441 |
| J (J/mm$^2$) | 0.963 | 0.784 | 1.186 | 0.508 | 0.671 | 0.374 | 1.034 | 0.528 |

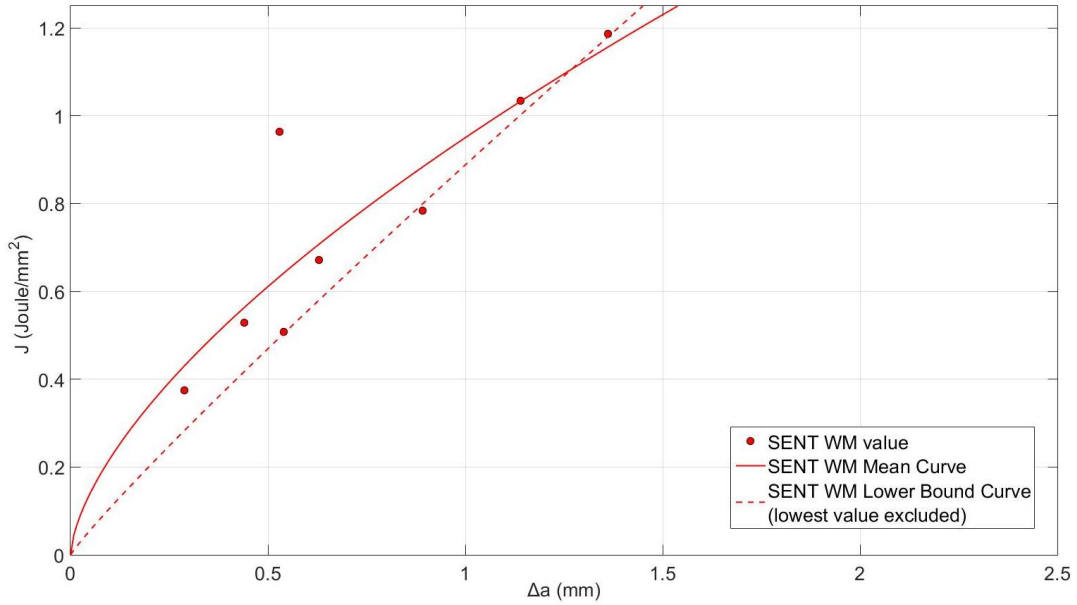


*Figure 40.J R-curve of SENT weld metal notched specimens*

J values of the FL notched SENT specimens and R curve are given in Table 23 and Figure 41, respectively.

*Table 23. J values of fusion line notched SENT specimens*

| | PJ22 | PJ23 | PJ24 | PJ25 | PJ26 | PJ27 | PJ28 | PJ29 | PJ30 |
|---|---|---|---|---|---|---|---|---|---|
| $a_0$ (mm) | 6.69 | 6.71 | 6.49 | 6.55 | 6.57 | 6.38 | 6.09 | 6.18 | 6.00 |
| Δa (mm) | 0.143 | 0.889 | 0.636 | 0.646 | 0.463 | 0.277 | 0.354 | 1.025 | 0.479 |
| J (J/mm$^2$) | 0.269 | 1.130 | 0.970 | 0.789 | 0.669 | 0.546 | 0.464 | 1.071 | 0.619 |

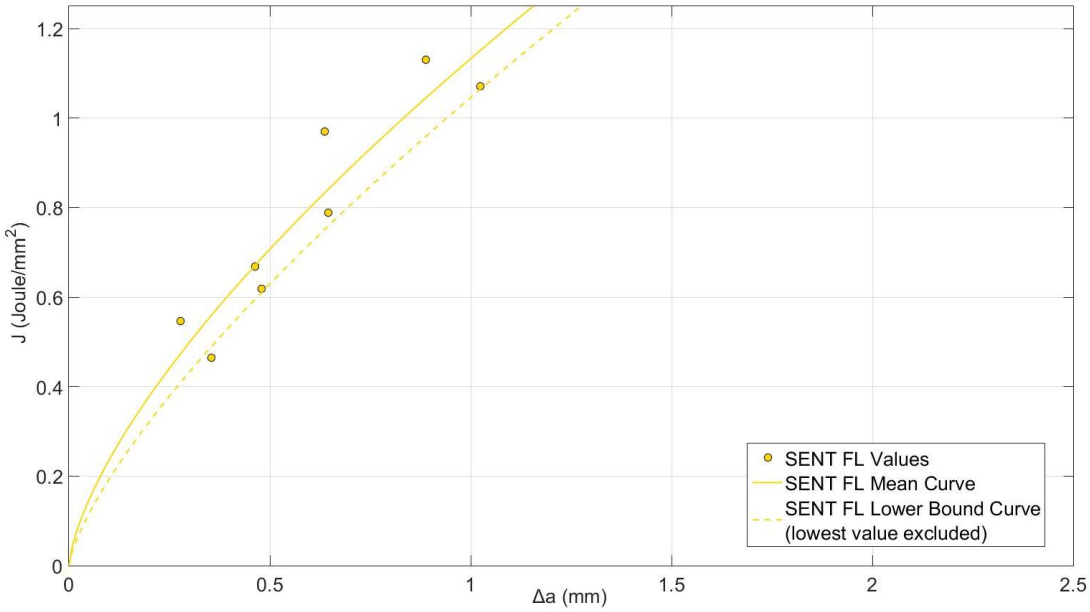


*Figure 41. J R-curve of the SENT fusion line notched specimens.*

Specimen PJ22 exhibited brittle behavior and wasn't presented in the J R-curve. One more specimen (PJ23) was prepared to provide 8 data for the R-curve. Brittle behavior of specimen the PJ22 is a result of LBZ. The pre-crack tip was located near LBZ and under the load the specimen wasn't able to resist the crack. Post-test metallography photo in Figure 42 shows the distance between crack tip to fusion line. It is clearly visible that brittle crack propagation follows the fusion line neighboring CGHAZ where the suspected LBZs are located. The standard validates a specimen as FL notched when the distance between the pre-crack tip and the fusion line is lower than 0.5mm [2]. Although all fusion line specimens are in accordance with this criterion,

only PJ22 is failed. This can be explained by the random distribution of LBZ. Brittle behavior is observed when crack tip is close enough to LBZ and the load is high enough to start a chain reaction leading to the failure.

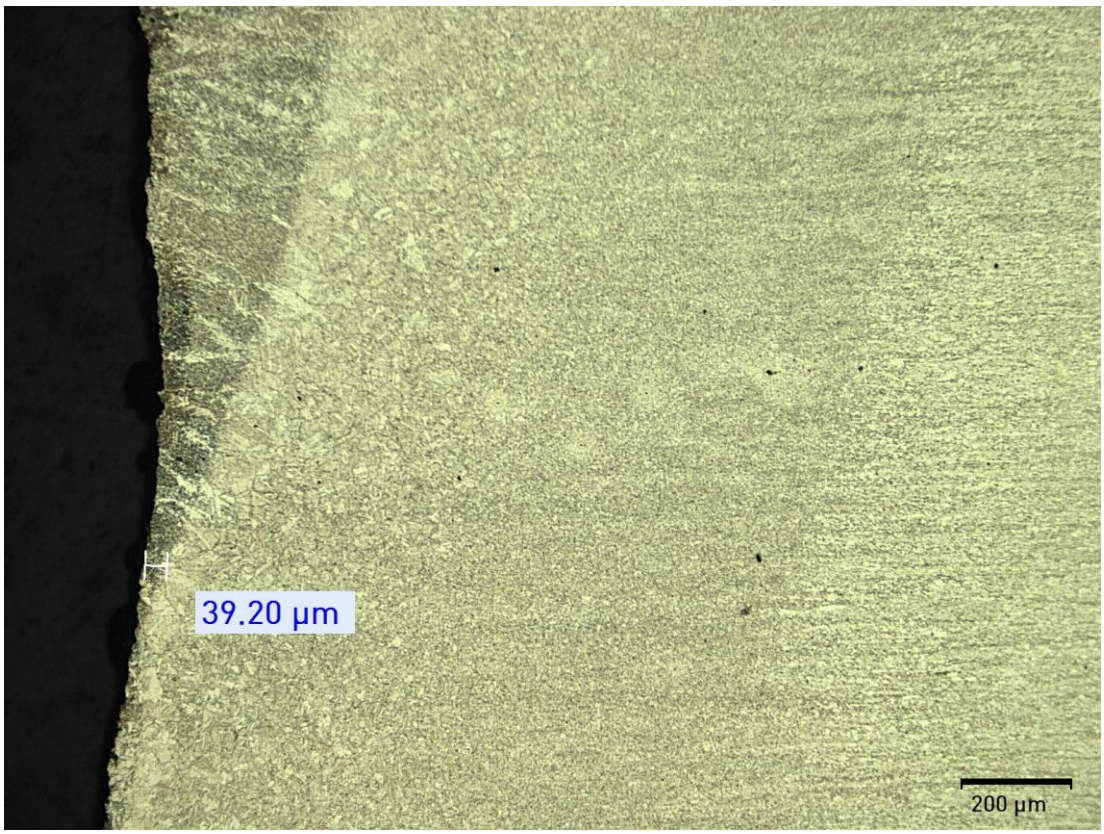


*Figure 42. Post test metallography of PJ22 showing the distance between pre-crack tip to fusion line.*

Fracture surfaces and the load vs crack opening displacement graphs of PJ22 and PJ23 are presented in Figure 43. Sudden load drop occurred just after passing the elastic zone caused the premature termination of the test of PJ22. Fracture surface of PJ23 shows the ductile crack propagation in dark brown region and deformation is easily observable on the side walls. On the other hand, fracture surface of PJ22 shows extremely small ductile crack propagation region and then a large brittle propagation region. Also there is no deformation on the side walls between two crack fronts.

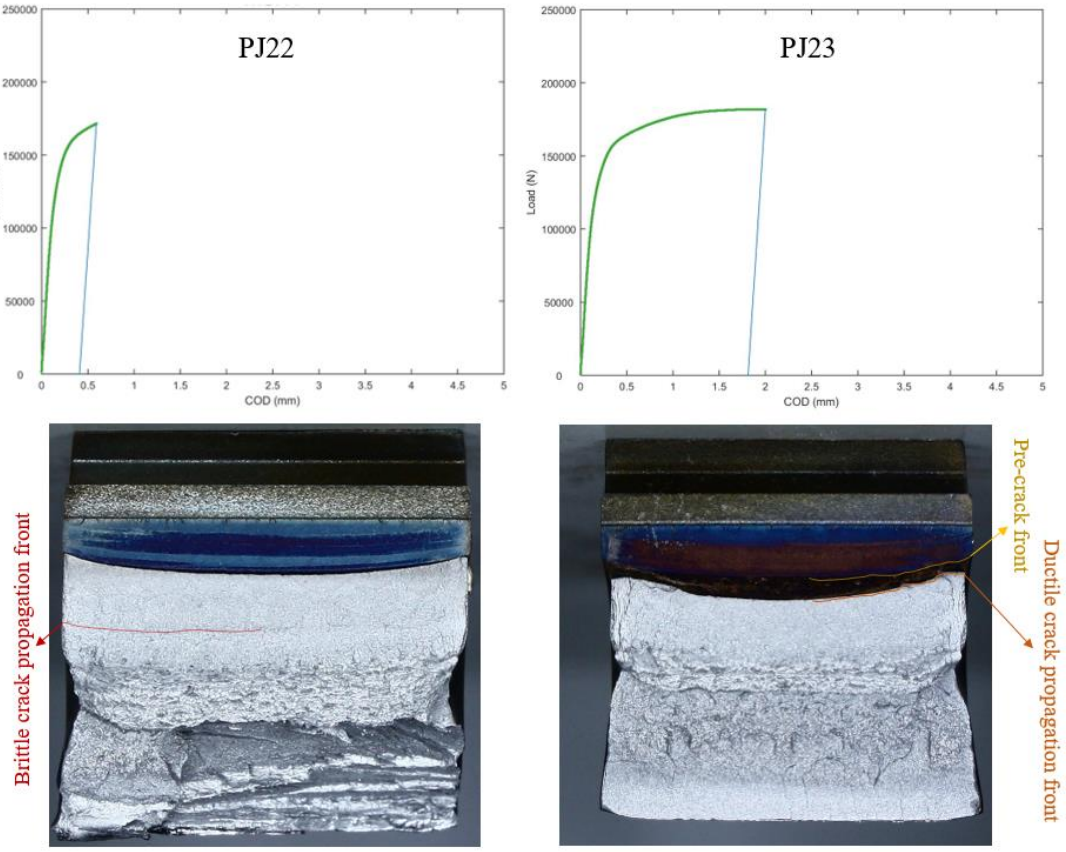


*Figure 43. Fracture surface and load vs crack opening displacement graph comparison of PJ22 and PJ23.*

*Table 24. Equations of the R-curves*

| Specimen Type | Notch Location | J R-curve equation |
|---|---|---|
| SENB | Weld Metal | $J=0.612\Delta a^{0.468}$ |
| SENB | Fusion Line | $J=0.937\Delta a^{0.534}$ |
| SENT | Weld Metal | $J=0.950\Delta a^{0.637}$ |
| SENT | Fusion Line | $J=1.113\Delta a^{0.681}$ |

The minimum required fracture toughness parameters presented in ECA were determined with finite element analysis (FEA) by a few companies that have highest expertise and experience in line pipe field. Meshing and loading the pipe and modeling a crack behavior realistically is not standardized yet even though there are open-ended recommendations on standards. The minimum single CTOD value of 0.25 mm is

required for acceptance of flaw size sets defined in option 1 in Annex A of API 1104 [1]. The minimum result obtained from CTOD single values testing is 0.423 ensures the criterion. However, this procedure is designated for seismic fault zone where high strain is expected. Equations of the R-curves are tabulated in Table 24.

# CHAPTER 5

# DISCUSSION

## 5.1 Crack tip constraint

Mean R-curves presented in Figure 44 shows that weld metal curves are limit state for both SENB and SENT specimens. Lower weld metal average in terms of fracture toughness is expected but generally catastrophic failures are observed on the FL notched specimens due to LBZ explained in the previous section [30]. The lowest J value is obtained from a FL specimen (PJ22). The result is not presented in R-curve which characterize elastic-plastic behavior under stable tearing since the specimen exhibited brittle behavior and unstable tearing.

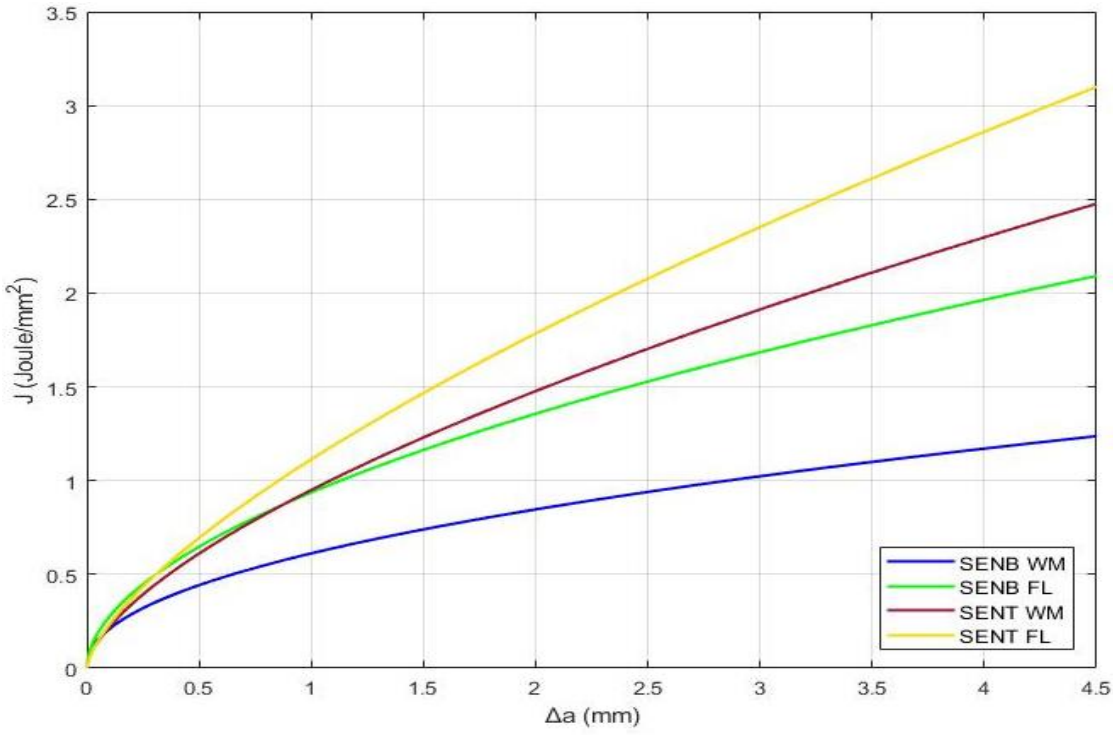


*Figure 44. Mean R-curves.*

The tearing resistance of SENT specimens is higher than that of the SENB specimens as shown in Figure 44. The main differences are: are $a_o/W$ ratio and different load types. $a_o/W$ ratio is 0.5 for the SENB specimens and 0.3 for the SENT specimens due the limitations of related standards. DNVGL-RP-F108 [37] and BS 8571 [38] standards for the SENT test require the $a_o/W$ range to be between 0.2 and 0.5 and ISO 12135 [36] for SENB test requires the $a_o/W$ range to be between 0.45 and 0.70. All J calculation formulas are applicable only in the defined ranges of the standards. Moore et al reported that $a_o/W$ range will be further reduced between 0.3 and 0.5 in the next revision of BS 8571 since excessive variations occur is seen in the tearing resistance curves [50].

The constraint on crack tip is the function of the load type, material property and specimen geometry [51]. Higher constraint lowers the resistance to tearing [52]. Base metal specimens were prepared and tested for the comparison of different load types with same $a_o/W$ ratio and same load types with the different $a_o/W$ ratio presented in Figure 45. The CTOD values of the SENT specimens are almost 75% higher than those of the SENB specimens for $a_o/W=0.5$ ratio. SENB specimens with $a_o/W=0.5$ have almost 80% higher CTOD values than SENB specimens for $a_o/W=0.65$.

Deeper notched SENB specimens have the worse results as reported by Thaulow et al [53]. Best results were obtained from the shallower notched specimens under tensile load. This conclusion is in agreement with literature [52, 54]. SENT specimens with shallower notches are not only less conservative but also more realistic since pipeline girth welds are predominantly loaded in tension and flaw sizes are controlled by the weld pass height which is 2-6 mm [37]. Consequently, R-curves generated from the SENT specimens with $a_o/W=0.3$ is the most realistic option in accordance with the existing standards.

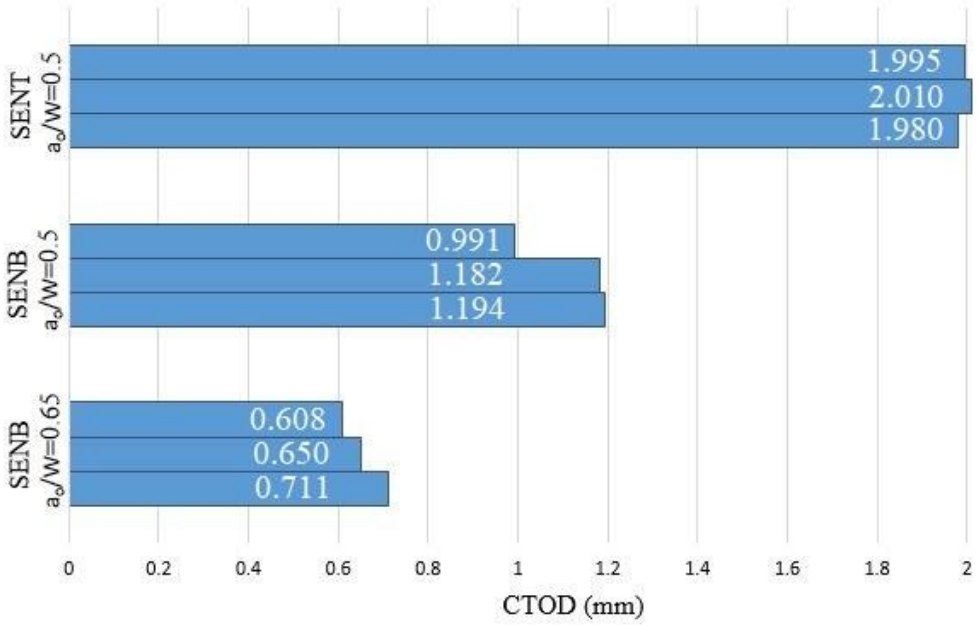


*Figure 45. Base metal CTOD values.*

Crack tip constraint alteration leads to considerable changes on fracture toughness parameters. Conventional specimens such as compact tension specimen and then, SENB specimen are becoming obsolete due to over-conservative assessments raised from the application of high constraint fracture toughness values [55]. Many recent studies are examining SENT specimens with finite element analysis (FEA) presenting the specimens as a more realistic alternative with lower constraint [56, 57, 58]. There are many numerical investigations employing FEA in literature, however, experimental results are rarely presented due to complexity of the testing and evaluation of the results. Tearing resistance curves presented in Figure 44 and single CTOD values presented in Figure 45 are both declare the validity of those analyses with clear experimental results.

5.2 Deformation at crack tip

For a material with a simple elastic – perfectly plastic response, equation 1 implies that a zone is formed at the crack-tip proximity where the material is plastically deformed Figure 46.

$$\sigma_{i,j} = \frac{K}{\sqrt{2\pi r}} f(\theta) \quad (5)$$

where r and θ are polar coordinates of a region under stress and at a crack-tip proximity. In other words, the stress field at the crack tip, which is quite high, contributes to the formation of a plastic zone at the proximity of crack tip. Plasticity in the plastic zone is a factor to determine its locus due to the redistribution of stresses that might be estimated employing methods based on LEFM. It plays an important role in estimation of crack initiation and propagation behaviors because it determines the state of stress, which in turn affects the direction of planes where the maximum shear stress is available.

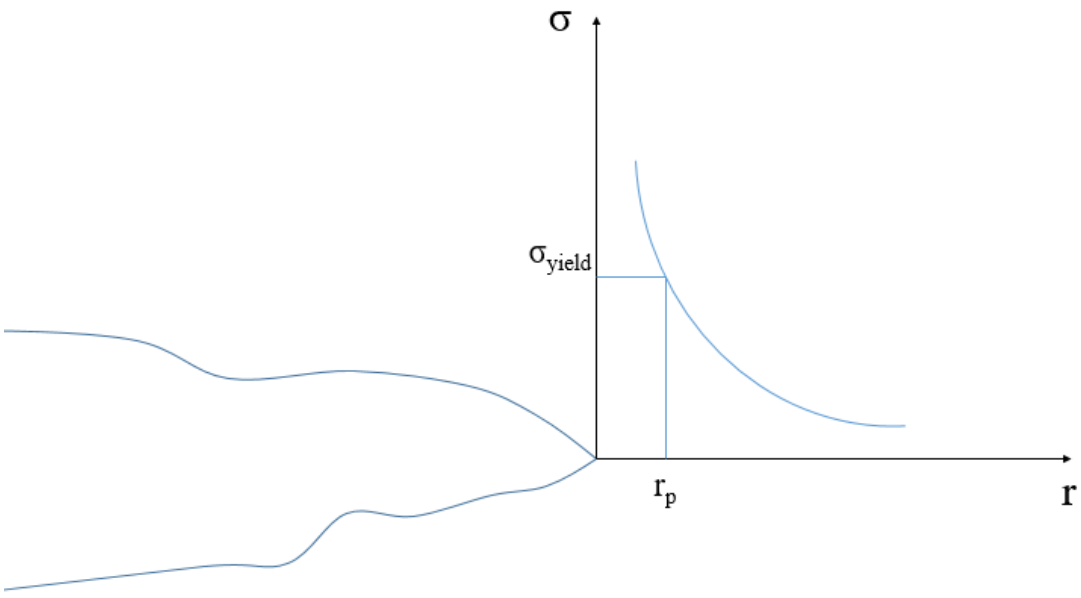


*Figure 46. Stress vs crack tip radius at the crack tip proximty.*

Employing the Mises shear strain energy criterion, analytical models to predict plastic zone locus have been provided by researchers since late fifties [59, 60, 61]. Harmain and Provan [62] contributed to these deterministic efforts and their model was based on Tresca criterion. Jing et al. [63] compared Tresca and Mises yield criteria on the closed-form solutions for the mode II crack tip plastic zone. Based on Yu's [64] unified strength teory, Qiang et al. [65] and Zhang et al. [66] solutions for modes I, II, II and mixed mode I/II under small-scale yielding were also developed. These studies provided more realistic solutions in terms of material versatility. Following finite element analyses based studies [67, 68] have been contributed to the development of the models, however these models were generally limited to isotropic materials.

In elastic-plastic fracture mechanics, the crack tip stress field is conventionally described by a single parameter, which is either J-integral or CTOD. Fracture toughness of a material is determined testing, usually, single-edge notched specimens. However, as previously mentioned in this dissertation, recent studies suggest that conventional single parameter approach sometimes may not be validated because the crack tip stress fields are affected by the crack tip constraint, which is induced by some geometrical and physical conditions [69, 70].

After fracture toughness parameters of base metal specimens are evaluated cross section of fractured surfaces are examined as presented in Figure 47. The force applied to a cracked body is either fully utilized in crack extension as in LEFM or a portion of the force utilized in deforming the material around the crack as in EPFM. Crack tip plasticity is the plastic deformation occurs around the crack tip [31].

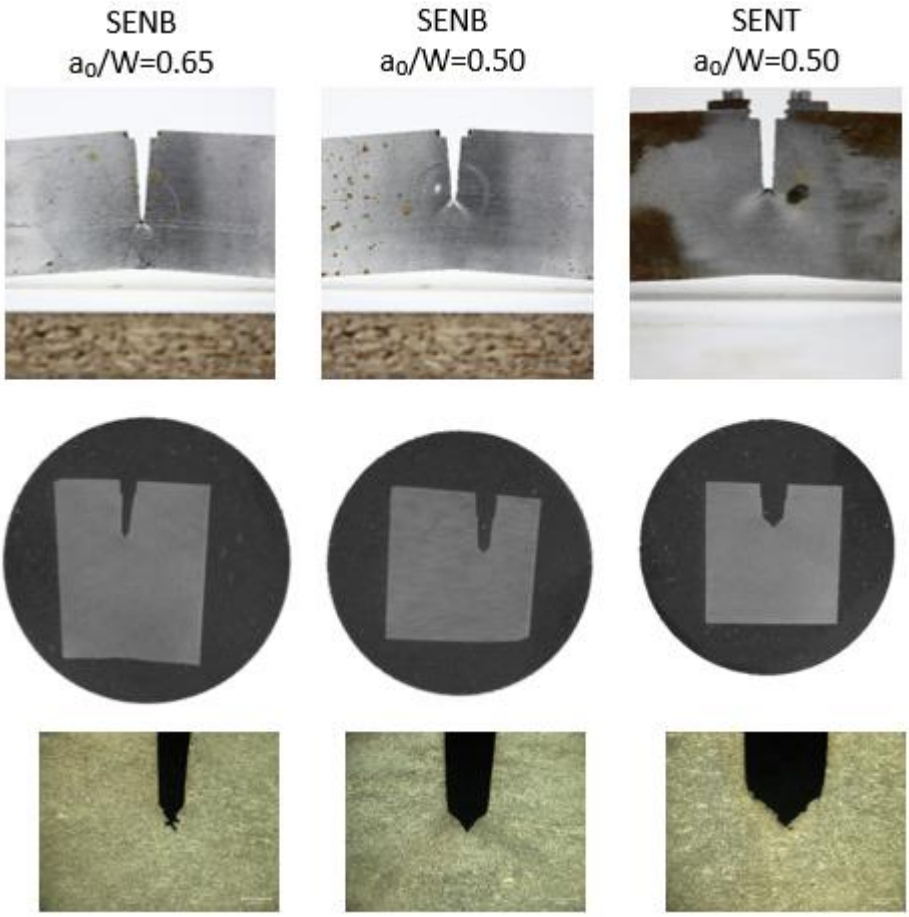


*Figure 47. Cross sections of base metal specimens.*

Crack tip plasticity is higher when the resistance to tearing is stronger. Better resistance is expressed with higher fracture toughness parameters and lower crack tip constraint. Higher plastic deformation is seen as cleavage in Figure 47. SENB specimen with 0.65 $a_o$/W ratio has the highest crack tip constraint, thus, it has the lowest cleavage. SENT specimen with 0.50 $a_o$/W ratio has the highest cleavage since it has the highest crack tip plasticity. CTOD values also support this conclusion.

The SENB specimen with 0.65 $a_o$/W ratio and SENT specimen with 0.50 $a_o$/W ratio are subjected to HV0.5 scanning since these two specimens are representing two extremes in terms of CTOD values and crack tip constraint. Contour maps of micro hardness variance are presented in Figure 48.

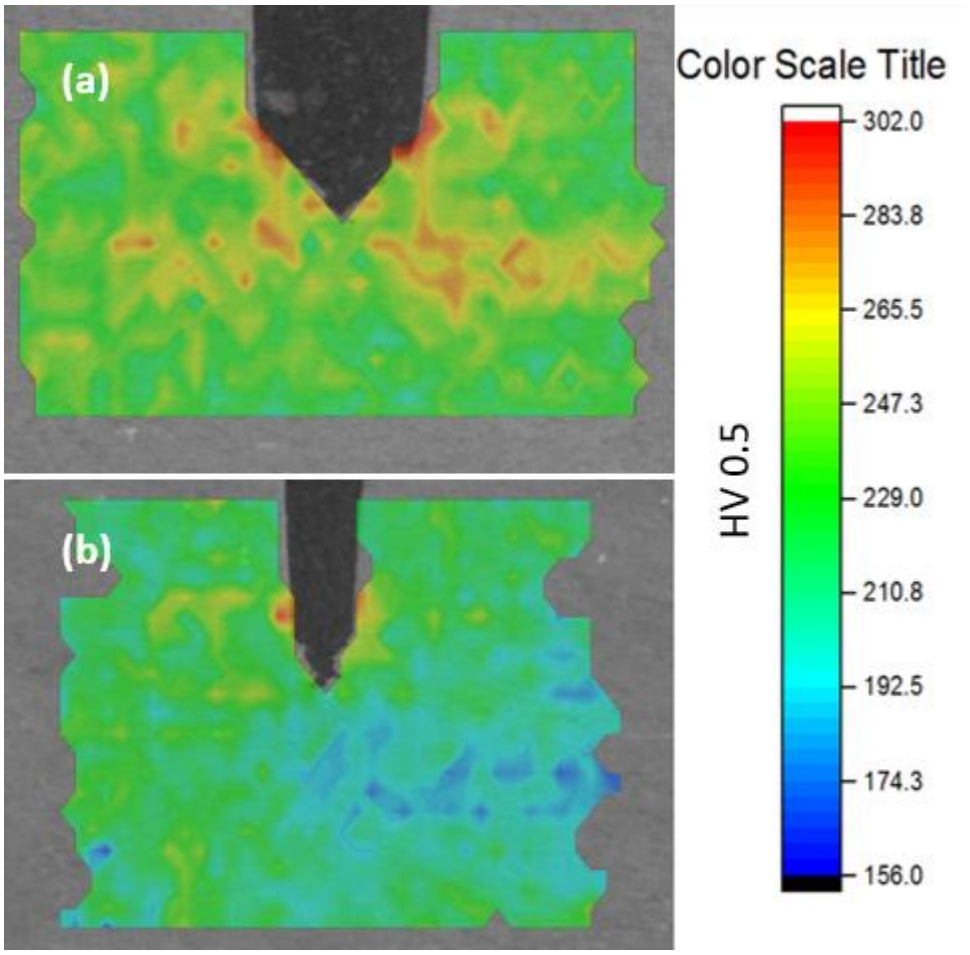


*Figure 48. Contour map of micro hardness varience (a) SENT specimen with 0.50 $a_o/W$ ratio and (b) SENB specimen with 0.65 $a_o/W$ ratio.*

Crack tip plasticity is visualized in terms of strain hardening due to plastic deformation around the crack tip. Our analysis proposed that crack tip plasticity levels in SENB specimens are lower than the ones in SENT specimens. SENT specimens had higher CTOD values compared to SENB specimens. In other words, motive behind the resistance to tearing is expressed in terms of strain. The highest strain hardening is seen at the onset of crack propagation which is called stretch zone.

## 5.3 The stretch zone

At critical strain, the pre-existing crack in a ductile material first blunts and voids are then formed ahead of the crack tip. These voids finally coalesce with the tip leading to the crack propagation [31]. The crack tip plasticity manifests itself as a stretch zone ahead of the fatigue pre-crack. In other words, the plastic deformation at the crack tip yields blunting and formation of the stretch zone. According to the standards [36, 37], values of initiation toughness, in terms of J or δ, may be determined from the stretch zone width (SZW).

The stretch zone is an intermediate zone between the end of the fatigue pre-crack and the beginning of the crack produced by monotonic loading. SZW is generally about 100 μm and less for low alloy steels. Therefore, determination of initiation toughness values requires the use of SEM. Fracture surface of a SENT specimen (PJ28) under SEM is presented in Figure 49. Since the appearance of this zone is ductile like the fatigue pre-crack zone, it is distinguished by a hillier relief and more elongated dimples at the end line of fatigue pre-crack as presented in Figure 50. An operator who has experience in the interpretation of SEM fractographs is essential to be able to examine the zone and determine the size of it. As similar to the pre-crack length and crack extension measurements, local SZWs are measured at the nine positions shown in Figure 49. At least five measurements shall be made at each of the nine local SZW as presented in Figure 51.

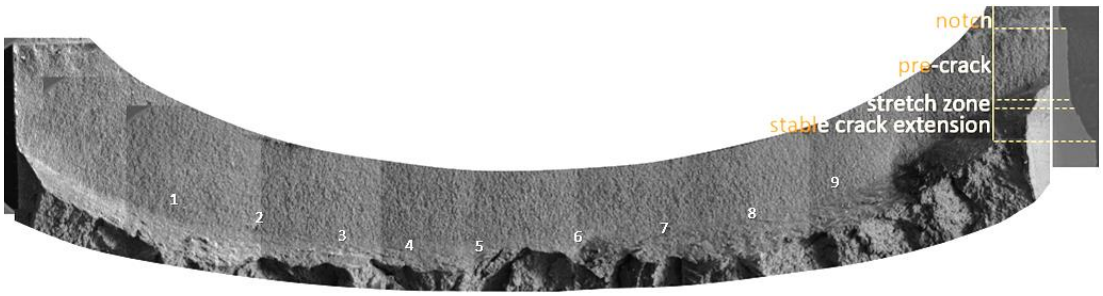


*Figure 49. Fracture surface of a SENT specimen (PJ28).*

Paranjpe and Banerjee [71], Mills [72], Amouzouvi and Bassim [73], Yin et al. [74] and Doig et al. [75] conducted empirical studies to evaluate the fracture toughness using SZW measurement. Despite the fact that an initiation toughness definition that based on SZW provides more realistic fracture resistance analyses, the experience required and the scatter of the values make this approach tricky and critical. The scatter comes from local metallurgical characteristics of the material, as well as variation in crack tip constraints through the cracking line. A large scatter in the SZW measurements was found independently by researchers during a round robin test [76]. Therefore, there are also attempts available to evaluate SZW numerically [77].

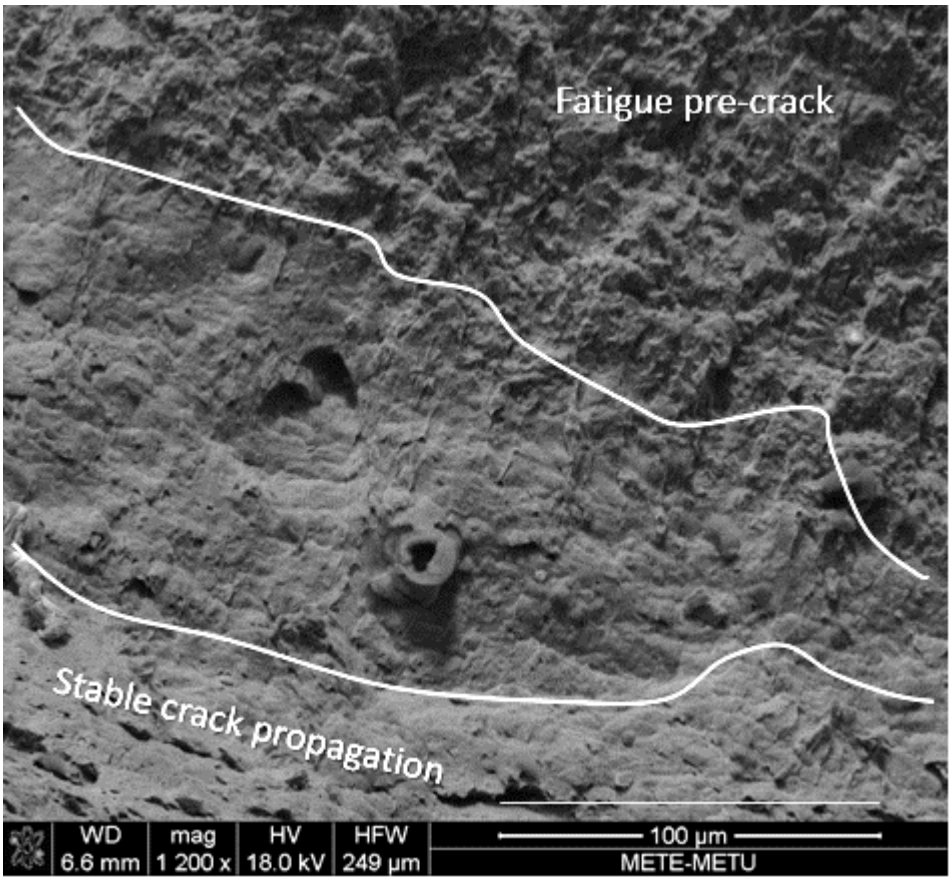


*Figure 50. Stretch zone between fatigue pre-crack and stable crack propagation.*

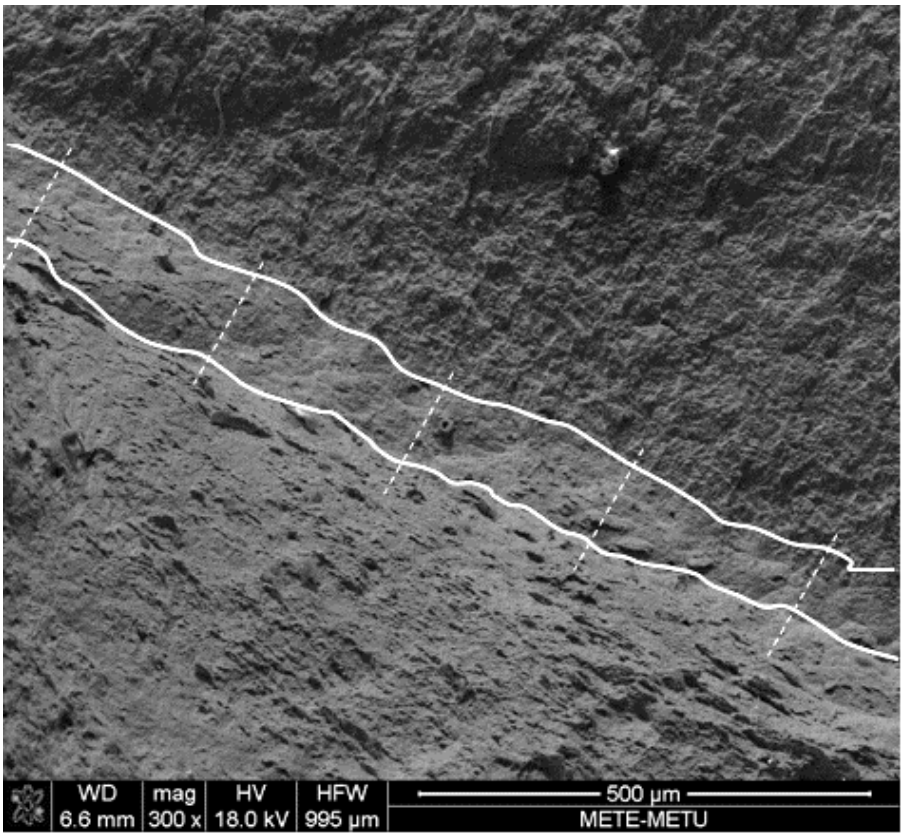


*Figure 51. Five measurement taken from one of the 9 local points on Figure 49.*

Stretch zone height (SZH) has emerged to determine the crack initiation line and calculation of initiation toughness. Weidner et al. [78] demonstrates a new method to determine SZW and SZH using a 3D imaging interface integrated to SEM as presented in Figure 52. SZW from top view in Figure 51 is calibrated using plateau metallography efforts presented in Figure 53. 45 measurements are taken per a SENT specimen (PJ28) and a SENB specimen (PJ8), which are both notched from fusion line, to calculate SZW and $J_{initiation}$ as tabulated in Table 25.

*Table 25. Stretch zone width and J values.*

| | PJ28 (SENT) | PJ8 (SENB) |
|---|---|---|
| Mean SZW (µm) | 96.6 | 55.4 |
| Standard deviation | 14.5 | 11.6 |
| Resistance curve equation | $J=1.113\Delta a^{0.681}$ | $J=0.937\Delta a^{0.534}$ |
| $J_{initiation}$ ($J/mm^2$) | 0.231 | 0.200 |

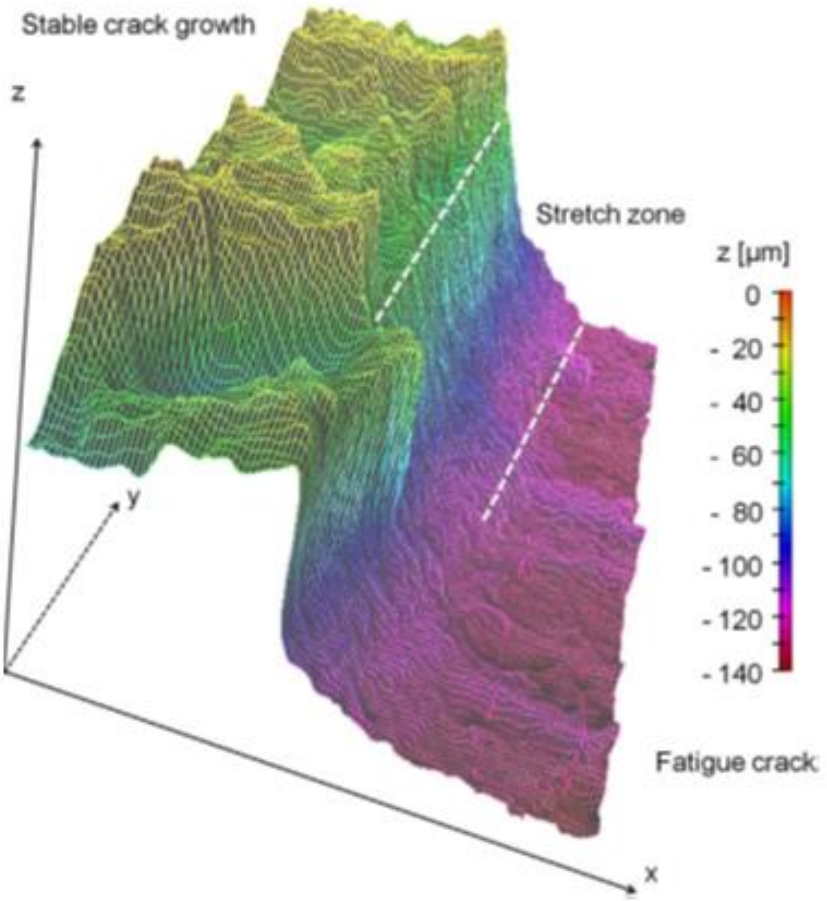


*Figure 52. SZW and SZH using a 3D imaging interface integrated to SEM [78].*

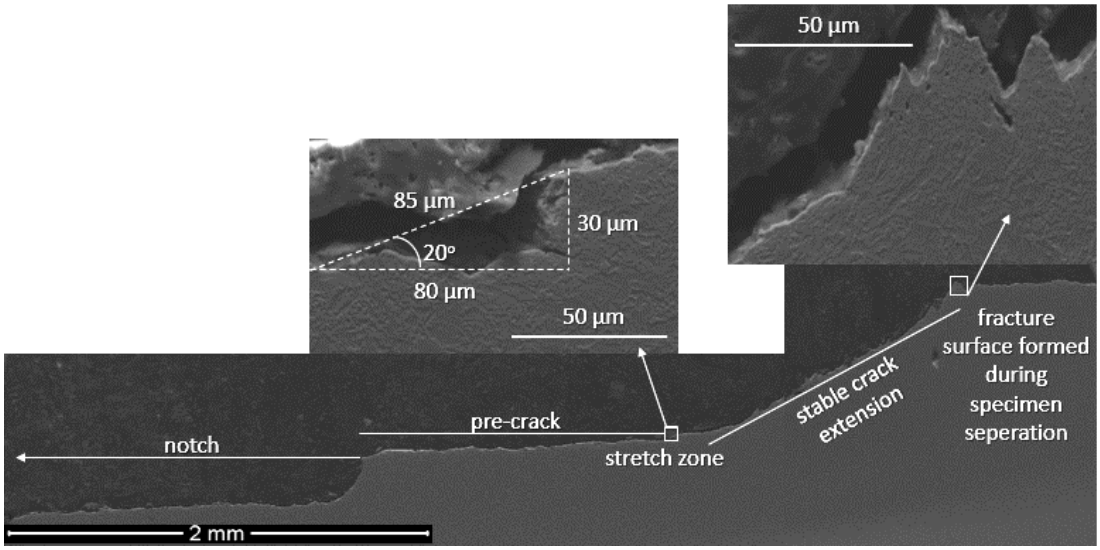


*Figure 53. Calibration of SZW from top view in Figure 51.*

The SENT specimen has a bigger stretch zone compared to the SENB specimen, which means the SENT specimen has a better resistance to crack initiation. This resistance can be expressed by $J_{initiation}$ and it is presented in Figure 54 and Figure 55 for SENT and SENB FL R-curves, respectively. Resistance curves with SZW measurements are presenting both tear initiation and propagation in terms of fracture toughness.

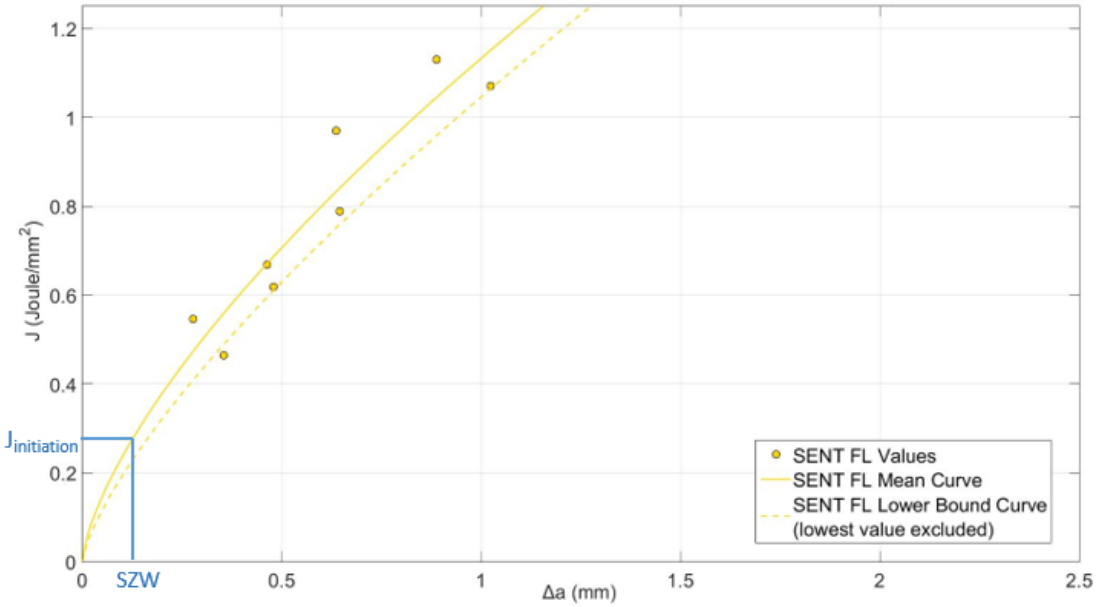


*Figure 54. J initiation and SZW on SENT FL mean resistance curve.*

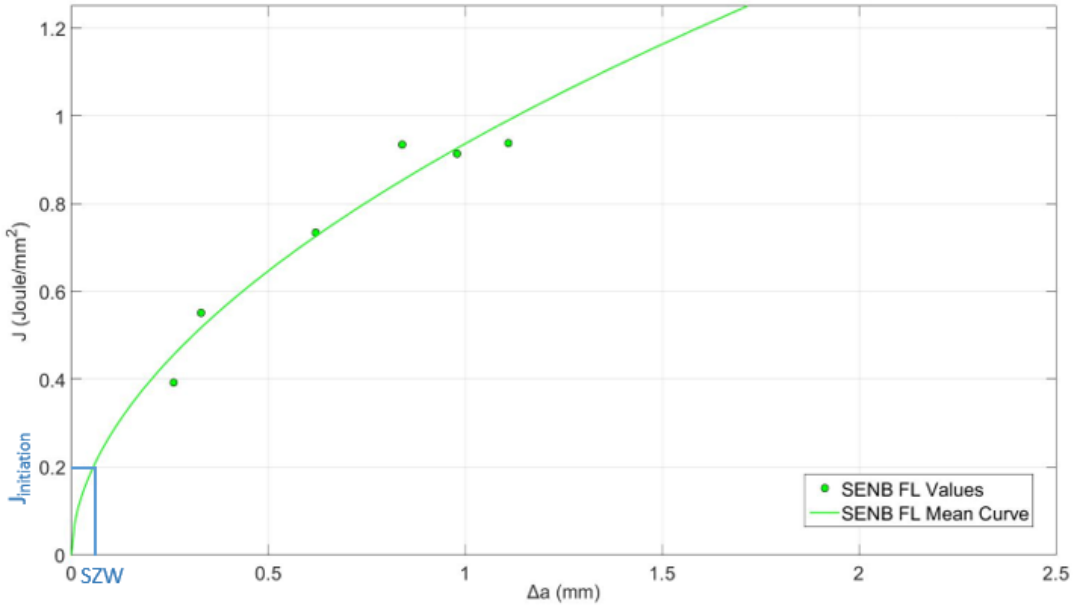


*Figure 55. J initiation and SZW on SENB FL mean resistance curve.*

## 5.4 Damage micro-mechanisms

Variation in the damage micro mechanisms were examined using post-test metallography on parent and as-welded material specimens under SEM. Cracking plateaus of parent material specimens, where relatively homogenous microstructures were available, provided relatively more clear images of damage mechanisms. On the one hand, relatively uniform damage fields that surround the stable crack extension indicate that predominantly fracture mode I has been experienced during the testing of single-edge notch specimens, either under tensioning or bending (Figure 56). On the other hand, two distinguished fracture mechanisms were observed on SENB specimens of both $a_o$/W parameters, whereas only tensile fracture mechanism was available in SENT specimens, which is typical void growth and coalescence as presented in Figure 57. The fracture mechanisms observed on SENB specimens were slightly similar to the ones that would be observed on post-test compact tear specimens (CTS) [79]. Besides blunting, shear mechanism is more apparent at the stretch zone of SENB specimen with $a_o$/W of 0.65 (Figure 58), as well as the tip of stable crack extension (Figure 59).

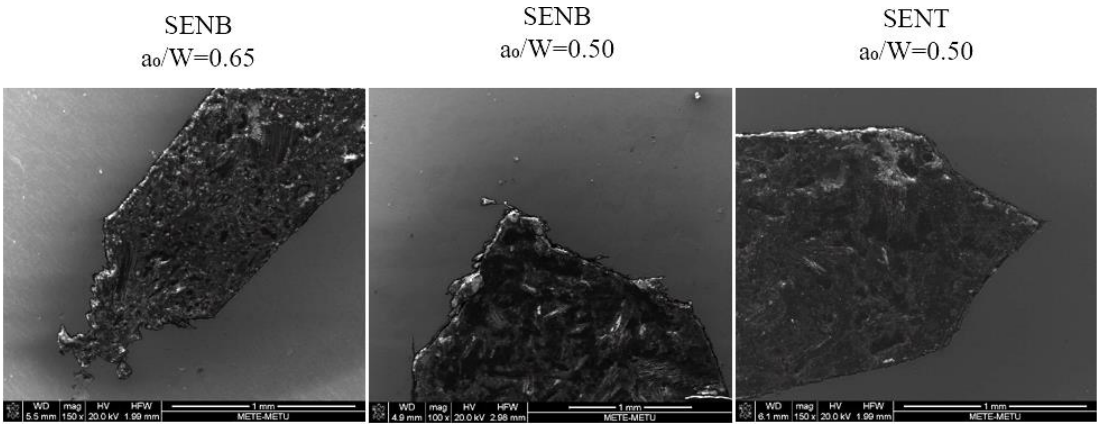


*Figure 56. Final crack fronts of base metal specimens.*

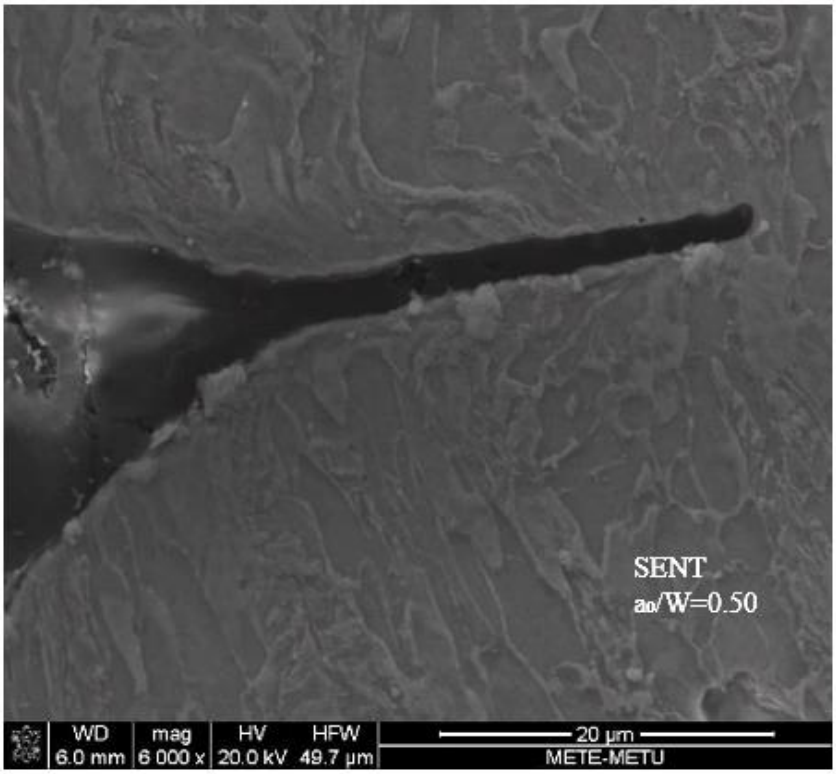


*Figure 57. Final crack tip of the SENT specimen.*

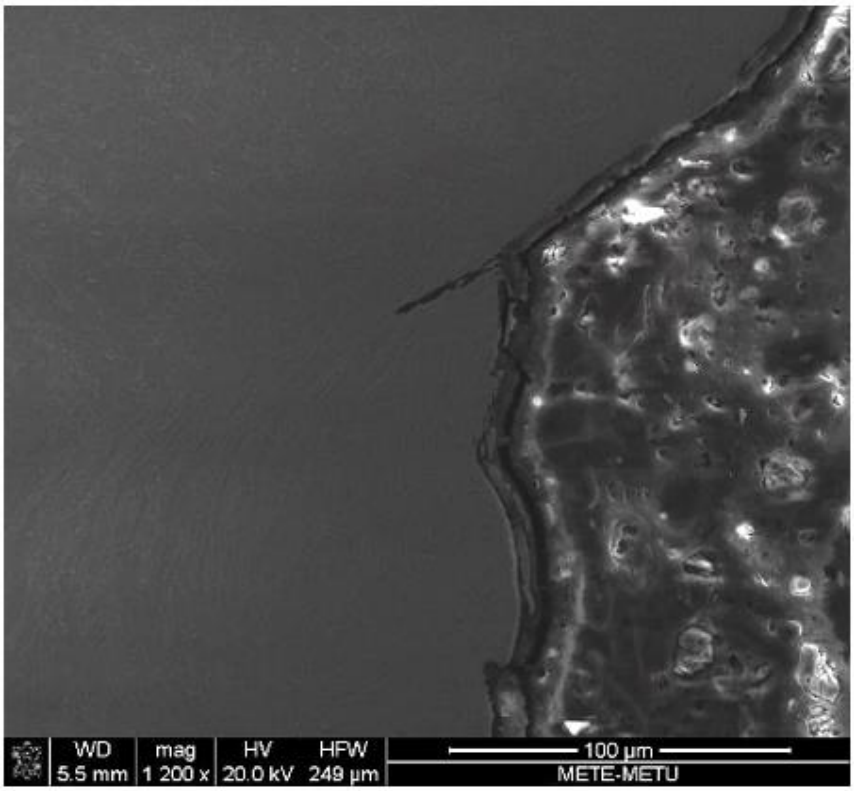


*Figure 58. Stretch zone of SENB specimen with $a_o/W$ of 0.65.*

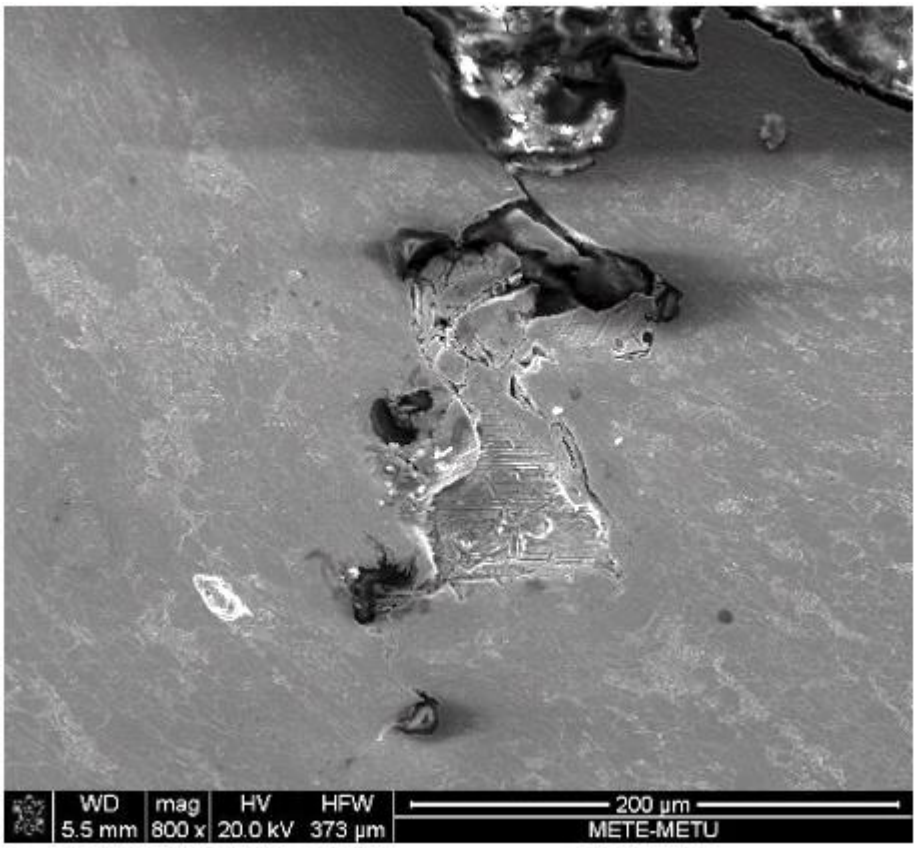


*Figure 59. Tip of stable crack extension of SENB specimen with $a_o/W$ of 0.65.*

In practical situations, such as reeled laying of off-shore pipelines, artcic pipelines, high-temperature / high-pressure pipelines or pipelines in areas with significant expected ground movement, loading conditions can be very complex. Sustained loads, seismic loads, thermal loads at various operating conditions, the reaction force due to pressure safety valves and forces induced by surge and nominal develop stresses in the system that may result in ductile mixed-mode fracture where pre-existing flaws are available [80]. Lower fracture resistance of the SENB specimens compared to the SENT specimens is related to localised micro shear mechanism.

# CHAPTER 6

# CONCLUSION & FUTURE RECOMMENDATIONS

## 6.1 Conclusion

Fracture toughness behavior of as welded 24.01 mm thick with 48” outside diameter line pipe steel grade X70M was investigated in terms of elastic-plastic fracture mechanics (EPFM) parameters. Critical crack tip opening displacement (CTOD) values were calculated and J R-curves were generated after the integrity of the joint is validated by conventional non-destructive and destructive tests. Both single edge notched bend (SENB) and single edge notched tension (SENT) specimens notched from weld metal and fusion line were prepared, tested and compared. Specimens further subjected to metallography and micro hardness measurements. Results were evaluated with the models and analysis reported in literature. The following conclusions can be drawn from this study:

- The SENT specimens demonstrate better resistance to both located crack and propagation of tearing compared to the SENB specimens due to lower crack tip constraint. Because of realistic predominant load type and lower standardized $a_o/W$ range, SENT specimen testing is a strong alternative for engineering critical assessments of line pipes.
- Weld metal notched specimens have lower values in terms of fracture toughness, yet, catastrophic failures are seen from the fusion line notched specimens due to local brittle zones (LBZs). LBZs are detrimental to fracture toughness are detected by micro hardness scanning in inter-critically reheated coarse grain heat affected zone (IRCGHAZ).
- Increasing the $a_o/W$ detrimentally affects the fracture resistance by increasing crack tip constraint. Shallower notched specimens which represent the

restrictions of line pipes with multi-pass girth welds accurately should be employed for better fracture toughness results.

- Strain field at the proximity of crack tip can be indirectly presented in terms of micro-hardness distribution since higher strain hardening is a manifestation of better fracture toughness.
- FL notched SENT specimens have larger stretch zone width (SZW) compared to the SENB specimens. Thus, they have higher resistance to crack initiation. Resistance to tearing initiation can be expressed as $J_{initiation}$ by using resistance curve equation.
- Both tearing initiation toughness values obtained from the resistance curves and the single critical values can be used for evaluating the fracture initiation resistance to a located flaw. However, determining the values of initiation toughness over resistance curves can be a better option in comparison to the single values if the stretch zone is measured properly, since the tearing length is neglected in critical single value calculations.
- Even though fracture mode I has been experienced predominantly in both the SENB and SENT tests, localised micro shear mechanism increases the vulnerability of the SENB specimens to crack growth.

## 6.2 Future recommendations

Stress-strain field at the proximity of crack tip may be modelled by employing finite element analysis (FEA). A comparison between experimental strain hardening measurements and stress-strain field may be used for more realistic estimations in computed models.

Measuring SZW properly has a vital role on determining the initiation toughness parameters. A guideline for interpreting SEM fractographs may contribute to standardization of initiation toughness determination over resistance curves.

## REFERENCES


[1] American Petroleum Institute, API 1104 Welding of Pipelines and Related Facilities, Washington, D.C.: API Publishing Services, 2005.

[2] Det Norske Veritas, DNVGL-ST-F101 Submarine pipeline systems, 2017.

[3] AFCEN, Design and Construction Rules for Mechanical Components of PWR Nuclear Islands, 2017.

[4] American Petroleum Institute, API 5L Specification for Line Pipe, NW, Washington, DC: API Publishing Services, 2013.

[5] EN 10025-4 Hot rolled products of structural steels. Technical delivery conditions for thermomechanical rolled weldable fine grain structural steels, 2004.

[6] Det Norske Veritas, DNVGL-OS-B101, 2017.

[7] S. Hashemi, "On the relation of microstructure and impact toughness characteristics of DSAW steel of grade API X70," *Fatigue & Fracture of Engineering Materials & Structures,* no. 32, pp. 33-40, 2009.

[8] G. Khalaj, "Artificial neural networks application to predict the ultimate tensile strength of X70 pipeline steels," *Neural Comput & Applic,* no. 23, pp. 2301-2308, 2013.

[9] Y. Kim, "Effects of Molybdenum and Vanadium Addition on Tensile and Charpy Impact Properties of API X70 Linepipe Steels," *Metallurgical and Materials Transactions A,* no. 38, pp. 1731-1742, 2007.

[10] S. Shin, B. Hwang, S. Lee, N. Kim and S. Ahn, "Correlation of microstructure and charpy impact properties in API X70 and X80 line-pipe steels," *Materials Science and Engineering A,* no. 458, pp. 281-289, 2007.

[11] L. Godefroid, "Microstructure and Mechanical Properties of Two APISteels for Iron Ore Pipelines," *Materials Research,* pp. 114-120, 2014.

[12] TANAP Natural Gas Transmission Company, "Trans Anatolian Natural Gas Pipeline Project," [Online]. Available: http://www.tanap.com/tanap-project/photo-galery/. [Accessed 6 May 2018].

[13] M. J. Kaiser, "Offshore pipeline construction cost in the U.S. Gulf of Mexico," *Marine Policy,* no. 82, pp. 147-166, 2017.

[14] J. F. Kiefner and C. Trench, "Oil Pipeline Characteristics and Risk Factors: Illustrations from the Decade of Construction," American Petroleum Institute, 2001.

[15] G. Krauss and S. Thomson, "Ferritic microstructures in continuously cooled low- and ultra-low carbon steels," *Iron and Steel Industry of Japan International,* vol. 35, no. 8, pp. 937-345, 1995.

[16] S. Shanmugam, R. Misra and J. Hartmann, "Microstructure of high strength niobium-containing pipeline steel," *Materials Science and Engineering A,* no. 441, pp. 215-229, 2006.

[17] R. Parthiban, S. Chowdhury, K. Harikumar and S. Sankaran, "Evolution of microstructure and its influence on tensile properties in thermo-mechanically controlled processed (TMCP) quench and partition (Q & P) steel," *Materials Scienece & Engineering A,* no. 705, pp. 376-384, 2017.

[18] S. K. Sharma and S. Maheshwari, "A review on welding of high strength oil and gas pipeline steels," *Journal of Natural Gas Science and Engineering,* no. 38, pp. 203-217, 2017.

[19] International Organization for Standardization, ISO 15614-1 Specification and qualification of welding procedures for metallic materials -- Welding procedure test -- Part 1: Arc and gas welding of steels and arc welding of nickel and nickel alloys, 2017.

[20] American Society of Mechanical Engineers, BPVC Section IX-Welding, Brazing, and Fusing Qualifications, ASME, 2017.

[21] American Welding Society, AWS D1.1 STRUCTURAL WELDING - STEEL, 2007.

[22] R. Celin, J. Burja and G. Kosec, "A comparison of as-welded and simulated heat affected zone (HAZ) microstructures," *Materials and Technology*, no. 50, pp. 455-460, 2016.

[23] J. Lee, J. Ju, J. Jang, W. Kim and D. Kwon, "Weld crack assessments in API X65 pipeline: failure assessment diagrams with variations in representative mechanical properties," *Materials Scienece and Engineering A*, no. 373, pp. 122-130, 2004.

[24] V. Gunaraj and N. Murugan, "Prediction of Heat-Affected Zone Characteristics in Submerged Arc Welding of Structural Steel Pipes," *Welding Journal*, pp. 94-98, 2002.

[25] D. Fairchild and J. e. Koo, "Local Brittle Zones in Structural Welds," *Welding Metallurgy of Structural Steels*, pp. 303-318, 1987.

[26] I. Milne, O. Ritchie and B. Karihaloo, Comprehensive Structural Integrity, 2003.

[27] P. Moore and G. Booth, The Welding Engineer's Guide to Fracture and Fatigue, Cambridge, UK: Woodhead Publishing, 2015.

[28] British Standards Institution, BS 7910 Guide to methods for assessing the acceptability of flaws in metallic structures, 2013.

[29] J. Landes and D. Shaffer, "Statistical characterisation of fracture in the transition regime," in *Fracture Mechanics STP 700*, American Society for Testing and Materials, 1980, pp. 368-383.

[30] S. Machida, H. Yoshinari and Y. Suzuki, "A Statistical Study on the Effect of Local Brittle Zones (LBZs) on the Fracture Toughness (Crack Tip Opening Displacement) of Multipass Welded Joints," in *Fracture Mechanics STP 700*, American Society for Testing and Materials, 1994, pp. 264-290.

[31] T. Anderson, Fracture Mechanics: Fundamentals and Applications, CRC Press, 2004.

[32] G. Irwin, "Analysis of stresses and strains near the end of a crack traversing a plate," *Journal of Applied Mechanics*, no. 24, pp. 361-364, 1957.

[33] A. A. Wells, "Application of fracture mechanics at and beyond general yielding," *British Weld Journal*, no. 10, pp. 563-570, 1963.

[34] J. Rice, "A path indipendent integral and the approximate analysis of strain concentration by notches and cracks," *Journal of Applied Mechanics*, no. 35, pp. 379-386, 1968.

[35] American Society for Testing and Materials, ASTM E1820 Standard Test Method for Measurement of Fracture Toughness, 2017.

[36] The International Organisation for Standardization, ISO 12135 Metallic materials in Unified method of test for the determination of quasistatic fracture toughness, 2015.

[37] Det Norske Veritas, DNVGL-RP-F108 Assessment of flaws in pipeline and riser girth welds, 2017.

[38] British Standards Institution, BS 8571 Method of test for determination of fracture toughness in metallic materials using single edge notched tension (SENT) specimens, 2014.

[39] American Welding Society, AWS A5.18 Specification for Carbon Steel Electrodes and Rods for Gas Shielded Arc Welding, 2005.

[40] American Welding Society, AWS A5.28 Specification for Low-Alloy Steel Electrodes and Rods for Gas Shielded Arc Welding, 2005.

[41] The International Organization for Standardization, ISO 5173 Destructive tests on welds in metallic materials in Bend tests, 2009.

[42] International Organization for Standardization, ISO/TR 16060 Destructive tests on welds in metallic materials -- Etchants for macroscopic and microscopic examination, 2003.

[43] The International Organization for Standardization, ISO 6507 Destructive tests on welds in metallic materials, 2012.

[44] The International Organization for Standardization, ISO 6892-1 Metallic materials — Tensile testing, in Part 1: Method of test at room temperature., 2009.

[45] The International Organization for Standardization, ISO 15653 Metallic materials in Method of test for the determination of quasistatic fracture toughness of welds, 2010.

[46] M. Mohammadijoo, J. Valloton, L. Collins, H. Henein and D. Ivey, "Characterization of martensite-austenite constituents and micro-hardness in intercritical reheated and coarse-grained heat affected zones of API X70," *Materials Characterization,* Vols. 321-331, no. 142, 2018.

[47] G. Spanos, R. W. Fonda, R. A. Vandermeer and A. Matuszeski, "Microstructural changes in HSLA-100 steel thermally cycled to simulate the heat-affected zone during welding," *Metallurgical and Materials Transactions A,* vol. 26, no. 12, pp. 3277-3293, 1995.

[48] M. Cagirici, Investigation of Key-Hole Weldability of Line Pipe Steel Grade X70M in Terms of Fracture Toughness Properties, Ankara: MSc Thesis, 2016.

[49] G. Donato, R. Magnabosco and C. Ruggieri, "Effects of weld strength mismatch on J and CTOD estimation procedure for SE(B) specimens," *International Journal of Fracture,* vol. 159, no. 1, pp. 1-20, 2009.

[50] P. Moore and H. Pisarski, "SENT testing standard BS 8571 and its ongoing development," *International Journal of Pressure Vessels and Piping,* no. 156, pp. 2-7, 2017.

[51] A. Karstensen, A. Horn and M. Goldthorpe, "Constraint loss in welds due to geometry, loading mode and strength mismatch," in *2nd International Symposium on High Strength Steel*, Stiklestad, SINTEF, Norway, 2002.

[52] H. Pisarski and C. Wignall, "Fracture toughness estimation for pipeline girth welds," in *International Pipeline Conference,* Alberta, Canada, 2002.

[53] C. Thaulow, E. Østby, B. Nyhus, Z. L. Zhang and B. Skallerud, "Constraint correction of high strength steel Selection of test specimens and application of direct calculations," *Engineering Fracture Mechanics,* no. 71, pp. 2417-2433, 2004.

[54] M. Verstraete, S. Hertelé, R. Denys, K. Van Minnenbruggen and W. De Waele, "Evaluation and interpretation of ductile crack extension in SENT specimens using unloading compliance technique," *Engineering Fracture Mechanics,* no. 115, pp. 190-203, 2014.

[55] Y. Matvienko and G. Nikishkov, "Two-parameter J-A concept in connection with crack-tip constraint," *Theoretical and Applied Fracture Mechanics,* no. 92, pp. 306-317, 2017.

[56] X.-K. Zhu, "Full-range stress intensity factor solutions for clamped SENT specimens," *International Journal of Pressure Vessels and Piping,* no. 149, pp. 1-13, 2017.

[57] S. Tiku, N. Pussegoda, M. Ghovanlou, W. Tyson and A. Dinovitzer, "Standardisation of SENT (or SE(T)) fracture toughness measurement: results of a round robin on a draft test procedure," in *11th International Pipeline Conference*, Calgary, Alberta, Canada, 2016.

[58] S. Cravero and C. Ruggieri, "Correlation of fracture behavior in high pressure pipelines with axial flaws using constraint designed test specimens—Part I: Plane-strain analyses," *Engineering Fracture Mechanics*, no. 72, pp. 1344-1360, 2005.

[59] G. Irwin, "Plastic zone near a crack and fracture toughness," in *7th Saga More Ordnance Materials Conference*, New York, 1963.

[60] D. Dugdale, "Yielding of steel sheets containing slits," *Journal of Mechanics and Physics of Solids*, no. 8, pp. 100-106, 1960.

[61] J. Hult and F. McClintock, "Elastic-plastic stress and strain distributions around sharp notches under repeated shear," in *9th International Congress on Applied Mechanics*, Brussels, 1957.

[62] G. Harmain and J. Provan, "Fatigue crack-tip plasticity revisited – the issue of shape addressed," *Theoretical and Applied Fracture Mechanics,* no. 26, pp. 63-79, 1997.

[63] P. Jing, T. Khraishi and L. Gorbatikh, "Closed-form solutions for the mode II crack tip plastic zone shape," *International Journal of Fracture,* no. 122, pp. 137-142, 2003.

[64] M. Yu, "Advances in strength theories for materials under complex stress state in the 20th Century," *Journal of Applied Mechanics,* no. 55, pp. 169-218, 2002.

[65] H. Qiang, N. Lu and B. Liu, "Unified solutions of crack tip plastic zone under small scale yielding," *Journal of Applied Mechanics,* no. 35, pp. 34-38, 1999.

[66] Y. Zhang, H. Qiang and Y. Yang, "Unified solutions to mixed mode crack tip under small scale yielding," *Journal of Applied Mechanics,* no. 43, pp. 50-54, 2007.

[67] X. Wu and Y. Dzenis, "Closed-form solution for the size of plastic zone in an edge-cracked strip.," *International Journal of Engineering Sciences ,* no. 40, pp. 1751-1759, 2002.

[68] K. Benrahou, M. Benguediab and M. Belhouari, "Estimation of the plastic zone by finite element method under mixed mode loading," *Computational Materials Science,* no. 38, pp. 595-601, 2007.

[69] H. Yuan and W. Brocks, "Quantification of constraint effects in elastic-plastic crack front fields," *Journal of the Mechanics and Physics of Solids,* no. 46, pp. 219-241, 1998.

[70] C. Betegón and J. Hancock, "Two-parameter characterized of elastic–plastic crack-tip fields," *Journal of Applied Mechanics,* no. 58, pp. 104-110, 1991.

[71] S. Paranjpe and S. Banerjee, "Interrelation of crack opening displacement and J-integral," *Engineering Fracture Mechanics,* no. 11, pp. 43-53, 1979.

[72] W. Mills, "On the relationship between stretch zone formation and the J integral for high strain-hardening materials," *Journal of Testing and Evaluation,* vol. 1, no. 9, pp. 56-62, 1981.

[73] K. Amouzouvi and M. Bassim, "Determination of fracture toughness from stretch zone width measurement in predeformed AISI Type 4340 steel," *Materials Science and Engineering,* no. 55, pp. 257-262, 1982.

[74] S. Yin, R. Gerbrands and M. Hartevelt, "An investigation of the blunting line," *Engineering Fracture Mechanics,* vol. 5, no. 18, pp. 1025-1036, 1983.

[75] P. Doig, R. Smith and P. Flewitt, "The use of stretch zone width measurements in the determination of fracture toughness of low strength steels," *Engineering Fracture Mechanics,* vol. 4, no. 19, pp. 653-664, 1984.

[76] J. Heerens, A. Cornec and K. Schwalb, "Results of a round robin on stretch zone width determination," *Fatigue & Fracture of Engineering Materials & Structures*, no. 11, pp. 19-29, 1987.

[77] S. Saxena, N. Ramakrishnan and B. Dutta, "Determination of stretch zone width using fem," *Engineering Fracture Mechanics* , no. 76, pp. 911-920, 2009.

[78] A. Weidner, T. Mottitschka, H. Biermann and S. Henkel, "Determination of stretch zone width and height by powerful 3D SEM imaging technology," *Engineering Fracture Mechanics* , no. 108, pp. 294-304, 2013.

[79] A. Pirondi and C. Donne, "Characterisation of ductile mixed-mode fracture with the crack-tip displacement vector," *Engineering Fracture Mechanics*, no. 68, pp. 1385-1402, 2001.

[80] P. Jia, H. Jing, L. Xu, Y. Han and Z. L., "A modified engineering critical assessment method for deeply-embedded cracks in metallic pipelines subjected to large plastic strain," *Engineering Fracture Mechanics*, no. In Press, 2017.